

Methodical developments and applications of scanning electrochemical microscopy



Dissertation

zur Erlangung des Doktorgrades der Naturwissenschaften (Dr. rer. nat.)
der Fakultät für Chemie und Pharmazie
der Universität Regensburg

vorgelegt von
Johannes Michael Eidschink
aus Kirchroth
im Jahr 2024

Die vorliegende Dissertation entstand im Zeitraum zwischen März 2021 und Juli 2024 am Institut für Analytische Chemie, Chemo- und Biosensorik der naturwissenschaftlichen Fakultät IV - Chemie und Pharmazie - der Universität Regensburg.

Die Arbeit wurde angeleitet von Prof. Dr. Frank-Michael Matysik.

Das Promotionsgesuch wurde eingereicht am: 05. August 2024

Termin des Kolloquiums: 10. Oktober 2024

Prüfungsausschuss:

Vorsitzender: Prof. Dr. Oliver Tepner

Erstgutachter: Prof. Dr. Frank-Michael Matysik

Zweitgutachter: Prof. Dr. Gerd-Uwe Flechsig

Drittprüfer: Prof. Dr. Werner Kunz

Danksagung

Grundsätzlich möchte ich mich bei allen Personen bedanken, welche mich auf meinem Weg zur Promotion begleitet haben.

Mein Dank gilt dabei insbesondere den folgenden Personen:

Herrn Prof. Dr. Frank-Michael Matysik danke ich für die Anleitung der Promotion und die Tätigkeit als Erstgutachter und -prüfer der Dissertation.

Herrn Prof. Dr. Oliver Tepner danke ich für die Tätigkeit als Vorsitzender des Prüfungsausschusses.

Bei Herrn Prof. Dr. Gerd-Uwe Flechsig möchte ich mich für die Tätigkeit als Zweitgutachter und -prüfer danken.

Herrn Prof. Dr. Werner Kunz gilt mein Dank für die Tätigkeit als Drittprüfer.

Dr. Thomas Herl danke ich für die Betreuung während meines Forschungspraktikums und der Masterarbeit, den fortwährenden wissenschaftlichen Austausch und seine graphische Zuarbeit.

Meinen aktuellen und ehemaligen Arbeitskollegen des AK Matysik, insbesondere Dr. Daniel Böhm, Nicole Herl, Martin Koall, Dr. Timo Raith, Joachim Rewitzer, und Dr. Stefan Wert möchte ich danken für die angenehme Arbeitsatmosphäre und inspirierende Diskussionen.

Meinen Kooperationspartnern im Rahmen wissenschaftlicher Forschungsaufenthalte, Dr. Katarzyna Jedlińska, Dr. Rene Pfeifer, und Michal Zelenský für die erfüllende Zusammenarbeit und den Wissensaustausch.

Meinen Freunden und Kommilitonen, welche mich vom Studium bis zur Promotion begleitet und angespornt haben.

Meiner Familie, insbesondere Monika Eidenschink, Helmut Eidenschink, Centa Eiglsperger, Johann Eiglsperger, und Karin Buchecker, danke ich für die immerwährende Unterstützung auch und besonders in schwierigen Zeiten.

Table of contents

Table of contents.....	I
List of publications.....	III
Conference contributions.....	VII
Declaration of collaboration	VIII
List of abbreviations	IX
1 Introduction	1
2 Theoretical background.....	6
2.1 Electrochemistry.....	6
2.1.1 Fundamentals	6
2.1.2 Mass transfer	8
2.1.3 Behaviour of ultramicroelectrodes in comparison to macro electrodes	10
2.2 Scanning electrochemical microscopy.....	14
2.2.1 Instrumental setup.....	14
2.2.2 Types of SECM probes and their characteristics	15
2.2.3 Operational modes.....	18
2.3 Scanning ion conductance microscopy	25
2.3.1 Instrumental setup.....	25
2.3.2 Working principles and operational modes	26
3 Experimental	32
3.1 Chemicals, instrumentation, materials, and software.....	32
3.2 Preparation of solutions – aqueous and non-aqueous.....	35
3.3 Fabrication of probes for scanning electrochemical microscopy and scanning ion conductance microscopy	36
3.4 Sample preparation for aqueous and non-aqueous environments.....	38
3.5 SECM setup and initial experimental procedures	40

4	Results and discussion.....	43
4.1	Simultaneous scanning ion conductance and electrochemical microscopy in lithium-ion battery research	43
4.1.1	Introduction	46
4.1.2	Results and discussion.....	48
4.1.3	Conclusion	55
4.1.4	Experimental section	56
4.1.5	Supporting information	60
4.2	Development of an <i>in situ</i> mediator dosing concept for scanning electrochemical microscopy in lithium-ion battery research	67
4.2.1	Introduction	69
4.2.2	Results and discussion.....	71
4.2.3	Conclusion	78
4.2.4	Experimental section	79
4.2.5	Supporting information	84
4.2.6	Unpublished data	87
4.3	Characterisation of as-grown and chemically-mechanically polished boron-doped diamond electrodes by means of feedback mode scanning electrochemical microscopy ..	91
4.3.1	Introduction	92
4.3.2	Results and discussion.....	94
4.3.3	Conclusion	104
4.3.4	Experimental section	105
5	Summary.....	111
6	Zusammenfassung in deutscher Sprache	114
7	Eidesstattliche Erklärung.....	117

List of publications

Peer-reviewed articles

Chem-mechanical polishing influenced morphology, spectral and electrochemical characteristics of boron doped diamond

Zelenský M, Fischer J, Baluchová S, Klimša L, Kopeček J, Vondráček M, Fekete L, Eidenschink J, Matysik F-M, Mandal S, Williams OA, Hromadová M, Mortet V, Schwarzová-Pecková K, Taylor A.

Carbon 203 (2023) 363-376.

Abstract

In this study complex characterization and comparison of as-grown and chemical-mechanical (CM) polished ultra-thin (≤ 500 nm) boron doped diamond (BDD) electrodes with various boron content ($0.58\text{--}4.4 \times 10^{21} \text{ cm}^{-3}$, deposited with B/C 500–8000 ppm) was performed. Atomic force and scanning electron microscopy were used to compare morphological changes and confirm the reduction in roughness down to ≤ 2 nm. High-quality CM polishing enabled electron backscatter diffraction leading to the evaluation of grain size distribution (mean $0.3 \mu\text{m}$) and preferred grain texture, $\{011\}$. X-ray photoelectron spectroscopy confirmed an increase in the B content on the surface of CM polished electrodes as a result of exposure of boron atoms incorporated into the bulk for highly doped BDD₄₀₀₀ and BDD₈₀₀₀ electrodes. Additionally, CM polished BDD electrodes are shown to possess uniform distribution of conductivity as proved by scanning electrochemical microscopy. This was reflected in faster heterogeneous electron transfer kinetics for inner-sphere redox markers ($[\text{Fe}(\text{CN})_6]^{3-/4-}$ and dopamine) and higher values of double layer capacitance in comparison with as-grown electrodes. These changes were more pronounced for low doped electrodes. Finally, the improvement in electrochemical characteristics was demonstrated by superior electroanalytical performance of CM polished BDD electrodes for dopamine detection.

Simultaneous Scanning Ion Conductance and Electrochemical Microscopy in Lithium-Ion Battery Research

Eidenschink J, Matysik F-M

ChemElectroChem 11 (2024) e202300577.

Abstract

Deeper understanding of processes involved in operation of lithium-ion batteries (LIBs) is necessary to further optimize them for future applications. Extensive research was conducted on the formation of a solid electrolyte interphase (SEI) on negative battery electrodes, still leaving several questions unanswered. Scanning probe microscopies (SPMs) enable *in situ* and *operando* investigations and have the potential to explain some phenomena. Scanning electrochemical microscopy (SECM) and scanning ion conductance microscopy (SICM) could be employed in LIB studies. A novel SICM method based on the redox couple ferrocene/ferrocenium is introduced for applications in carbonate solvents widely used in LIBs. Proof of concept measurements were conducted with a micro milled copper circuit board as model substrate. Furthermore, the proposed SICM approach was hyphenated with feedback mode SECM resulting in the simultaneous mapping of morphology and electrochemical activity. A flexible dual-probe arrangement was developed enabling usage of both SPM techniques at the same time, and furthermore, an easy replacement of both individual probes if needed. The setup was applied in the characterisation of commercial graphite electrodes for LIBs before and after conducting a pre-charging protocol. Changes in electrochemical activity and topography of the graphite electrode were resolved in simultaneously generated SECM/SICM recordings.

Stamping Platinum Electrodes – Design, Fabrication, and Characterization

Jedlińska K, Eidenschink J, Matysik F-M, Baś B

Journal of The Electrochemical Society 171 (2024) 077502.

Abstract

This communication introduces a quick and easy method to modify a typical disk electrode's surface geometry. The method involves masking fragments of the flat surface of the working electrode, by applying a specific thin layer of chemically stable insulating material, leaving unvarnished, electrochemically active surface. Desired shapes are achieved by using a properly laserengraved stainless-steel plate and a stamper to transfer the profiled varnish from the steel plate to the surface of the electrode. Three shapes - microdisk, microband, and ring electrodes - were applied to a platinum disk electrode, validated through optical and scanning electrochemical microscopies, and cyclic voltammetry.

Development of an *in situ* Mediator Dosing Concept for Scanning Electrochemical Microscopy in Lithium-Ion Battery Research

Eidenschink J, Matysik F-M

ChemElectroChem 11 (2024) e202400311.

Abstract

In scanning electrochemical microscopy (SECM), the addition of a redox active species plays an essential role. Those deliberately added mediators may alter results in scanning electrochemical microscopy (SECM) studies. In investigations of lithium-ion battery (LIB) materials, especially of the positive electrode, the oxidation potentials of commonly used mediator substances such as ferrocene are located within the operation potential of the electrode. Thus, they possibly interfere with the regular charge/discharge processes. *In situ* studies are therefore in need of approaches reducing or eliminating the use of mediators. Within this publication, a novel mediator dosing (MD) concept is introduced. A capillary was closely positioned at the tip of the scanning probe. By gravity flow, stable flow rates of mediator solution of up to $32.4 \pm 0.6 \mu\text{L h}^{-1}$ were achieved. These low amounts were found to be sufficient to form a ferrocene zone at the probe tip enabling feedback mode SECM measurements with comparable quality to measurements directly in ferrocene solution. Proof of concept experiments were conducted by investigation of a thin-film electrode with a micro-structured surface. Furthermore, the MD concept was applied in imaging experiments of a commercially available LIB graphite electrode.

Conference contributions

Oral presentations

2021 **3rd Cross-Border Seminar on Electroanalytical Chemistry (CBSEC)**, online, 08.-09.04.2021

Investigation of the electrochemical behaviour of cysteine based on capillary electrophoresis-mass spectrometry

2021 **17th International Students Conference “Modern Analytical Chemistry”**, Prague, Czech Republic, 16.-17.09.2021

Investigation of the oxidation behaviour of cysteine by means of electrochemistry hyphenated to capillary electrophoresis and mass spectrometry

2022 **4th Cross-Border Seminar on Electroanalytical Chemistry (CBSEC)**, Prague, Czech Republic, 11.-13.04.2022

Imaging of the surface activity of boron-doped diamond samples by means of scanning electrochemical microscopy

2022 **Electrochemistry 2022**, Berlin, Germany, 27.-30.09.2022

Investigation of boron-doped diamond samples with the feedback mode of scanning electrochemical microscopy

2023 **5th Cross-Border Seminar on Electroanalytical Chemistry (CBSEC)**, Waldmünchen, Germany, 04.-06.04.2023

Development of a mediator dosing concept for lithium-ion battery studies by means of scanning electrochemical microscopy

2024 **6th Cross-Border Seminar on Electroanalytical Chemistry (CBSEC)**, Prague, Czech Republic, 26.-27.03.2024

Scanning ion conductance microscopy in lithium-ion battery research and its hyphenation to scanning electrochemical microscopy

Declaration of collaboration

Most of the practical and theoretical work of this thesis was performed solely by the author. Parts of the obtained results were achieved in cooperation with other researchers. In accordance with § 8 Abs. 1 Satz 2 Punkt 7 of the Ordnung zum Erwerb des akademischen Grades eines Doktors der Naturwissenschaften (Dr. rer. nat.) an der Universität Regensburg vom 18. Juni 2009 (Änderungssatzung vom 18. Dezember 2023), the nature of these collaborations is described in this section.

4.1. Simultaneous scanning ion conductance and electrochemical microscopy in lithium-ion battery research

All experimental works, data evaluation, and writing were done by the author. Graphical abstract and front cover were designed together with Martin Koall and Dr. Thomas Herl. The project was supervised by Prof. Dr. Frank-Michael Matysik.

4.2. Development of an *in situ* mediator dosing concept for scanning electrochemical microscopy in lithium-ion battery research

Conceptual design, experimental works, data evaluation, and writing were performed solely by the author. Prof. Dr. Frank-Michael Matysik supervised the project.

4.3. Characterisation of as-grown and chemically-mechanically polished boron-doped diamond electrodes by means of feedback mode scanning electrochemical microscopy

BDD electrodes were provided by Michal Zelenský. Parts of the SECM measurements and sample preparation were performed in collaboration with Michal Zelenský. Parts of the SECM measurements, SECM data evaluation, and writing of the SECM section of the publication were done by the author. The corresponding section within this thesis was written solely by the author. The project was supervised by Dr. Karolina Schwarzová-Pecková and Prof. Dr. Frank-Michael Matysik.

List of abbreviations

Abbreviations used within this thesis are summarized in this section. They are listed in alphabetic order with their respective full name and unit in Table I.

Table I. Alphabetic list of abbreviations.

Abbreviation	Full name	Unit
A	Area	[m ²]
AC	Alternating current	
AE	Auxiliary or counter electrode	
AFM	Atomic force microscopy	
ag	As-grown	
a _i	Activity of species i	
BDD	Boron-doped diamond	
C	Capacitance	[F]
CFIA	Capillary flow injection analysis	
c _i	Concentration of species i	[mol L ⁻¹]
cmp	Chemically-mechanically polishing	
CV	Cyclic voltammetry Cyclic voltammogram	
CVD	Chemical vapour deposition	
D	Diffusion coefficient	[cm ² s ⁻¹]
d	Tip-to-substrate distance	[m]
DC	Direct current	
DMC	Dimethyl carbonate	
E	Potential	[V]
E ⁰	Standard electrode potential	[V]
E ^{0'}	Formal standard electrode potential	[V]
e ⁻	Electron	

EBDS	Electron backscatter diffraction	
EC	Ethylene carbonate	
EIS	Electrochemical impedance spectroscopy	
EMC	Ethyl methyl carbonate	
F	Faraday constant	$[9.6485 \times 10^4 \text{ C mol}^{-1}]$
FB	Feedback	
Fc	Ferrocene	
FcMeOH	Ferrocene methanol	
HET	Heterogeneous electron transfer	
I, i	Current	[A]
ID	Inner diameter	[m]
I_T	Normalised tip current	
J	Flux	$[\text{mol cm}^{-2} \text{ s}^{-1}]$
k_0	Heterogeneous electron transfer rate constant	$[\text{cm s}^{-1}]$
L	Normalised tip-to-substrate distance	
l	Length	[m]
LIB	Lithium-ion battery	
LSV	Linear sweep voltammetry Linear sweep voltammogram	
MD	Mediator dosing	
n	Number of exchanged electrons	
O	Oxidized species	
OD	Outer diameter	[m]
PAC	Probe approach curve	
PEEK	Polyether ether ketone	
PSC	Probe scan curve	
PTFE	Polytetrafluoroethylene	
PVC	Polyvinyl chloride	

R	Electrical resistance Ideal gas constant Reduced species	[Ω] [8.3145 J mol ⁻¹ K ⁻¹]
r	Radius	[m]
RC	Redox competition	
RE	Reference electrode	
SECM	Scanning electrochemical microscopy	
SEI	Solid-electrolyte interphase	
SEM	Scanning electron microscopy	
SG/TC	Substrate generation/tip collection	
SICM	Scanning ion conductance microscopy	
SPM	Scanning probe microscopy	
T	Temperature	[K]
t	Time	[s]
TG/SC	Tip generation/substrate collection	
U	Potential	[V]
UME	Ultramicroelectrode	
V	Volume	[m ³]
WE	Working electrode	
XPS	X-ray photoelectron spectroscopy	
z	Number of transferred electrons	
κ	Dimensionless rate constant	
κ_e	Conductivity	[S m ⁻¹]
Φ	Electric field potential	[V]
v	Flow velocity	[m s ⁻¹]

1 Introduction

Introduced in 1989 by the working groups of Bard [1] and Engstrom, [2] scanning electrochemical microscopy (SECM) is a representative of the family of scanning probe microscopy (SPM) techniques. Since then, it became a powerful analytical tool in a wide variety of applications. Usually, in the operation of a SECM setup, a micro- or nanometre sized electrode is utilized as probe. Application of a suitable potential leads to the conversion of an added redox-active species, and the recorded current delivers localized information regarding the electrochemical activity and morphology of a substrate of interest. [3]

The technique is routinely applied in studies of biological samples, [4-7] corrosion research, [8-10] probing of kinetics, [11-14] and many more. [15-17] Furthermore, since its introduction SECM was continuously improved by the development of new operational modes, [18-20] instrumental advances, [21-24] and the hyphenation to complementary techniques like atomic force microscopy (AFM) [25] or scanning ion conductance microscopy (SICM). [26,27] The latter was first described by Hansma *et al.* [28] and it is highly suitable for the combination with the SECM. Both techniques are non-contact, enabling studies of sensitive substrates, and they deliver complementary information, i. e. information on the electrochemical activity generated from the SECM and morphological information obtained from the SICM technique. Furthermore, via the distance-dependency of the SICM signal, the hyphenation enables SECM measurements under constant-distance conditions.

Recently, studies of energy storage devices such as lithium-ion batteries (LIBs) became a hot topic in SPM research. The highly reactive nature of LIB materials demands working under inert conditions and is therefore quite challenging. Nevertheless, enabling deeper understanding of battery chemistry as well as the ability to study electrode materials under *in situ* [29] and even *in operando* [30,31] conditions drove the recent progress in SECM and other SPM techniques. SECM was employed in probing the physical swelling of graphite composite electrodes, [32] formation of the solid-electrolyte interphase (SEI) on various electrode materials, [33-36] characterisation of positive electrode materials, [37,38] or investigations of the Li^+ ion flux. [39,40] Stand-alone SICM in LIB research is still underrepresented with only few applications. [41-43] The complexity of battery chemistry calls for further development of existing techniques in order to fully understand processes involved in the operation of LIBs. The limitation of SECM, i. e. difficult separation of the influence of topography and electrochemical activity on the signal, can be overcome by coupling to complementary techniques. The hyphenation of AFM-SECM was already displayed in the context of LIB research, [44] while the coupling of SECM and SICM was not yet achieved in LIB media.

The objective of the presented thesis can be summarized in four bullet points:

- Modification of the existing SECM setup for experiments under inert conditions
- Development of a straightforward SICM method for application in LIB research and the hyphenation to SECM
- Development of a novel mediator dosing concept for measuring in SECM feedback mode with reduced mediator introduction in the context of LIBs
- Characterisation of novel electrode materials and concepts in cooperation with international research partners

References

- [1] A. J. Bard, F. R. F. Fan, J. Kwak, O. Lev, *Anal. Chem.* 1989, 61, 132.
- [2] R. C. Engstrom, C. M. Pharr, *Anal. Chem.* 1989, 61, 1099A-1104A.
- [3] D. Polcari, P. Dauphin-Ducharme, J. Mauzeroll, *Chem. Rev.* 2016, 116, 13234.
- [4] S. Bergner, J. Wegener, F.-M. Matysik, *Anal. Chem.* 2011, 83, 169.
- [5] D. Zhan, X. Li, A. B. Nepomnyashchii, M. A. Alpuche-Aviles, F.-R. F. Fan, A. J. Bard, *J. Electroanal. Chem.* 2013, 688, 61.
- [6] T. Raith, A. Kröninger, M. J. Mickert, H. H. Gorris, F.-M. Matysik, *Talanta* 2020, 214, 120844.
- [7] I. Morkvenaite-Vilkonciene, A. Kisieliute, W. Nogala, A. Popov, B. Brasiunas, M. Kamarauskas, A. Ramanavicius, S. Linfield, A. Ramanaviciene, *Electrochim. Acta* 2023, 463, 142790.
- [8] J. Izquierdo, M. B. González-Marrero, M. Bozorg, B. M. Fernández-Pérez, H. C. Vasconcelos, J. J. Santana, R. M. Souto, *Electrochim. Acta* 2016, 203, 366.
- [9] M. C. L. de Oliveira, R. M. P. Da Silva, R. M. Souto, R. A. Antunes, *J. Magnes. Alloys* 2022, 10, 2997.
- [10] J. Izquierdo, A. Eifert, C. Kranz, R. M. Souto, *Electrochim. Acta* 2017, 247, 588.
- [11] H. V. Patten, K. E. Meadows, L. A. Hutton, J. G. Iacobini, D. Battistel, K. McKelvey, A. W. Colburn, M. E. Newton, J. V. Macpherson, P. R. Unwin, *Angew. Chem. Int. Ed.* 2012, 51, 7002.
- [12] Z. Liang, H. S. Ahn, A. J. Bard, *J. Am. Chem. Soc.* 2017, 139, 4854.
- [13] Q.-H. Zhang, X.-R. Li, P. Liu, X.-Z. Meng, L.-K. Wu, Z.-Z. Luo, F.-H. Cao, *Int. J. Hydrogen Energ.* 2021, 46, 39665.
- [14] Q. Huang, P. Li, M. Wang, Y. Shen, *J. Electroanal. Chem.* 2024, 118061.
- [15] A. Asserghine, M. Medvidović-Kosanović, L. Nagy, R. M. Souto, G. Nagy, *Sensor. Actuat. B-Chem.* 2020, 320, 128339.
- [16] S. Wert, H. Iken, M. J. Schöning, F.-M. Matysik, *Electroanal.* 2021, 33, 1143.
- [17] S. Wert, C. Iffelsberger, K. A. Novčić, F.-M. Matysik, M. Pumera, *Appl. Mater. Today* 2022, 26, 101309.
- [18] K. Eckhard, X. Chen, F. Turcu, W. Schuhmann, *Phys. Chem. Chem. Phys.* 2006, 8, 5359.
- [19] C.-L. Lin, J. Rodríguez-López, A. J. Bard, *Anal. Chem.* 2009, 81, 8868.

- [20] Y. Wang, K. Kececi, J. Velmurugan, M. V. Mirkin, *Chem. Sci.* 2013, 4, 3606.
- [21] C. Iffelsberger, P. Vatsyayan, F.-M. Matysik, *Anal. Chem.* 2017, 89, 1658.
- [22] A. Hengstenberg, C. Kranz, W. Schuhmann, *Chem. Eur. J.* 2000, 6, 1547.
- [23] Z. J. Barton, J. Rodríguez-López, *Anal. Chem.* 2017, 89, 2708.
- [24] A. Boika, Z. Zhao, *Electrochem. Commun.* 2016, 68, 36.
- [25] C. Kranz, G. Friedbacher, B. Mizaikoff, A. Lugstein, J. Smoliner, E. Bertagnolli, *Anal. Chem.* 2001, 73, 2491.
- [26] Y. Takahashi, A. I. Shevchuk, P. Novak, Y. Murakami, H. Shiku, Y. E. Korchev, T. Matsue, *J. Am. Chem. Soc.* 2010, 132, 10118.
- [27] S. Wert, S. Baluchová, K. Schwarzová-Pecková, S. Sedláková, A. Taylor, F.-M. Matysik, *Monatsh. Chem.* 2020, 151, 1249.
- [28] P. K. Hansma, B. Drake, O. Marti, S. A. Gould, C. B. Prater, *Science* 1989, 243, 641.
- [29] X. Zeng, D. Liu, S. Wang, S. Liu, X. Cai, L. Zhang, R. Zhao, B. Li, F. Kang, *ACS Appl. Mater. Inter.* 2020, 12, 37047.
- [30] M. R. Krumov, S. Lang, L. Johnson, H. D. Abruña, *ACS Appl. Mater. Inter.* 2023, 15, 47692.
- [31] G. Zampardi, F. La Mantia, W. Schuhmann, *Electrochem. Commun.* 2015, 58, 1.
- [32] H. Bülter, F. Peters, J. Schwenzel, G. Wittstock, *J. Electrochem. Soc.* 2016, 163, A27-A34.
- [33] H. Bülter, F. Peters, J. Schwenzel, G. Wittstock, *Angew. Chem. Int. Ed.* 2014, 53, 10531.
- [34] E. Ventosa, P. Wilde, A.-H. Zinn, M. Trautmann, A. Ludwig, W. Schuhmann, *Chem. Commun.* 2016, 52, 6825.
- [35] E. Ventosa, E. Madej, G. Zampardi, B. Mei, P. Weide, H. Antoni, F. La Mantia, M. Muhler, W. Schuhmann, *ACS Appl. Mater. Inter.* 2017, 9, 3123.
- [36] B. Krueger, L. Balboa, J. F. Dohmann, M. Winter, P. Bieker, G. Wittstock, *ChemElectroChem* 2020, 7, 3590.
- [37] G. Zampardi, R. Trocoli, W. Schuhmann, F. La Mantia, *Phys. Chem. Chem. Phys.* 2017, 19, 28381.
- [38] A. Mishra, D. Sarbapalli, M. S. Hossain, Z. T. Gossage, Z. Li, A. Urban, J. Rodríguez-López, *J. Electrochem. Soc.* 2022, 169, 86501.
- [39] Z. T. Gossage, J. Hui, Y. Zeng, H. Flores-Zuleta, J. Rodríguez-López, *Chem. Sci.* 2019, 10, 10749.

- [40] Y. Zeng, Z. T. Gossage, D. Sarbapalli, J. Hui, J. Rodríguez-López, *ChemElectroChem* 2022, 9.
- [41] A. L. Lipson, R. S. Ginder, M. C. Hersam, *Adv. Mater.* 2011, 23, 5613.
- [42] A. L. Lipson, K. Puntambekar, D. J. Comstock, X. Meng, M. L. Geier, J. W. Elam, M. C. Hersam, *Chem. Mater.* 2014, 26, 935.
- [43] Y. Takahashi, D. Takamatsu, Y. Korchev, T. Fukuma, *JACS. Au* 2023, 3, 1089.
- [44] G. Zampardi, S. Klink, V. Kuznetsov, T. Erichsen, A. Maljusch, F. La Mantia, W. Schuhmann, E. Ventosa, *ChemElectroChem* 2015, 2, 1607.

2 Theoretical background

2.1 Electrochemistry

2.1.1 Fundamentals

Electrochemistry is a discipline in chemistry studying conversion processes involving electron transfer at the electrolyte/electrode interface. Equation 2.1 shows a typical reaction in the electrochemical investigation of an active species, with n as the number of exchanged electrons, and O and R being the oxidized or reduced form of the species, respectively. [1,2]



In a potential region where the electron transfer is thermodynamically favourable the reaction takes place. The electrochemical potential E of such a reaction is described by the Nernst equation (equation 2.2) taking into account the standard electrode potential E^0 and the activities a_O and a_R of the active species. R is the ideal gas constant ($8.314 \text{ J mol}^{-1} \text{ K}^{-1}$), T is the temperature in K, z resembles the number of transferred electrons, and F is the Faraday constant ($9.6485 \times 10^4 \text{ C mol}^{-1}$). [3,4]

$$E = E^0 + \frac{RT}{zF} \ln \frac{a_O}{a_R} \quad (2.2)$$

Since activities are difficult to access, often a modified version of the Nernst equation, as shown in equation 2.3, is applied. The formal electrode potential $E^{0'}$ incorporates the activity coefficients of O and R as well as the standard electrode potential. Therefore, the concentrations of O and R (c_O and c_R) can be used in the logarithmic term. [5]

$$E = E^{0'} + \frac{RT}{zF} \ln \frac{c_O}{c_R} \quad (2.3)$$

Electrochemical investigations typically are conducted in a three-electrode arrangement as illustrated in Figure 2.1. [2] All electrodes are connected to a potentiostat in order to control the applied potential and record the current signal. The reaction of interest occurs at the working electrode (WE), which is potential biased to a reference electrode (RE). The resulting current flows between the WE and a third electrode, the counter or auxiliary electrode (AE). The three

electrodes are immersed in an electrolyte solution containing the active species and often a supporting electrolyte. Ideally, the measurement of the potential against the RE should be currentless, otherwise, the effective potential of the working electrode (E_{eff}) differs from the applied potential according to equation 2.4 with the resistance of the electrolyte solution ($R_{solution}$). Furthermore, reactions at the RE could alter its potential. To minimize the current towards the RE, it is typically connected to a high ohmic resistance. [1,5]

$$E_{eff} = E - I_{RE} \cdot R_{solution} \quad (2.4)$$

The application of a potential to the WE leads to a current flowing between WE and AE. Two different kinds of processes contribute to this current, namely faradaic, and non-faradaic processes. The resulting current can, therefore, be described as the sum of faradaic (I_F) and non-faradaic or capacitive current (I_C) as shown in equation 2.5.

$$I = I_F + I_C \quad (2.5)$$

Non-faradaic currents originate from the charging of an electrical double layer, which is formed at the electrode upon application of a potential. There is no conversion of the active species involved. This process can be described as the charging of a capacitor. Therefore, the time-dependent current I_C is calculated according to equation 2.6 with the double-layer capacitance C_{dl} . [1,5]

$$I_C = \frac{E_{eff}}{R_{solution}} \cdot \exp\left(-\frac{t}{R_{solution}C_{dl}}\right) \quad (2.6)$$

The faradaic current is the current generated from the electrochemical conversion of the active species at the electrolyte/electrode interface. It follows Faraday's law and therefore, current and the amount of converted species are directly proportional. Since analytical information is delivered in the faradaic current, a high ratio of the currents I_F/I_C is desirable.

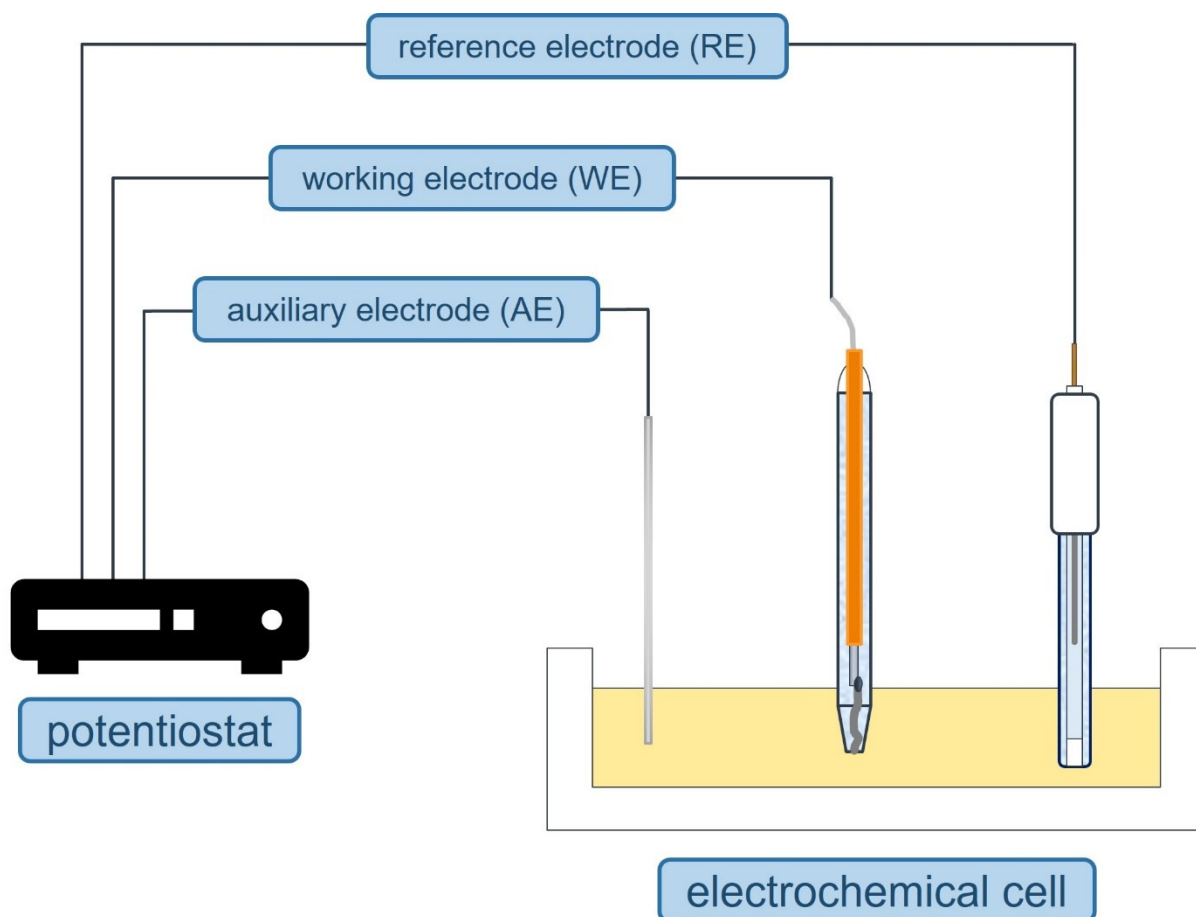


Figure 2.1. Illustration of the essential components of an instrumental setup utilized in electrochemical experiments. It consists of a working electrode, an auxiliary electrode, and a reference electrode immersed in an electrolyte solution and connected to a potentiostat.

2.1.2 Mass transfer

Mass transfer in a solution can be comprised of up to three individual factors, diffusion, migration, and convection. Diffusion describes the movement of a species because of a gradient in chemical potential. Migration represents the movement of charged particles in an electrical field. Convection accounts for the movement of a species in solution resulting from density gradients or by stirring. The Nernst-Planck equation (equation 2.7) describes the unidirectional flux J of a species i in a solution. It contains three terms accounting for the individual influence of the three mass transfer contributions. The first term represents the flux due to diffusion. It is directly proportional to the concentration gradient of species i . The second term describes the influence of migration on the flux. Convection affecting the flux of i is represented by the third term. [2,5]

$$J_i(x) = - \underbrace{D_i \frac{\partial c_i(x)}{\partial x}}_{\text{diffusion}} - \underbrace{\frac{z_i F}{RT} D_i c_i \frac{\partial \phi(x)}{\partial x}}_{\text{migration}} + \underbrace{c_i v(x)}_{\text{convection}} \quad (2.7)$$

In this equation, $J_i(x)$ represents the flux of species i in direction x , D_i is the diffusion coefficient of i , $dc_i(x)/dx$ is the concentration gradient of i at distance x , $d\phi(x)/dx$ describes the potential gradient, z_i is the charge of i , c_i is the concentration of species i , and $v(x)$ represents the velocity of a volume element in solution moving along the x -axis.

Depending on the experimental parameters, one or more of the contributing factors can be neglected. Measuring in quiescent solution results in no convection in the solution, i. e. the convection term is eliminated. Addition of a supporting electrolyte which is inert under the experimental conditions and is added in much higher concentration than the studied species suppresses migrative effects on the active species.

Therefore, if the contributions of migration and convection are suppressed, the mass transfer of species i is only dependent on the diffusion. In this case, equation 2.8, also known as Fick's first law, describes the flux of species i . It is directly proportional to the concentration gradient. [1,3]

$$-J_i(x) = D_i \frac{\partial c_i(x)}{\partial x} \quad (2.8)$$

Accounting for the temporal change of the concentration of i in relation to its flux, Fick's second law is obtained. Equation 2.9 represents the case of unidirectional diffusion in x -direction. [1,3]

$$\frac{\partial c_i(x,t)}{\partial t} = D_i \left(\frac{\partial^2 c_i(x,t)}{\partial x^2} \right) \quad (2.9)$$

If more than one dimension needs to be considered, equation 2.10 is applied. It represents the general form of Fick's second law with the Laplacian operator ∇^2 which takes into account the geometry of the used electrode. [3,5]

$$\frac{\partial c_i}{\partial t} = D_i \cdot \nabla^2 c_i \quad (2.10)$$

Equation 2.9 describes purely linear diffusion. It is valid for planar macro electrodes surrounded by an insulating layer, since in this case the radial diffusion taking place only at the electrode's borders is negligible. Reducing the electrode dimensions increases the influence of radial diffusion until it can't be neglected anymore. The extreme is reached in the case of

ultramicroelectrodes (UMEs), where the observed diffusion is mainly hemispherical. Diffusion profiles for both cases are schematically depicted in Figure 2.2. The hemispherical diffusion profile leads to the possibility of obtaining constant current signals with UMEs as discussed in more detail in the following section. [3]

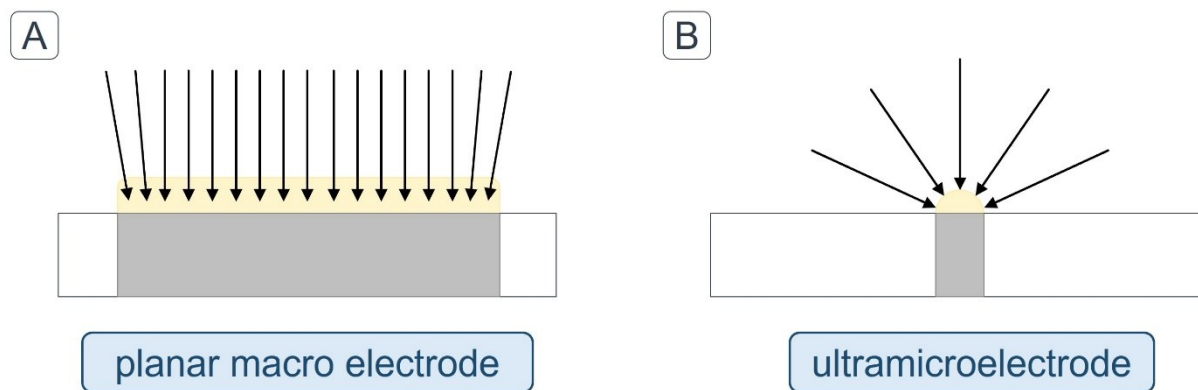


Figure 2.2. Different types of diffusion. A) Mostly planar diffusion towards the surface of a planar macro electrode. B) Radial diffusion towards an ultramicroelectrode. Adapted from [3].

2.1.3 Behaviour of ultramicroelectrodes in comparison to macro electrodes

Solving Fick's second law for a planar macro electrode results in equation 2.11, also known as the Cottrell equation, with A as the active area of the electrode. It describes the temporal change of the recorded current $i(t)$ for a diffusion-limited conversion of the active species. [1,4]

$$i(t) = \frac{nFAD_i^{1/2}c_i}{\pi^{1/2}t^{1/2}} \quad (2.11)$$

So-called UMEs possess certain advantages for the usage in electrochemical investigations. An UME is defined as an electrode with at least one dimension smaller than 25 μm . [6] In this section, their electrochemical behaviour is discussed in comparison to conventional macro electrodes. UMEs exhibit higher current densities than macro electrodes, however, in a non-uniform manner since the current density is higher at the electrode's border and lower in the centre. Typically, currents in the nano- or picoampere region are obtained with UMEs. Due to the low currents, the ohmic drop can be neglected. [4,6,12]

Fick's second law for a disk-shaped UME is given in equation 2.12, with r and z as the radial or linear distance from the electrode centre, respectively. [4]

$$\frac{\partial c_i(r,z,t)}{\partial t} = D_i \left(\frac{\partial^2 c_i}{\partial r^2} + \frac{1}{r} \frac{\partial c_i}{\partial r} + \frac{\partial^2 c_i}{\partial z^2} \right) \quad (2.12)$$

The solution of this equation is not trivial. However, it contains a time-independent component leading to the most beneficial property of an UME, a constant current signal in the case of a diffusion-limited reaction. Therefore, depending on the UME dimensions a stationary diffusion-limited current is reached after a certain amount of time. For the case of a disk-shaped UME, this steady-state current i_∞ can be calculated according to equation 2.13 with the radius of the electrode ($r_{\text{electrode}}$) and under the assumption of an infinite thickness of the insulating layer surrounding the electrode. [6,12]

$$i_\infty = 4nFc_iD_i r_{\text{electrode}} \quad (2.13)$$

Voltammetric experiments are a group of techniques often conducted in electrochemical investigations. In the following, two common techniques, chronoamperometry and cyclic voltammetry (CV), are discussed with respect to the current responses of macro- and ultramicroelectrodes as WEs.

In chronoamperometry, a constant potential is applied to the WE at the start of the experiment t_{start} , as shown in Figure 2.3A. The corresponding current-time plots, so-called chronoamperograms, recorded with a macro- and an ultramicroelectrode are illustrated in Figure 2.3B. Initially, high currents are obtained with both types of electrodes originating from the charging of the electrochemical double layer as well as the high concentration of the active species at the electrode surface in the beginning of the experiment. In the case of a macro electrode, the further temporal change of the recorded current is described by the Cottrell equation (equation 2.11, previous section). However, no steady-state current is reached because of the continuous growth of the diffusion layer. In contrast, the usage of an UME results in a steady-state current response after a short period of time. [1,4]

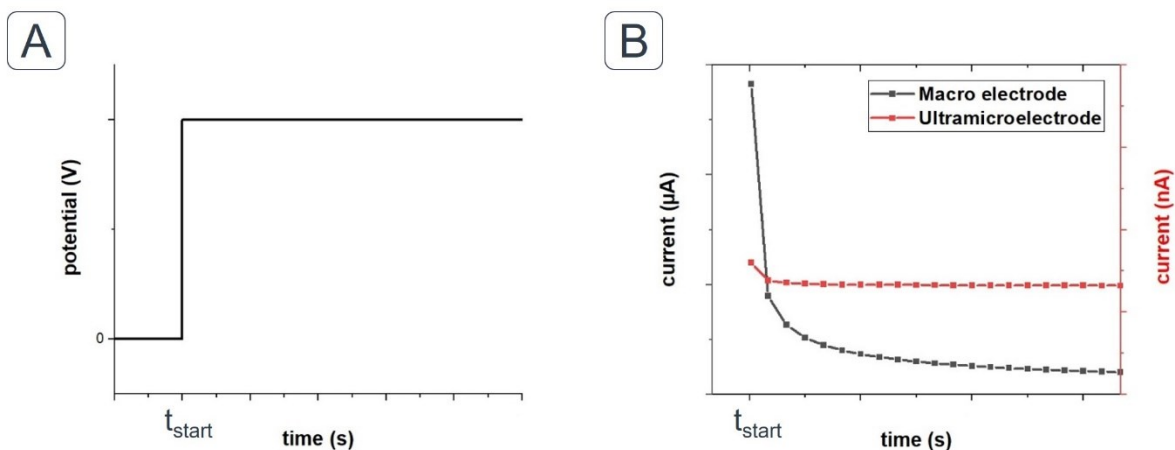


Figure 2.3. Chronoamperometric experiment. A) Application of a constant potential bias to the working electrode at a starting point, t_{start} . B) Chronoamperograms: Current response of a macro electrode and an ultramicroelectrode after a potential is applied. Adapted from [1,4].

In CV, the current response of the WE is recorded while its potential bias is changed periodically as illustrated in Figure 2.4A. Starting from a defined starting potential E_{start} , the potential of the WE is changed with a constant scan rate until a defined reversal potential E_{vertex} is reached. Both potentials are usually chosen based on the redox potential of the studied species. After the forward scan, the potential bias is changed in the opposite direction until the initial potential is reached. The corresponding current responses, cyclic voltammograms (also abbreviated as CV), are shown in Figure 2.4B and C for a one-electron transfer reaction, for example, in the case of ferrocene methanol as active species. With a macro electrode, a characteristic “duck”-shaped CV is obtained with pronounced peaks related to the oxidation or reduction of the active species, respectively. The typical shape is caused by the formation and the growth of the diffusion layer. At the peak potential, every molecule of the active species reaching the electrode surface is directly converted, the diffusion limit of the reaction is reached and the current signal decreases according to the Cottrell equation even with further increase of the potential. In contrast, the usage of an UME results in the recording of a sigmoidal-shaped CV. The shape is explained by the formation of a stable diffusion layer thickness and the reach of steady-state currents for oxidation or reduction, respectively. [1,5]

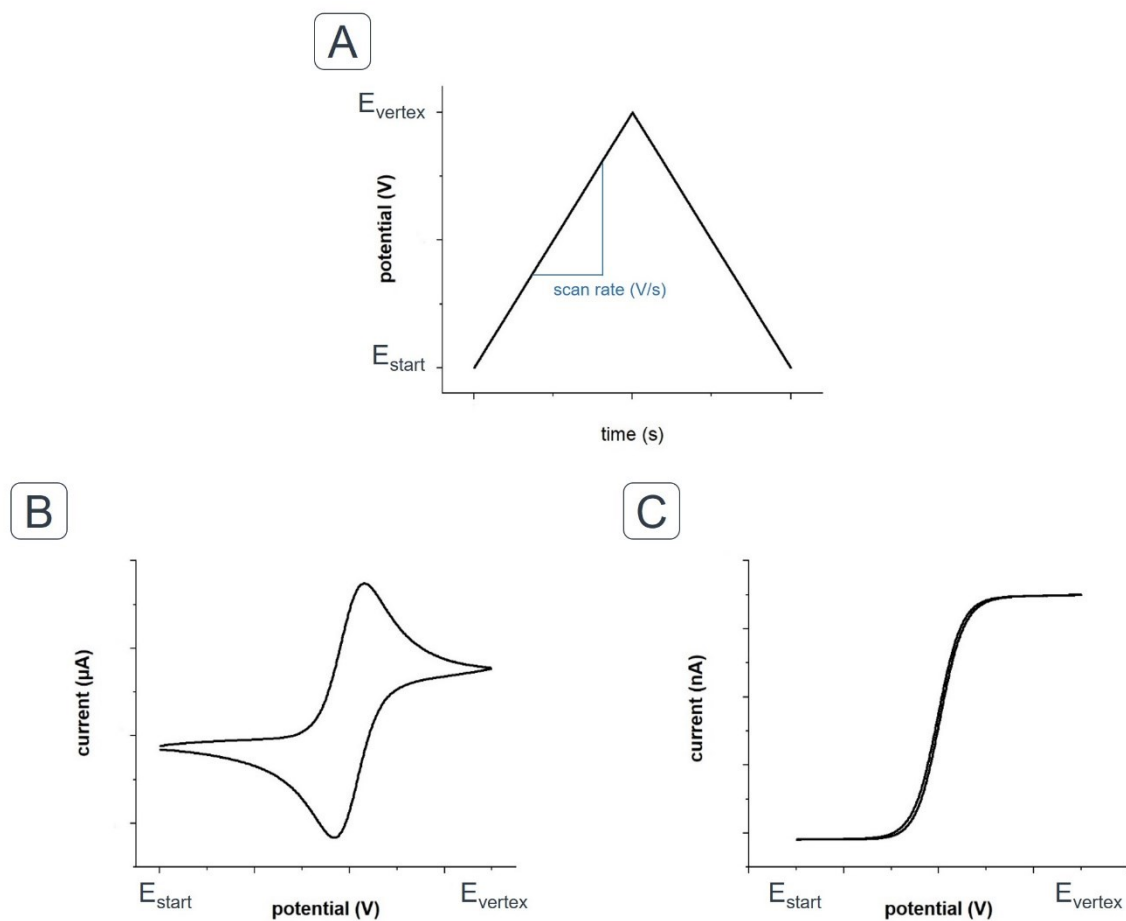


Figure 2.4. Cyclic voltammetry. A) A potential sweep between a starting potential (E_{start}) and a turning potential (E_{vertex}) is conducted at a defined scan rate. B) Corresponding cyclic voltammogram recorded with a macro electrode. C) Typical current response of an ultramicroelectrode. Adapted from [1,5].

2.2 Scanning electrochemical microscopy

Scanning electrochemical microscopy (SECM) is a scanning probe microscopy (SPM) technique which was introduced in the late 1980s by the two research groups of Bard [7] and Engstrom. [8] Since then, it has become a well-established electroanalytical tool with countless applications and target substrates, as discussed in various recent review articles. [9-11] Furthermore, instrumental and experimental developments led to the creation of a variety of powerful operational modes.

The general principle of SECM is scanning an electrode with micro- or nanometre dimensions of the active electrode area across a substrate which is submerged in an electrolyte solution. The current response recorded by the scanned probe delivers localized information about the substrate's topography as well as its electrochemical activity. [12]

In the following section, basic principles regarding the SECM instrumental setup and its operation are presented.

2.2.1 Instrumental setup

The typical components of a SECM setup are illustrated in Figure 2.5. A positioning unit consisting of piezo elements and stepper motors is used to precisely control the position of the SECM probe in three dimensions (x-, y-, and z-axis) with nanometre resolution. To control and record potentials and currents at up to two working electrodes, a low current bipotentiostat is necessary. It is capable of precise measurements of currents in the pA range or even lower. Control of instrumental parameters and probe positioning as well as data acquisition are carried out with a computer. Measurements are conducted in an electrochemical cell with the sample usually mounted at the bottom of the cell. It is filled with a solution containing supporting electrolyte and often an additionally added redox-active species needed for the electrochemical reaction at the probe electrode. In the context of SECM, this species is called mediator, and its selection is based on several aspects, for example, biocompatibility in biological studies or solubility. [6] Hexacyanoferrate(III), ferrocene, or its derivatives are a few examples of frequently used mediators. A three- or four electrode arrangement is used, depending on the choice of the operational mode. It is comprised of a reference electrode, for example an Ag/AgCl/3 M KCl electrode, an auxiliary electrode, and one or two working electrodes, the SECM probe and in some modes the substrate of interest. [12]

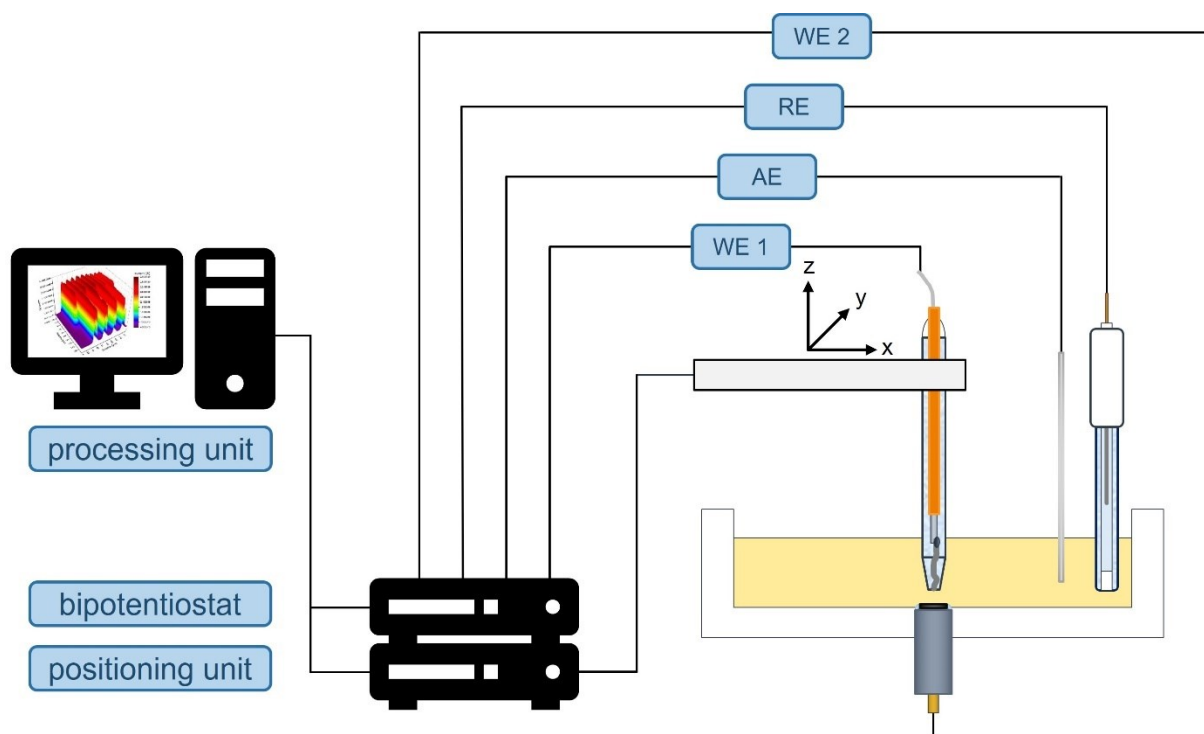


Figure 2.5. Illustration of a scanning electrochemical microscopy setup with the most important components. It consists of an electrochemical cell operated usually in a three- or four-electrode arrangement, a bipotentiostat, a positioning unit, and a processing unit. The cell is filled with electrolyte solution, often containing a redox-active species needed for the generation of current signal. Adapted from [4,12].

2.2.2 Types of SECM probes and their characteristics

The probably most important part dictating the performance of the SECM setup is the employed probe. The achievable resolution strongly depends on the size of the active electrode area, smaller dimensions result in more finely resolved details. Over the years, many electrode materials such as carbon, [13] gold, [14] or platinum [15] and different geometries, for example, ring [16] or disk-shaped [17] electrodes were successfully used in SECM studies. Furthermore, not only amperometric but also potentiometric probes were introduced for the selective detection of ions, for example, Li^+ [18] or Zn^{2+} . [19] The most frequently used ion-selective SECM probes so far are H^+ -dependent, enabling the localized measurement of the pH.

Nevertheless, a vast majority of SECM experiments are performed with amperometric probes. [6] Within those, the mostly used probes are UMES with a disk-geometry of which a schematic depiction is given in Figure 2.6. They often consist of a micro wire, a glass capillary, and a piece of jumper wire for the electrical connection. Although ready-to-use SECM probes

are commercially available, mostly they are self-produced following published fabrication protocols. [20,21] Briefly, the micro wire is soldered onto the jumper wire. Then, the assembly is inserted into a glass capillary. An insulating layer around the micro wire is achieved by melting the glass tip and thorough polishing results in a disk-shaped UME. Even sub nanometre sized probes are possible, for example, by etching of micro wires or usage of Wollaston wires. One important parameter in the characterisation of a SECM probe is the so-called R_g value. It is a dimensionless value, and it is defined as the ratio of the insulating layer thickness ($r_{insulation}$) and the active electrode dimension ($r_{electrode}$) according to equation 2.14.

$$R_g = \frac{r_{insulation}}{r_{electrode}} \quad (2.14)$$

The steady-state current of a disk-shaped UME is described by equation 2.15, as already discussed in section 2.1.3. However, this equation is only valid for an infinite thickness of the insulating layer surrounding the active electrode area. The resulting tip dimensions are not practical for SECM applications, since bigger tip dimensions result in a heightened risk of crashing the probe into the substrate. Therefore, smaller probe dimensions are preferable. While a decrease of the R_g value decreases the risk of crashes, it also negatively influences the contrast obtainable in a SECM experiment since the mediator diffusion from the sides of the probe is increased. A good compromise is found in the usage of probes with R_g values in the range of 2 to 10. [6]

$$i_{T,\infty} = 4nFc_iD_i r_{electrode} \quad (2.15)$$

Furthermore, with decreasing R_g value, the steady-state current recorded with the UME differs significantly from the current calculated according to equation 2.15. Therefore, a dimensionless compensation factor ($\beta(R_g)$) for this equation was introduced accounting for the discrepancy. It can be calculated for a given R_g value according to equation 2.16. Several calculated compensation factors for typical probe dimensions are summarized in Table 2.1. [22]

$$\beta(R_g) = 1 + \frac{0.23}{(R_g^3 - 0.81)^{0.36}} \quad (2.16)$$

Table 2.1. Exemplary R_g values of SECM probes and resulting compensation factors for equation 2.15. Adapted from [22].

R_g	50	20	10	5	4	3	2	1.5	1.1
$\beta(R_g)$	1.00	1.01	1.02	1.04	1.05	1.07	1.11	1.16	1.29

With the inclusion of the introduced compensation factor, equation 2.17 is obtained. It is valid for disk-shaped electrodes with a finite thickness of the insulation layer.

$$i_{T,\infty}(R_g) = 4nFc_iD_i r_{electrode} \beta(R_g) \quad (2.17)$$

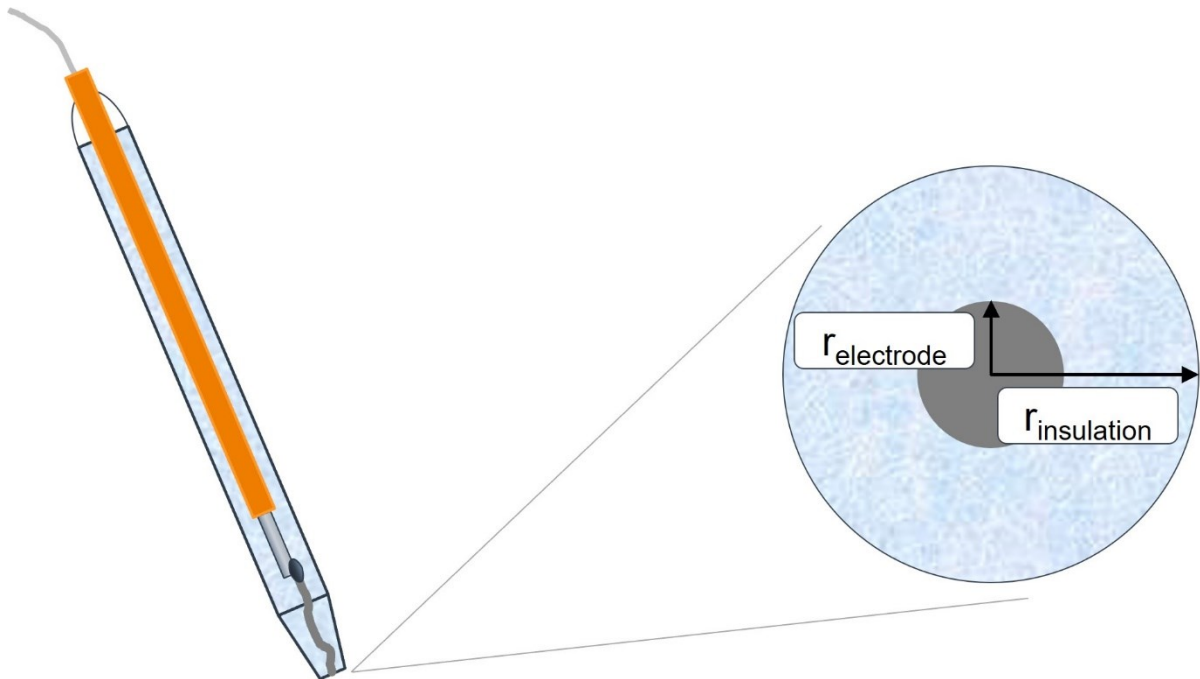


Figure 2.6. Scheme of an ultramicroelectrode usually employed as working electrode in SECM experiments. An important characteristic is the dimensionless R_g value, given as the ratio of insulation ($r_{insulation}$) to electrode radius ($r_{electrode}$).

In order to be able to compare individual measurements and data obtained from different probe sizes, it is common practise to normalise probe travel distances as well as probe currents according to equations 2.18 and 2.19. Both parameters are represented as dimensionless values. The normalised distance (L) is given as a ratio of the actual distance (d) and the radius of the active electrode area ($r_{\text{electrode}}$). Probe currents (i_T) are normalised relative to the steady-state current of the probe in bulk solution ($i_{T,\infty}$). [12]

$$L = \frac{d}{r_{\text{electrode}}} \quad (2.18)$$

$$I_T = \frac{i_T(d)}{i_{T,\infty}} \quad (2.19)$$

2.2.3 Operational modes

A SECM setup can be operated in a variety of different operational modes. Historically, the first introduced modes were the feedback (FB) and generator/collector (G/C) modes. [7,8] Since those early years, other modes and modified versions of existing methods were developed, for example the redox competition mode or potentiometric measurements.

Feedback mode

The FB mode is the most common operational mode of SECM. [6] Typically, a two- or three-electrode assembly is used, with the SECM probe as WE, an AE, and, optionally, a RE. The substrate of interest is unbiased in the FB mode. Furthermore, a mediator is added either in reduced or oxidised form of a quasi-reversible redox couple. A fixed potential bias is applied to the probe which is suitable for the oxidation or reduction of the added mediator substance. In the following discussion, the mediator is presumed in its reduced form, and it is oxidized at the SECM probe. The underlying principles are illustrated in Figure 2.7. Far away from the substrate, i. e. normalised distances of $L > 10$, a steady-state current is measured resulting from the diffusion-limited reaction of the mediator (Figure 2.7A). Closer to the surface, i. e. $L < 10$, the signal is either increasing or decreasing, depending on whether the surface is conductive or insulating. While approaching a conductive surface, a conductor, the current signal increases even above the bulk current signal. The oxidised mediator species can be reduced again at a conductive surface, forming a redox cycle. The locally increased flux of the

reduced mediator species towards the SECM probe results in the increase of the current signal, hereby referred to as positive feedback (Figure 2.7B). In contrary, in the case of a non-conductive and inert substrate, an insulator, approaching the surface of the substrate leads to a decrease of the measured current signal. This is due to an increased influence of the physical blocking by the substrate and the insulating layer of the probe resulting in hindered diffusion of the mediator towards the electrode. This effect is termed negative feedback (Figure 2.7C). Probe approach curves (PACs), a typical SECM measurement where the surface is directly approached (z-direction) with the SECM probe, for both cases, positive and negative FB, are shown in Figure 2.7D.

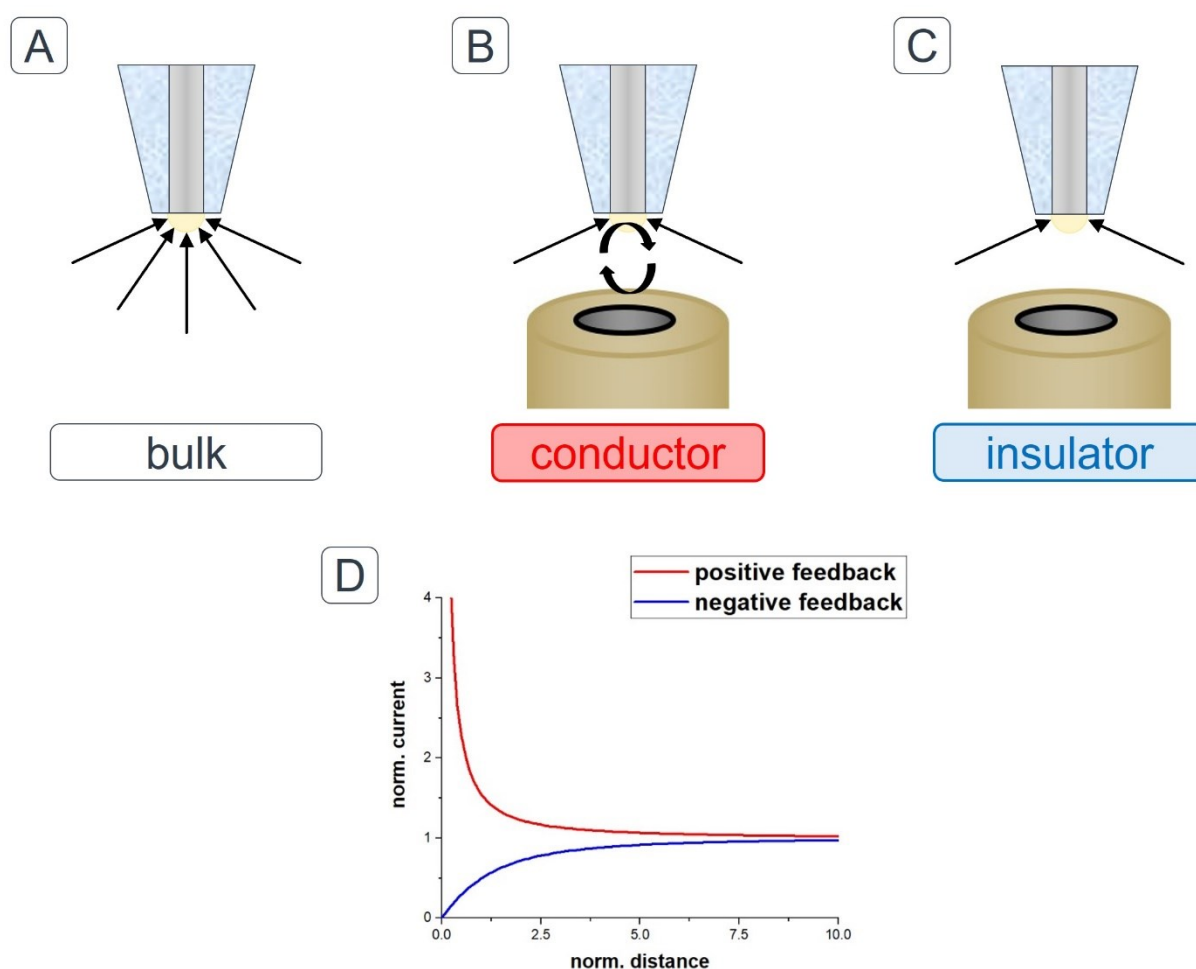


Figure 2.7. Fundamentals of the feedback operational mode of SECM. A) In bulk solution, a steady-state current is recorded with the UME, which is used to normalise current responses in measurements. B) Close to a conductor, the redox mediator is recycled resulting in an increased current response (positive feedback). C) When approaching an insulating surface, the diffusion of the redox mediator is hindered. This leads to a decrease in the recorded current signal (negative feedback). D) Probe approach curves for ideal positive (red curve) and negative (blue curve) feedback. Adapted from [12].

Several theoretical approximations to describe the current response in positive and negative FB were developed over the years. Equation 2.20 was reported by Cornut *et al.* in 2007. [23] It has only two variables, L and R_g, and the model is valid for R_g < 200 with an accuracy of ±0.01.

$$I_{T, \text{ negative FB}} = \frac{i_T}{i_{T,\infty}} \approx \frac{\frac{2.08}{R_g^{0.358}} \left(L - \frac{0.145}{R_g} \right) + 1.585}{\frac{2.08}{R_g^{0.358}} (L + 0.0023R_g) + 1.57 + \frac{\ln R_g}{L} + \frac{2}{\pi R_g} \ln \left(1 + \frac{\pi R_g}{2L} \right)} \quad (2.20)$$

Equation 2.21 for the mathematical modelling of the current signal under positive FB was reported by Amphlett *et al.* in 1998. [24] Since the positive FB is less dependent on the R_g value, the equation is much simpler in comparison to the description of the negative FB. The parameters A, B, C, and D are dependent on the R_g value. Numeric values valid for several R_g values are summarized in Table 2.2. Validity of the equation was reported for the listed parameters in the region of 0.04 < L < 10, with an error of less than 1%.

$$I_{T, \text{ positive FB}} = \frac{i_T}{i_{T,\infty}} \approx A + \left(\frac{B}{L} \right) + C \cdot \exp \left(\frac{D}{L} \right) \quad (2.21)$$

Table 2.2. R_g values and corresponding parameters A, B, C, and D for equation 2.21 as reported by [24,25]

R _g	A	B	C	D
1.1	0.5882629	0.6007009	0.3872741	-0.869822
1.5	0.6368360	0.6677381	0.3581836	-1.496865
2.0	0.6686604	0.6973984	0.3218171	-1.744691
5.1	0.63349	0.67476	0.36509	-1.42897
10	0.7449932	0.7582943	0.2353042	-1.683087

However, the proposed theoretical model for positive FB is only valid for diffusion-controlled regeneration of the mediator at the substrate surface. In the case of a kinetical limitation of the mediator regeneration, equations 2.22 to 2.25 need to be used. They are valid for an R_g of 10 and 0.1 ≤ L ≤ 1.5. [26,27] The first three equations (2.22 – 2.24) describe the individual contributions of negative FB (2.22), positive FB (2.23), and the kinetic component of the mediator regeneration (2.24) to the overall current recorded at the SECM probe. The

parameter κ in equation 2.24 is a dimensionless rate constant defined as $\kappa = k_{0\text{electrode}}/D$ with k_0 as heterogeneous electron transfer rate constant. [27] Equation 2.25 yields an approximation for the current response of the SECM probe approaching the substrate including the beforementioned individual contributions to the tip current. In practical application, the set of equations can be used to determine surface kinetics in a highly localized manner. Each PAC towards an individual position on a heterogeneously active substrate yields a localized k_0 by fitting experimental data with the mathematical approximation as a means measuring the local electrochemical activity of the substrate. PACs towards a surface with kinetically limited mediator regeneration are shown in Figure 2.8 together with the theoretical approximations for negative [23] and positive [24] FB.

$$I_T^{ins}(L) = \frac{i_T}{i_{T,\infty}} \approx \frac{1}{0.40472 + \frac{1.60185}{L} + 0.58819 \exp\left(\frac{-2.37294}{L}\right)} \quad (2.22)$$

$$I_T^{cond}(L) = \frac{i_T}{i_{T,\infty}} \approx 0.72627 + \frac{0.76651}{L} + 0.26015 \exp\left(\frac{-1.41332}{L}\right) \quad (2.23)$$

$$I_S^{kin}(L, k_0) = \frac{0.78377}{L\left(1 + \frac{1}{\kappa L}\right)} + \frac{0.68 + 0.3315 \exp\left(\frac{-1.0672}{L}\right)}{1 + \frac{\left(\frac{11}{\kappa L}\right) + 7.3}{110 - 40L}} \quad (2.24)$$

$$I_T(L) = \frac{i_T}{i_{T,\infty}} = I_T^{ins}(L) + I_S^{kin}(L) \left(1 - \frac{I_T^{ins}(L)}{I_T^{cond}(L)}\right) \quad (2.25)$$

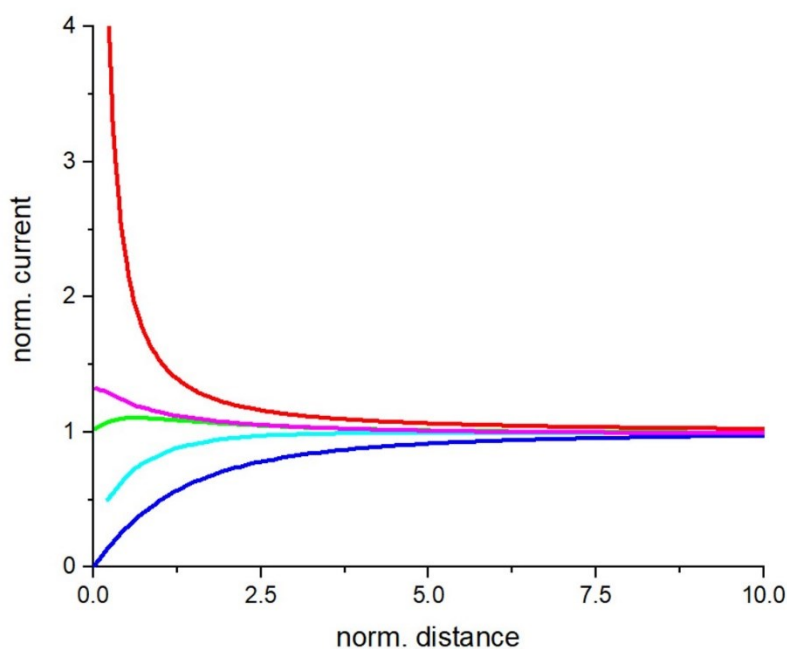


Figure 2.8. Illustrative current-distance curves for diffusion-controlled mediator recycling at the surface (positive feedback, red curve), hindered diffusion (negative feedback, blue curve), and kinetically limited recycling of the mediator (magenta, green, cyan curves). Adapted from [27].

The FB mode of SECM was applied in countless applications and for the characterisation of various kinds of substrates. [28,29] However, the co-dependency of the current signal from the electrochemical activity and topography of the substrate complicates data interpretation with non-ideal substrates, i. e. rough surfaces or heterogeneously active substrates. Therefore, much effort was and is dedicated to that issue. Distance control implemented with an oscillating probe as introduced by the Schumann research group [30] and termed shear force SECM, or the application of an alternating current (AC) to the SECM probe termed AC-SECM [31] are two examples of separating the influence of topography and electrochemical activity on the SECM signal. Furthermore, the hyphenation to complementary techniques, such as atomic force microscopy (AFM) [32] or scanning ion conductance microscopy (SICM), [33] is very promising and remains as a topic for further novel approaches in instrumental development of the SECM technique.

Generator/collector and other modes

Besides from the FB mode, in first SECM publications the so-called generator/collector (G/C) modes were introduced. A four-electrode setup is utilized, with the potentials and currents of the SECM probe and the substrate being controlled and recorded individually as two WEs. Amperometric as well as potentiometric probes were utilized in G/C experiments, since it is more common, the amperometric mode will be described in more detail. The role of the generator can be assigned to the SECM probe or the substrate, resulting in the different designations as either substrate generation/tip collection (SG/TC) or tip generation/substrate collection (TG/SC) mode. For simplification, in the following discussion the mediator species is presumed to exist only in its reduced form in the bulk solution at the start of the experiment. The principle of the SG/TC mode is depicted in Figure 2.9A. By a suitable potential bias, the reduced form of the active redox species is oxidized at the substrate electrode. The oxidized form then diffuses towards the SECM probe (collector), which is placed close to the substrate surface and has a potential applied sufficient for the reduction of the mediator. In contrast to the FB mode, the monitored reaction takes place at the whole active surface of the substrate. Therefore, no steady state is reached since the diffusion layer grows as long as the potential is applied to the substrate. Thus, a drift of the SECM signal is observed complicating data interpretation. Several ideas have been proposed over the years to address this issue. One approach is the so-called hydrodynamic SECM. It was termed and proposed by the Matysik group. [34] The introduction of forced convection by high precision stirring [35] or the usage of electrochemical flow cells [36] results in the formation of a steady diffusion layer at the substrate electrode, increasing the repeatability and the contrast of SG/TC measurements. Typically, the SG/TC mode is applied in corrosion research or enzymatic studies. [12]

In the TG/SC mode, the roles are reversed with the oxidation of the mediator at the SECM probe (generation) and its subsequent detection (collection) at the substrate. The principle is illustrated in Figure 2.9B. Since the area of the substrate is typically much larger than the tip electrode, the achievable collection efficiency in TG/SC mode is often close to 100%. It is, therefore, frequently applied in the monitoring of reaction kinetics. [6]

Another operational mode, which was introduced by the Schumann group in 2006 [37] is the redox competition (RC) mode of SECM. In this experiment, probe and substrate electrode are both biased to a potential at which the same reaction occurs, i. e., at both electrodes, the oxidation of the mediator species takes place. A more active substrate results in a reduced current recorded at the SECM probe. This leads to a significantly reduced background current and thus, an increased sensitivity in probing catalytic activities. Often, a constant potential is applied at the substrate, while the tip is operated with a pulse protocol. [4]

The direct mode of SECM is different from the other operational modes. In a direct mode experiment, the substrate is assigned as WE and the SECM probe as AE, resulting in a current flowing between them. An electric field is formed only in the small space in-between, enabling highly localized modifications of the substrate surface, which is the main application of the direct mode. Possibilities range from the etching of semiconductors to the controlled deposition of metals, enzymes, or even polymers. [6,12]

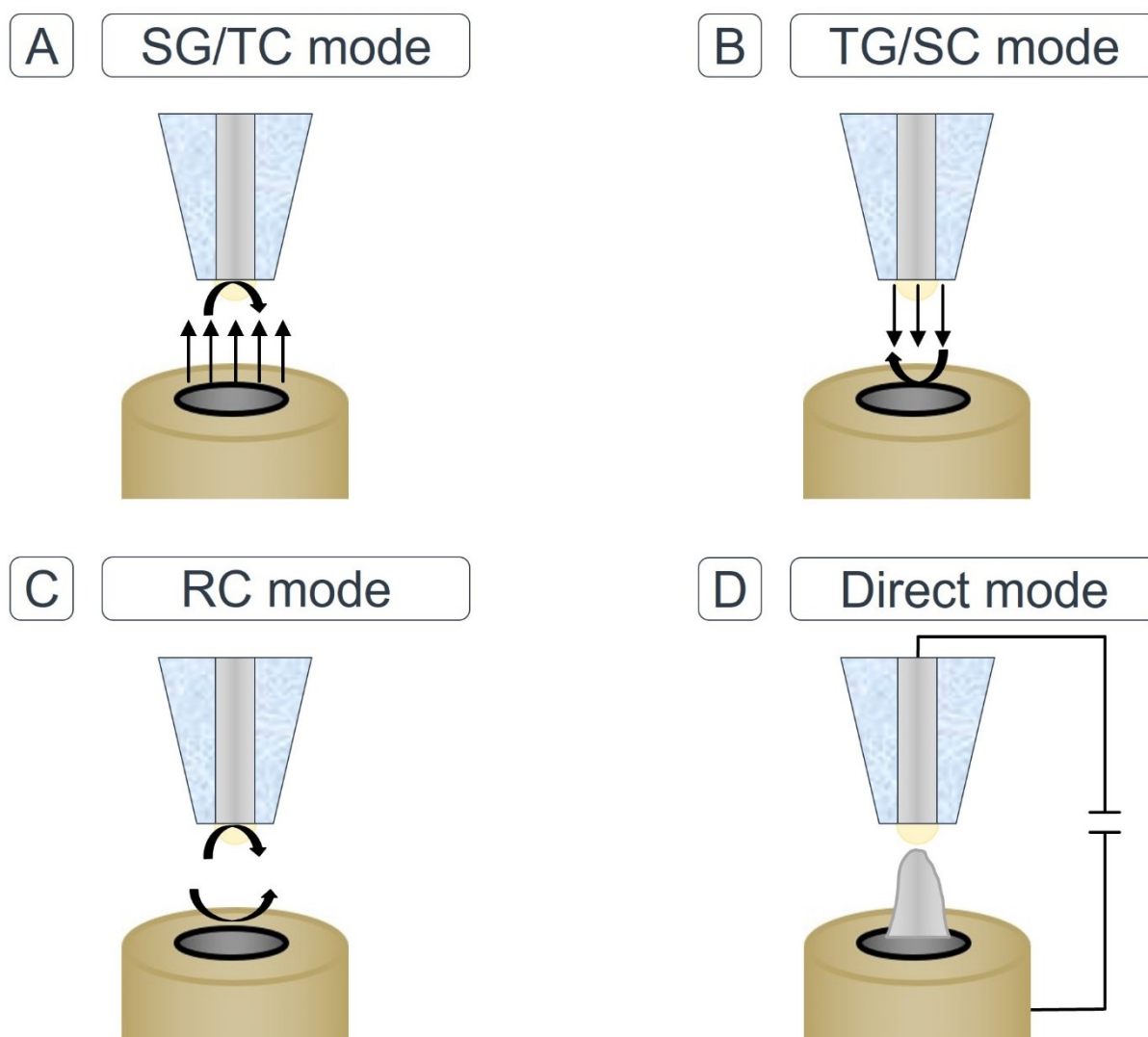


Figure 2.9. Schematics of SECM operational modes other than feedback mode. A) Substrate generation/tip collection mode (SG/TC). An electrochemically active species is generated at the sample surface and detected with the SECM probe at a suitable potential. B) Tip generation/substrate collection mode (TG/SC). The tip is used to generate the active species, which is then recorded with the substrate electrode. C) Redox competition (RC) mode. SECM probe and substrate are both polarized at a potential suitable to convert the electrochemically active substance. D) Direct mode. The substrate is connected as working electrode with the SECM probe as auxiliary. Application of a potential leads to the deposition of for example, a metal layer below the tip electrode. Adapted from [4].

2.3 Scanning ion conductance microscopy

Another member of the SPM family is scanning ion conductance microscopy (SICM). It was developed by Hansma *et al.*, who introduced the technique to the scientific community in 1989. [38] Typically, an electrolyte-filled capillary is scanned across the surface of a substrate immersed in an electrolyte solution. An ionic current measured between an electrode inserted into the pipette and another electrode immersed in the electrochemical cell delivers high-resolution topographical information without physical contact with the substrate. Therefore, the method is well-suited for investigations of delicate substrates, such as biological cells and even subcellular structures like proteins. [39-41]

In the subsequent section further instrumental details, the working principle, and operational modes of SICM are described.

2.3.1 Instrumental setup

The instrumental setup utilized in SICM experiments shares a lot of similarities with a SECM setup, as discussed in section 2.2.1. It is schematically depicted in Figure 2.10.

Typically, it consists of a precise positioning unit, a potentiostat, and a control unit. The main difference to the SECM is the electrode arrangement. In SICM, often two electrodes are used, a bath electrode immersed in the electrolyte solution and a second electrode which is inserted into an electrolyte-filled pipette used as the scanning probe. Chloridized silver wires (Ag/AgCl) are the most common material used as electrodes since they exhibit a stable potential over prolonged measurement times. However, also other materials such as platinum [42] or lithiated tin [43] were applied to specialised investigations. Typically, borosilicate or quartz glass capillaries which are manufactured with a pipette puller are employed with achievable inner tip diameters at the nanometre scale. The measurement cell as well as the pipette are filled with a suitable electrolyte solution. In most studies, potassium chloride solutions in variable concentrations are chosen. Studies were also conducted with physiological buffers, [44] or with asymmetric concentrations, [45] i. e. the concentrations of capillary filling solution and the bath solution are different. Furthermore, multifunctional probes were developed based on either multibarrel pipettes [46] or by implementing a ring electrode layer on the outside of the pipette. [16]

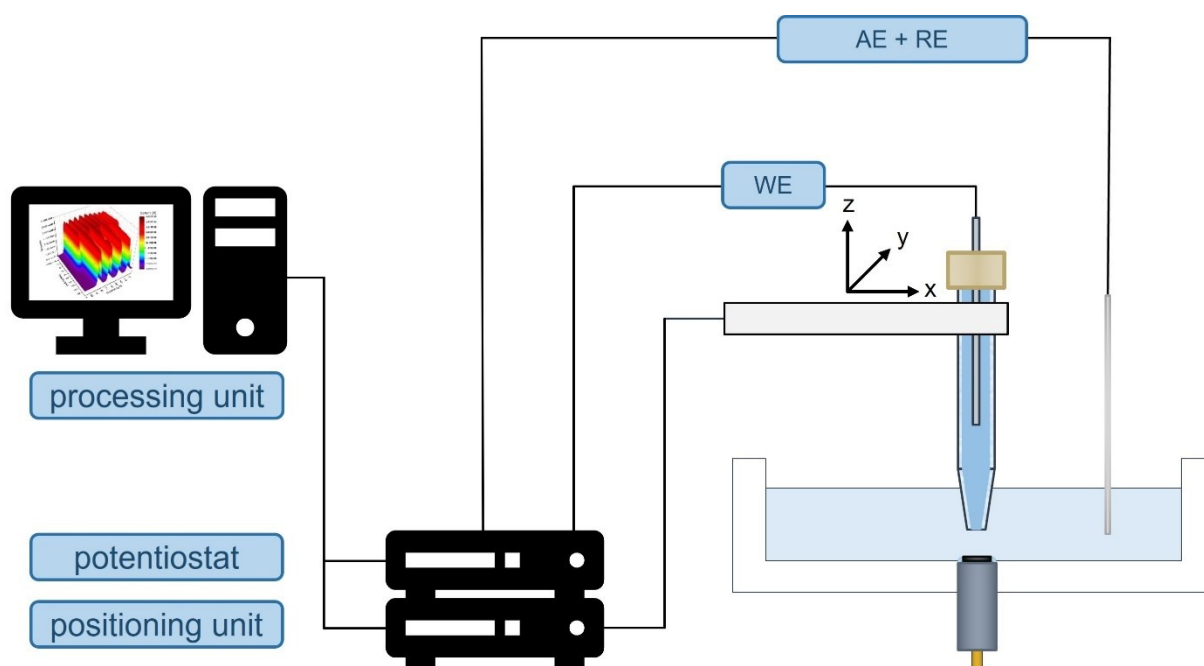


Figure 2.10. Typical components of a scanning ion conductance microscopy setup. The probe is an electrolyte-filled capillary with a quasi-reference electrode inserted, such as an Ag/AgCl wire. Application of a potential bias leads to an ionic current between the probe and a second quasi-reference electrode in the electrolyte solution. Furthermore, a potentiostat, a positioning unit, and a processing unit are needed.

2.3.2 Working principles and operational modes

The underlying principle in SICM is the measurement of an ion current between two quasi-reference electrodes, one positioned in the measurement solution, the bath electrode, and another one inserted into an electrolyte-filled pipette. If the pipette tip is in close proximity to a surface, the ion current is reduced because of an increased access resistance resulting from the blockage of the capillary orifice. The working distance of the method is defined by the tip dimensions. In bulk solution, a steady-state ion current is observable, while current changes typically occur at distances lower than the tip orifice diameter. [41]

Several operational modes of SICM were developed over the years. In the most trivial and originally published one, the direct current (DC) or non-modulated mode, [38] a constant potential bias is applied between the two electrodes as illustrated in Figure 2.11A. When approaching the surface, the ion current is decreases, resulting in current-distance curves as exemplary shown in Figure 2.11B. The changes in the measured ion current deliver direct information about the tip-substrate distance.

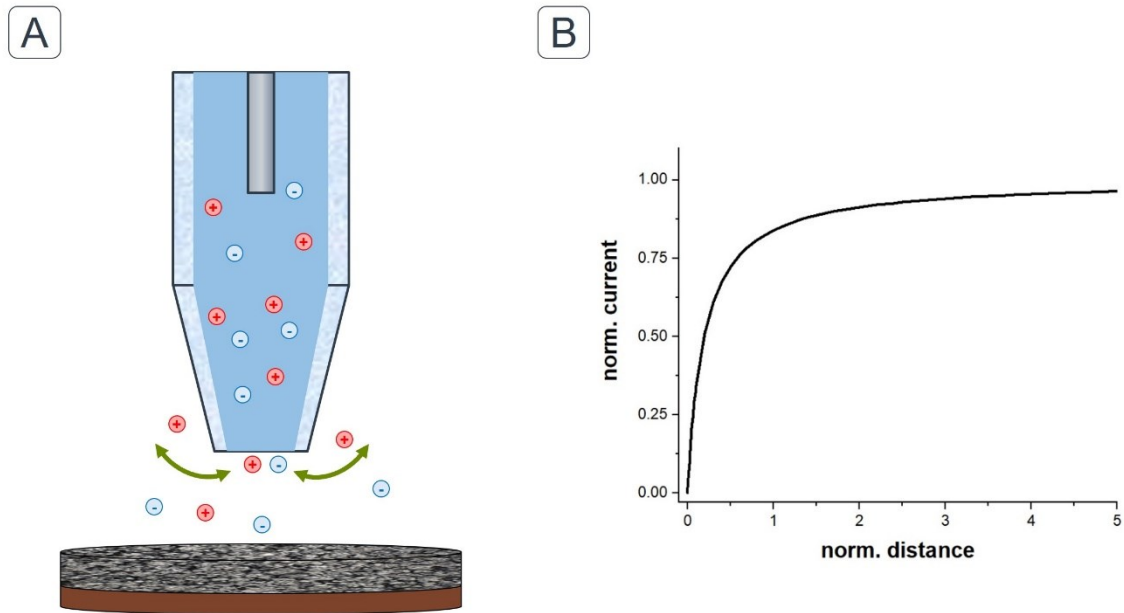


Figure 2.11. Working principle of the non-modulated SICM mode. A) An ionic current flows through the tip orifice of the probe by application of a suitable potential bias between the inserted electrode and a second electrode immersed in the electrochemical cell. Close to a surface, the measured current decreases, resulting from increased blockage of the tip opening. B) Typical current-distance curve obtained from approaching the surface of interest. Adapted from [41].

Since the introduction of SICM, several mathematical models have been proposed to describe the relation of tip dimensions and the tip-substrate distance. One of the more recent models published by Rheinlaender *et al.* [47] enables accurate modelling of an SICM approach curve. It considers several tip parameters, the tip-substrate distance (d), and the conductivity of the electrolyte solution (κ_e). The total resistance of the ion current could be divided into two contributions, the pipette resistance R_p and the access resistance R_z . R_p is defined according to equation 2.26. R_z is highly dependent on the tip-substrate distance and is described by equations 2.27 and 2.28.

$$R_p \approx \frac{1}{\kappa_e} \frac{1}{\pi r_i \tan \alpha} \quad (2.26)$$

$$R_z \left(\frac{d}{r_o} \leq 0.2 \right) \approx \frac{\ln \left(\frac{r_o}{r_i} \right)}{2\kappa_e \pi d} \quad (2.27)$$

$$R_z \left(\frac{d}{r_o} \geq 0.2 \right) \approx \frac{1}{4\kappa_e r_i} \left[1 + 0.2 \left(\frac{r_o}{d} \right)^{1.2} \right] \quad (2.28)$$

The tip orifice radius is defined as r_i , the total tip radius as r_o , and the tip inner cone angle as α . Both resistances, and the applied potential bias (U) contribute to the measured current according to equation 2.29. The steady-state current (i_∞) in bulk is defined by equation 2.30.

$$i(d) = \frac{U}{R_p + R_z} \approx i_\infty \frac{R_p + R_z(d \rightarrow \infty)}{R_p + R_z(d)} \quad (2.29)$$

$$i_\infty = \frac{U}{R_p + R_z(d \rightarrow \infty)} \approx \frac{\kappa_e U r_i}{\frac{1}{\pi \tan \alpha} + \frac{1}{4}} \quad (2.30)$$

After approaching the surface to a defined current target, e. g., to 90% of bulk current, scanning in lateral direction creates a topographic profile of the sample. To avoid crashes during the scan, the current signal is used to continuously adjust the z-position of the SICM probe, maintaining a constant tip-substrate distance. This way, in an imaging experiment, a topographical map of the substrate with direct access to three-dimensional information of surface details is obtained. It should be noted, however, that the DC mode of SICM often suffers from a drift of the current signal over extended measurement durations. This drawback led to the development of modulated operational modes. [4]

In the distance-modulated mode of SICM, the pipette is oscillated vertically with fixed amplitude via a piezo actuator while still a constant potential bias is applied as in the DC mode. In bulk, there is no influence on the current signal from the oscillation. Close to the substrate, an AC component is induced on the ion current, which could be isolated with the help of a lock-in amplifier and can be utilized as active distance control. Unlike the DC signal, the AC component is less influenced by thermal fluctuations or other interferences, effectively leading to improved sensitivity of the method. [4,41]

The relatively slow achievable scan rates in the distance-modulated mode originating from the physical limitations of the piezo actuator eventually led to the introduction of the voltage-modulated operational mode. Typically, the AC component is applied, and either phase or amplitude are modulated. Higher modulation frequencies in comparison to the distance-modulated mode result in faster scanning speeds.

Further recent improvements of the SICM technique include pulsed or hopping modes, and the hyphenation to complementary techniques, such as AFM [48] or SECM. [33]

References

- [1] J. Wang, Analytical electrochemistry, Wiley-VCH, Hoboken, 2006.
- [2] C. G. Zoski, Handbook of electrochemistry, Elsevier, Amsterdam, 2007.
- [3] C. M. A. Brett, A. M. O. Brett, Electrochemistry. Principles, methods, and applications, Oxford University Press, Oxford, 1993.
- [4] G. Wittstock, B. Speiser, J. Witt, Lehrbuch der Elektrochemie. Grundlagen, Methoden, Materialien, Anwendungen, Wiley-VCH, Weinheim, 2023.
- [5] A. J. Bard, L. R. Faulkner, Electrochemical methods. Fundamentals and applications, Wiley, New York, 2001.
- [6] D. Polcari, P. Dauphin-Ducharme, J. Mauzeroll, Chem. Rev. 2016, 116, 13234.
- [7] A. J. Bard, F. R. F. Fan, J. Kwak, O. Lev, Anal. Chem. 1989, 61, 132.
- [8] R. C. Engstrom, C. M. Pharr, Anal. Chem. 1989, 61, 1099A-1104A.
- [9] T. Kai, C. G. Zoski, A. J. Bard, Chem. Commun. 2018, 54, 1934.
- [10] C. L. Bentley, J. Edmondson, G. N. Meloni, D. Perry, V. Shkirskiy, P. R. Unwin, Anal. Chem. 2019, 91, 84.
- [11] A. Preet, T.-E. Lin, Catalysts 2021, 11, 594.
- [12] A. J. Bard, M. V. Mirkin, Scanning electrochemical microscopy, CRC Press, Boca Raton, 2012.
- [13] A. K. Satpati, A. J. Bard, Anal. Chem. 2012, 84, 9498.
- [14] S. Meltzer, D. Mandler, J. Electrochem. Soc. 1995, 142, L82-L84.
- [15] P. Hanekamp, T. Raith, C. Iffelsberger, T. Zankl, W. Robl, F.-M. Matysik, J. Appl. Electrochem. 2019, 49, 455.
- [16] S. Wert, S. Baluchová, K. Schwarzová-Pecková, S. Sedláková, A. Taylor, F.-M. Matysik, Monatsh. Chem. 2020, 151, 1249.
- [17] P. Vatsyayan, C. Iffelsberger, C. C. Mayorga-Martinez, F.-M. Matysik, Anal. Methods 2016, 8, 6847.
- [18] Z. T. Gossage, J. Hui, Y. Zeng, H. Flores-Zuleta, J. Rodríguez-López, Chem. Sci. 2019, 10, 10749.
- [19] C. Wei, A. J. Bard, G. Nagy, K. Toth, Anal. Chem. 1995, 67, 1346.
- [20] C. Lee, C. J. Miller, A. J. Bard, Anal. Chem. 1991, 63, 78.
- [21] C. G. Zoski, Electroanal. 2002, 14, 1041.
- [22] C. Lefrou, R. Cornut, ChemPhysChem 2010, 11, 547.

- [23] R. Cornut, C. Lefrou, *J. Electroanal. Chem.* 2007, 608, 59.
- [24] J. L. Amphlett, G. Denuault, *J. Phys. Chem. B* 1998, 102, 9946.
- [25] Y. Shao, M. V. Mirkin, *J. Phys. Chem. B* 1998, 102, 9915.
- [26] C. Wei, A. J. Bard, M. V. Mirkin, *J. Phys. Chem.* 1995, 99, 16033.
- [27] G. Wittstock, M. Burchardt, S. E. Pust, Y. Shen, C. Zhao, *Angew. Chem. Int. Ed.* 2007, 46, 1584.
- [28] S. Amemiya, A. J. Bard, F.-R. F. Fan, M. V. Mirkin, P. R. Unwin, *Annu. Rev. Anal. Chem.* 2008, 1, 95.
- [29] C. G. Zoski, *J. Electrochem. Soc.* 2016, 163, H3088-H3100.
- [30] A. Hengstenberg, C. Kranz, W. Schuhmann, *Chem. Eur. J.* 2000, 6, 1547.
- [31] M. A. Alpuche-Aviles, D. O. Wipf, *Anal. Chem.* 2001, 73, 4873.
- [32] J. V. Macpherson, P. R. Unwin, *Anal. Chem.* 2000, 72, 276.
- [33] Y. Takahashi, A. I. Shevchuk, P. Novak, Y. Murakami, H. Shiku, Y. E. Korchev, T. Matsue, *J. Am. Chem. Soc.* 2010, 132, 10118.
- [34] C. Iffelsberger, P. Vatsyayan, F.-M. Matysik, *Anal. Chem.* 2017, 89, 1658.
- [35] T. Raith, A. Kröniger, M. J. Mickert, H. H. Gorris, F.-M. Matysik, *Talanta* 2020, 214, 120844.
- [36] T. Raith, S. Wert, C. Iffelsberger, F.-M. Matysik, *Monatsh. Chem.* 2018, 149, 1671.
- [37] K. Eckhard, X. Chen, F. Turcu, W. Schuhmann, *Phys. Chem. Chem. Phys.* 2006, 8, 5359.
- [38] P. K. Hansma, B. Drake, O. Marti, S. A. C. Gould, C. B. Prater, *Science* 1989, 243, 641.
- [39] M. Nakajima, Y. Mizutani, F. Iwata, T. Ushiki, *Semin. Cell Biol.* 2018, 73, 125.
- [40] B.-C. Liu, X.-Y. Lu, X. Song, K.-Y. Lei, A. A. Alli, H.-F. Bao, D. C. Eaton, H.-P. Ma, *Front. Physio.* 2013, 3.
- [41] C. Zhu, K. Huang, N. P. Siepser, L. A. Baker, *Chem. Rev.* 2021, 121, 11726.
- [42] P. Zhang, N. Aydemir, M. Alkaisi, D. E. Williams, J. Travas-Sejdic, *ACS Appl. Mater. Inter.* 2018, 10, 11888.
- [43] A. L. Lipson, R. S. Ginder, M. C. Hersam, *Adv. Mater.* 2011, 23, 5613.
- [44] A. I. Shevchuk, G. I. Frolenkov, D. Sánchez, P. S. James, N. Freedman, M. J. Lab, R. Jones, D. Klenerman, Y. E. Korchev, *Angew. Chem. Int. Ed.* 2006, 45, 2212.
- [45] A. Page, M. Kang, A. Armitstead, D. Perry, P. R. Unwin, *Anal. Chem.* 2017, 89, 3021.
- [46] K. T. Rodolfa, A. Bruckbauer, D. Zhou, Y. E. Korchev, D. Klenerman, *Angew. Chem. Int. Ed.* 2005, 44, 6854.

- [47] J. Rheinlaender, T. E. Schäffer, *Anal. Chem.* 2017, 89, 11875.
- [48] L. Dowling-Carter, M. Aramesh, C. Forró, R. F. Tiefenauer, I. Shorubalko, J. Vörös, T. Zambelli, *J. Appl. Phys.* 2018, 124.

3 Experimental

3.1 Chemicals, instrumentation, materials, and software

All chemicals, instruments, materials, and software utilized within this thesis are listed in Tables 3.1 to 3.4 in the following section.

Table 3.1. Chemicals utilized within the experimental works.

Chemical	Supplier
Ferrocene methanol (FcMeOH, 97%)	Alfa Aesar (Haverhill, USA)
Hexaammineruthenium(III) chloride (99%)	ABCR (Karlsruhe, Germany)
Potassium chloride ($\geq 99.5\%$)	Carl Roth (Karlsruhe, Germany)
Potassium hexacyanoferrate(II) trihydrate ($\geq 99\%$)	Sigma-Aldrich (St. Louis, USA)
Potassium hexacyanoferrate(III) ($\geq 99\%$)	Sigma-Aldrich (St. Louis, USA)
Potassium nitrate ($\geq 99\%$)	Merck (Darmstadt, Germany)
Silver nitrate ($\geq 99\%$)	Sigma-Aldrich (St. Louis, USA)
Dimethyl carbonate (DMC, anhydrous, $\geq 99\%$)	Sigma-Aldrich (St. Louis, USA)
Ethyl methyl carbonate (EMC, 99%)	Sigma-Aldrich (St. Louis, USA)
Ethylene carbonate (EC, anhydrous, 99%)	Sigma-Aldrich (St. Louis, USA)
Ferrocene (Fc, 98%)	Sigma-Aldrich (St. Louis, USA)
Ferrocenium hexafluorophosphate (97%)	Sigma-Aldrich (St. Louis, USA)
Lithium hexafluorophosphate (battery grade, $\geq 99.99\%$)	Sigma-Aldrich (St. Louis, USA)
Tetrabutylammonium hexafluorophosphate ($\geq 99\%$)	Sigma-Aldrich (St. Louis, USA)

Table 3.2. Instrumentation employed within the experimental work of this thesis.

Instrument	Supplier
Digital microscope (DNT000006)	dnt Innovation (Leer, Germany)
Faraday cage (laboratory-constructed)	Mechanical workshop of the University of Regensburg (Regensburg, Germany)
Gloveboxes	GS Glovebox Systemtechnik (Malsch, Germany) Mecaplex (Grenchen, Switzerland) Mechanical workshop of the University of Regensburg (Regensburg, Germany)
Laboratory power supply (PPS-11360)	Voltcraft Conrad Electronic (Hirschau, Germany)
Milli-Q Advantage A10 system	Merck (Darmstadt, Germany)
Polishing device (laboratory-constructed)	Electrical and mechanical workshop of the University of Regensburg (Regensburg, Germany)
Scanning electrochemical microscope SECM 920C	CH Instruments (Austin, USA)
Soldering station WE CP-20	Weller (Wetzlar, Germany)
Syringe pump (UMP3)	WPI (Sarasota, USA)
VK-X3000 3D laser scanning microscope	Keyence (Osaka, Japan)
Wide stand microscope (100-300x magnification)	PEAK (Bornheim-Roisdorf, Germany)

Table 3.3. Materials used within the experimental works.

Material	Supplier
Ag/AgCl/3M KCl reference electrode (CHI111)	CH Instruments (Austin, USA)
Ag wire ($r = 0.25$ mm)	Advent Research Materials (Oxford, UK)
Al bottles ($V = 38$ & 125 mL), UN approval 1B1/X/250	Bürkle (Bad Bellingen, Germany)
Conductive silver epoxy resin (8331)	MG Chemicals (Burlington, Canada)
Epoxy resin (Resin L + Hardener S)	R&G Faserverbundwerkstoffe (Waldenbuch, Germany)
Fused-silica capillaries (OD = 360 μm , ID = 75 and 100 μm)	Polymicro Technologies (Phoenix, USA)
Jumper wire (insulation OD = 1.10 mm, cross-section = 0.20 mm ²)	Tru Components Conrad Electronic (Hirschau, Germany)
Lapping film sheets ($0.1 - 30$ μm grit size)	Precision Surfaces International (Houston, USA)
LIB graphite electrodes (Product ID 11124)	Customcells (Itzehoe, Germany)
Non-aqueous Ag/Ag ⁺ reference electrode (CHI112)	CH Instruments (Austin, USA)
Pt disk electrode (CHI102)	CH Instruments (Austin, USA)
Pt wires (radii of 6.25 μm , 12.5 μm , 0.25 mm, and 0.5 mm)	Advent Research Materials (Oxford, UK) Goodfellow (Huntingdon, UK)
Soda-lime glass capillaries (OD = 1.8 mm, ID = 1.15 mm)	Hilgenberg (Malsberg, Germany)
Thin-film electrodes (IDRA1)	Micrux Technologies (Gijón, Spain)

Table 3.4. Software used within the experimental works.

Software	Supplier
Office 365 (Excel, Powerpoint, Word)	Microsoft (Redmond, USA)
Origin 2019b	OriginLab (Northampton, USA)
SECM Software CHI920C	CH Instruments (Austin, USA)

3.2 Preparation of solutions – aqueous and non-aqueous

Parts of the presented experimental works were conducted in aqueous solutions, i. e. studies of boron-doped diamond (BDD) and stamping platinum electrodes. All solutions utilized within those topics were prepared with de-ionized water. The compositions of mediator solutions are summarized in Table 3.5. Respective electrolyte salts and mediator substances were dissolved at room temperature. De-gassing was achieved by treatment in an ultrasonic bath for 30 min at 50 °C. After storage at room temperature for 24 h, solutions were ready to use. Precipitates were removed prior to use with syringe filters.

Table 3.5. Composition of aqueous mediator solutions.

Mediator	Supporting electrolyte
1.5 mM FcMeOH	0.2 M KNO ₃
1.5 mM FcMeOH	1 M KNO ₃
1.5 mM Hexaammineruthenium(III)	1 M KNO ₃
1.5 mM Hexacyanoferrate(II)	1 M KNO ₃
1.5 mM Hexacyanoferrate(III)	1 M KNO ₃

Solutions utilized within LIB related experiments were prepared and stored inside an Argon-filled glovebox. The respective compositions are summarized in Table 3.6. Supporting electrolyte salts and mediator species were dissolved in organic solvent mixtures, which were prepared beforehand. After completed dissolution of mediator species and supporting electrolyte, the solutions were stored in certified Al bottles.

Table 3.6. Composition of non-aqueous mediator and electrolyte solutions.

Mediator	Supporting electrolyte	Solvent mixture
1.5 mM Fc	0.1 M LiPF ₆	EC:DMC (30:70 by wt.)
none	0.1 M LiPF ₆	EC:DMC (30:70 by wt.)
1.5 mM Fc	0.1 M TBAPF ₆	EC:DMC (30:70 by wt.)
none	0.1 M TBAPF ₆	EC:DMC (30:70 by wt.)
1.5 mM Fc	0.1 M LiPF ₆	EC:EMC (30:70 by wt.)
none	0.1 M LiPF ₆	EC:EMC (30:70 by wt.)
1.5 mM Fc + 1.5 mM FcPF ₆	0.1 M LiPF ₆	EC:EMC (30:70 by wt.)

3.3 Fabrication of probes for scanning electrochemical microscopy and scanning ion conductance microscopy

Platinum disk UMEs were routinely fabricated according to protocols published in literature. [1,2] All SECM experiments within this thesis were conducted with Pt UMEs with active electrode radii of either 6.25 or 12.5 μm , respective parameters are stated in the individual experiments. The necessary steps in the fabrication are illustrated in Figure 3.1. Briefly, roughly 1 cm of the insulating layer was removed from both ends of a piece of jumper wire. A Pt microwire with a length of approximately 1 cm was soldered onto one end. Then, the whole wire assembly was inserted into a pulled soda-lime glass capillary (tip opening diameter $\sim 100 \mu\text{m}$) until the Pt wire protruded from the tip opening by 1 mm. Afterwards, the tip was re-sealed by melting of the glass in a butane flame. Eventually, the Pt disk electrode was exposed by defined polishing in a laboratory-constructed polishing device equipped with lapping film sheets of grit sizes ranging from 0.1 up to 30 μm . The electrochemical performance of obtained SECM probes was assessed by CV and PACs [3,4] as described in more detail in section 2.2. The R_g value was estimated by optical microscopy at 100x magnification. In the case of deviations from the stated fabrication steps, they are described in the respective sections.

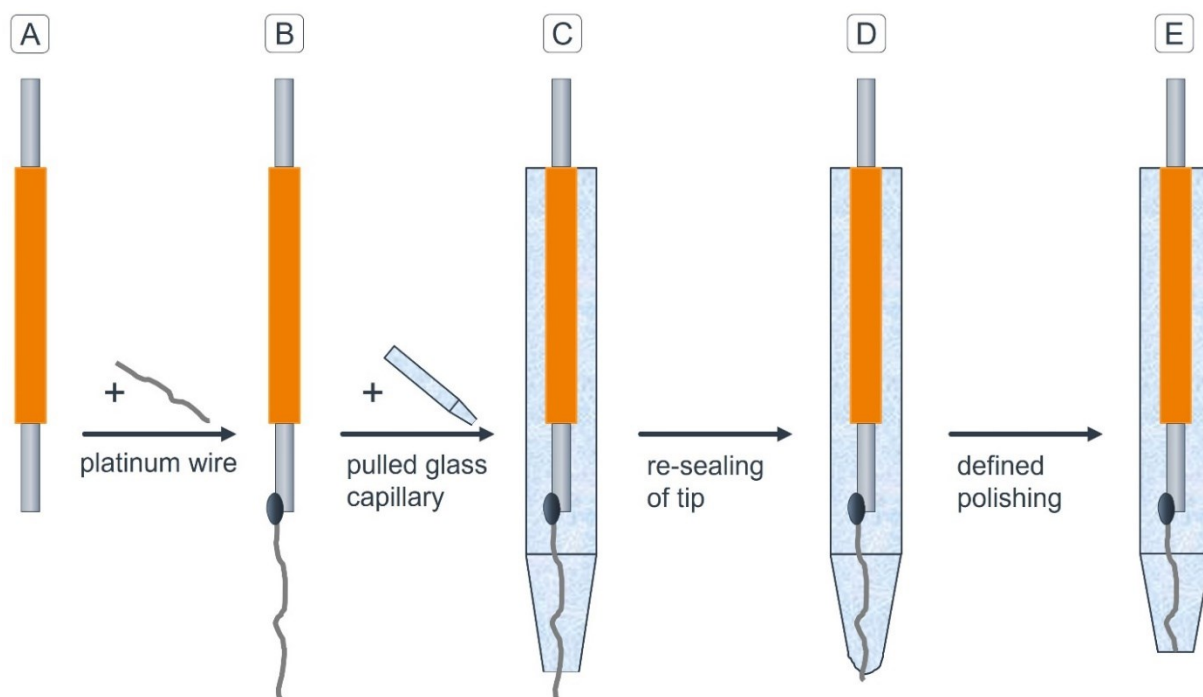


Figure 3.1. Fabrication steps for SECM probes. A) A small portion of the insulation from both ends of a jumper wire is removed. B) A platinum wire is soldered onto one end. C) The wire assembly is inserted into a pulled soda-lime glass capillary until approximately 1 mm of the platinum wire protruded from the tip. D) By heating in a butane flame, the tip is re-sealed. E) Defined polishing with lapping film sheets uncovers a disk-shaped platinum electrode.

SICM probes were produced from soda-lime glass capillaries also used in the UME fabrication. The individual steps are summarized in Figure 3.2. First, a glass capillary was re-sealed by melting the tip in a butane flame resulting in a conical decrease of the ID within the tip. By fine polishing, a tip opening is uncovered with IDs in the range of 10 to 30 μm . The obtained capillary was then thoroughly cleaned by flushing with a sequence of de-ionized water, isopropanol, and acetone followed by drying at ambient conditions for at least one hour. Aqueous SICM probes were then filled with 1 M KCl and an Ag/AgCl wire was inserted. Probes for usage within the LIB related experiments were transferred into an Argon-filled glovebox for further steps. In the latter case, the capillary was then filled with the respective electrolyte solution (1.5 mM Fc, 1.5 mM FcPF₆, 0.1 M LiPF₆, dissolved in EC:EMC 30:70 by wt.). Eventually, a Pt wire was inserted, and the probe was closed with a polyether ether ketone (PEEK) cap. Before utilization in experiments, the performance of an SICM probe was evaluated by chronoamperometry, linear sweep voltammetry (LSV), and PACs towards a model substrate.

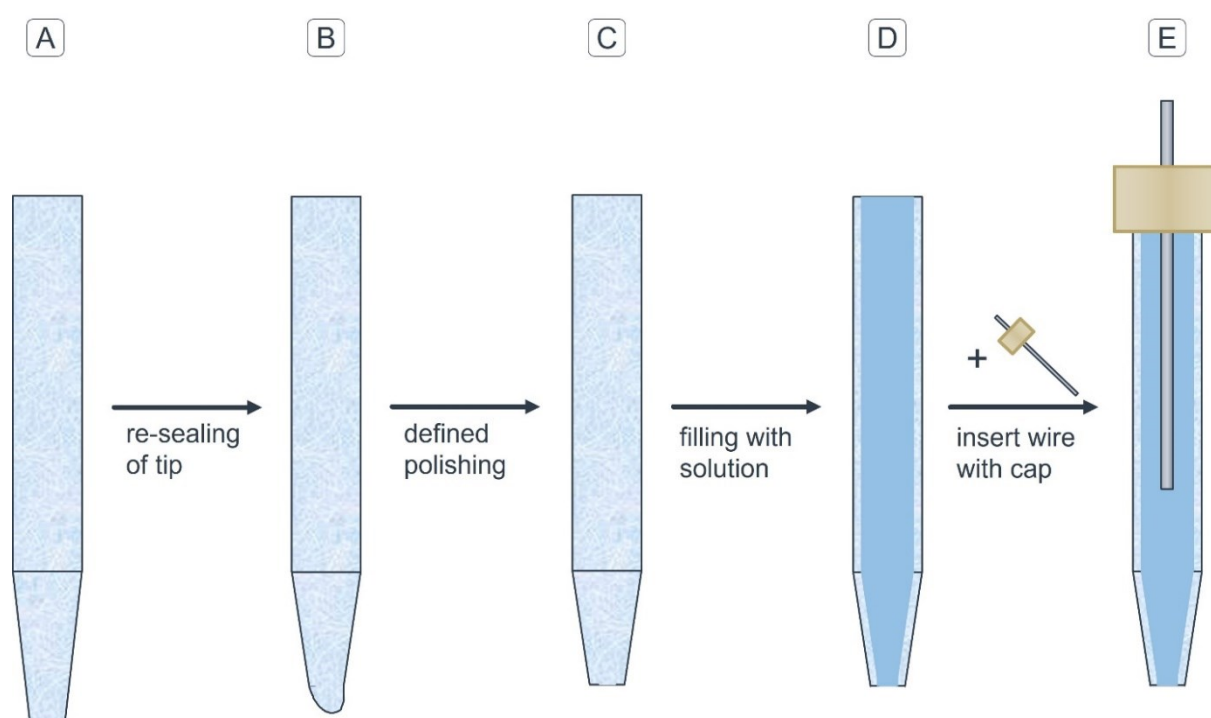


Figure 3.2. Steps in the fabrication of SICM probes. A) A soda-lime glass tube is pulled in a butane flame to a capillary with an opening diameter of approximately 100 μm . B) The tip is re-sealed by heating. C) Defined polishing of the tip exposed an opening with a diameter in the range of 10 to 30 μm . D) After thorough cleaning, the capillary is filled with electrolyte solution. E) A platinum wire is inserted into the capillary, and it is closed with a PEEK cap.

3.4 Sample preparation for aqueous and non-aqueous environments

Depending on the field of application, aqueous or non-aqueous, two different types of custom-made sample holders were used in the preparation of substrates. The steps in both cases are illustrated in Figure 3.3. For aqueous investigations, a holder made from polyvinyl chloride (PVC) with an inserted brass rod was used. If necessary, substrates were cut to fit the top of the sample holder. After cleaning of sample and sample holder with de-ionized water and isopropanol, a small portion of conductive silver epoxy adhesive was mixed and applied to ensure electrical connection between sample and brass rod. The substrate was gently positioned on top of the sample holder and a curing step for the conductive adhesive of at least six hours at ambient conditions was conducted. Then, the edges of the sample were sealed with epoxy resin, to prevent leakage of solutions below the sample. After another curing step of at least 24 hours, samples were ready for installation within the SECM electrochemical cell. Samples without the need of an electrical connection to the SECM, i. e. model substrates like the Micrux thin-film electrode, were fixed on microscope glass slides with epoxy resin. Since PVC was not suitable for usage in LIB solvents, another type of sample holder was designed. It was made from PEEK with an inserted brass rod and a screw cap containing an inlaid Viton gasket. All following fabrication steps were conducted within an Argon-filled glovebox. Circular pieces of LIB graphite electrode with a diameter of 4 mm were cut from larger sheets with a punching iron. A small amount of the conductive silver epoxy adhesive was applied, and a piece of graphite electrode was gently positioned on top of the sample holder. After a curing time of at least six hours, the screw cap was installed, and samples were ready for use.

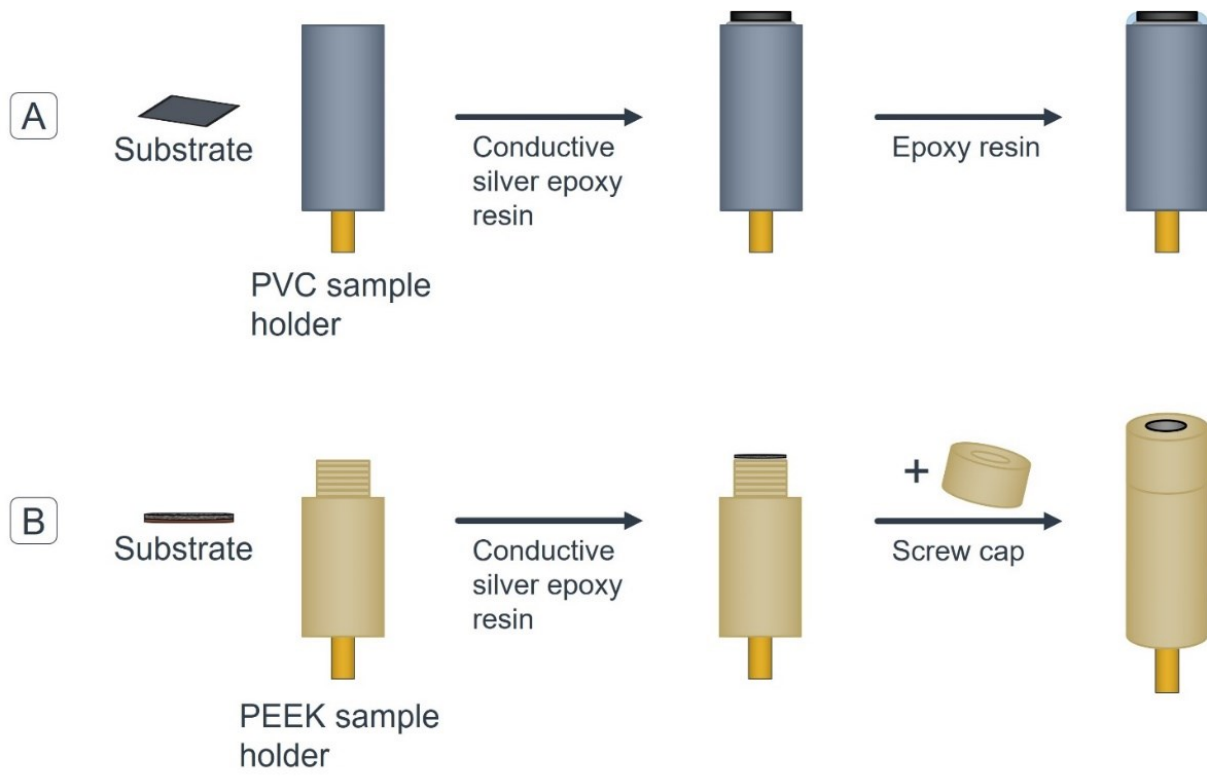


Figure 3.3. Illustration of sample preparation steps for aqueous and non-aqueous substrates. A) Substrates investigated in aqueous media are placed onto in-house fabricated PVC sample holders. Electrical contact is ensured by a conductive silver epoxy resin. After curing, an epoxy resin is applied to the sides of the substrate to prevent leakage of solution below the sample. B) For LIB materials, custom-made PEEK sample holders with a screw cap are used. Substrates are installed on the top and contacted with conductive silver epoxy resin. A screw cap with an inlaid Viton gasket prevents leakage of solution below the substrate.

3.5 SECM setup and initial experimental procedures

All SECM and SICM experiments were performed on a commercially available SECM 920C system. The instrumental setup was modified for measurements under inert conditions. Relevant details are shown in Figure 3.4.

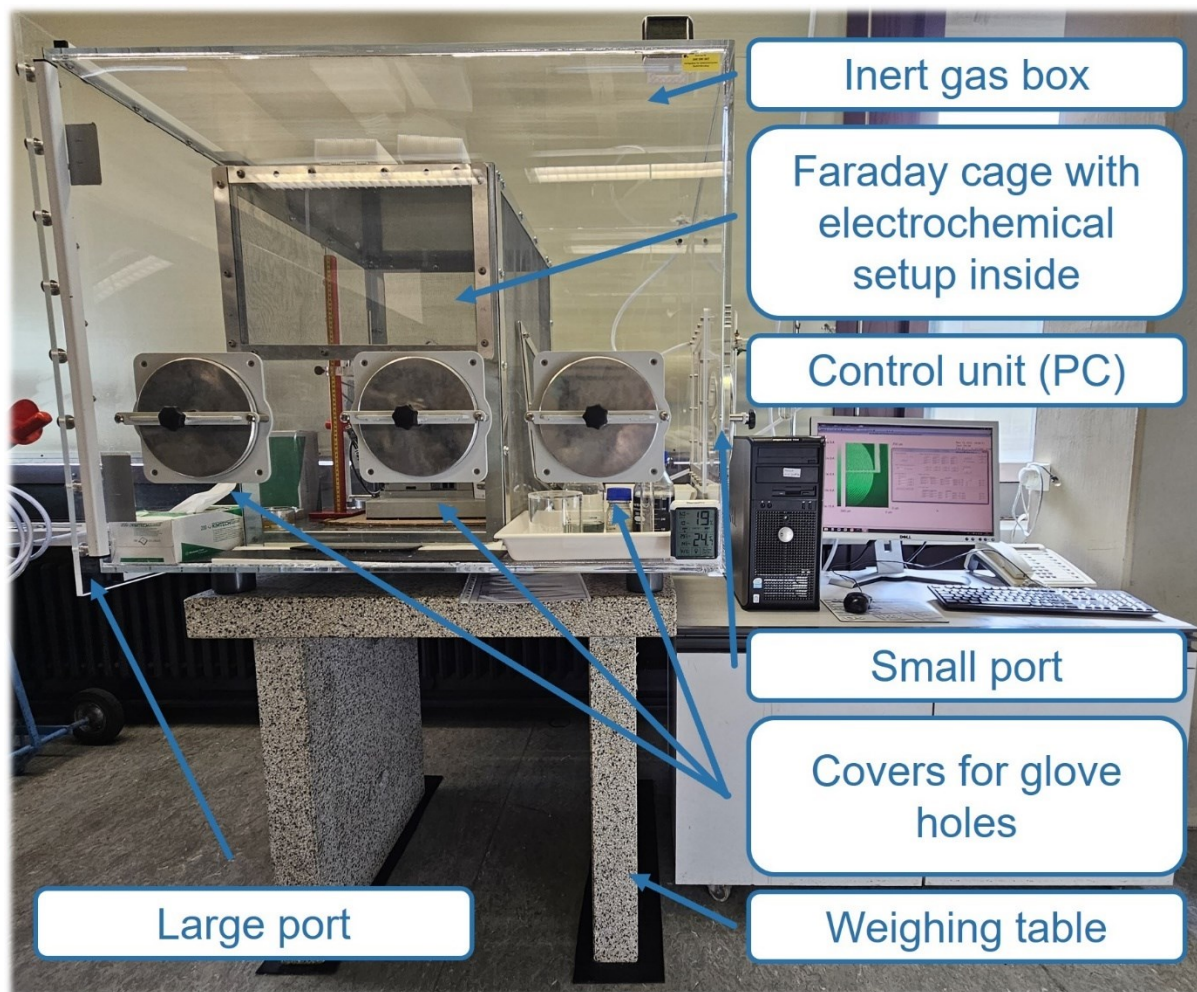


Figure 3.4. Photograph of the instrumental setup. The Faraday cage containing the electrochemical setup is placed within a plexiglass box filled with inert gas (Argon). Two ports, a large one on the left and a small one on the right side, enable introduction of probes, solution, samples, and other materials. Bipotentiostat and positioning control unit are placed behind the inert gas box with their electrical connections fed through gas-tight connectors. Glove holes and a permanent excess pressure inside the box allow manipulations on the electrochemical setup while maintaining an inert atmosphere. The plexiglass box is installed on top of a weighing table.

Due to the need of an oxygen and humidity free atmosphere for LIB related experiments, a plexiglass box was designed and fabricated in cooperation with the mechanical workshop of the University of Regensburg. It was equipped with two ports, a large one on the left and a

small one on the right side, for the introduction of probes, samples, and other materials. Via a gas intake, the box was flushed with Argon maintaining a permanent excess pressure inside secured with an overpressure protection installed in the gas outlet. Because of the excess pressure, the inert atmosphere inside of the plexiglass box could be sustained even when opening the glove hole covers for manipulations of the electrochemical setup, f. e., changing of electrolyte solutions or adjustment of probe assemblies. To reduce interference from vibrations and electromagnetic noise, the electrochemical setup and the positioning control unit were installed on a dampening mat inside a custom-made Faraday cage. Electrochemical cells made from polytetrafluoroethylene (PTFE) are mounted on a platform with three fine thread screws to adjust for sample tilt. Specific individual details of the setup are stated within the respective sections.

After assembly of the electrochemical setup, the function of an UME was tested by recording a CV in the respective mediator solution. In the case of a SICM probe, a linear sweep voltammogram (LSV) was recorded for evaluating the performance. If the probe performance was insufficient, the electrode surface was renewed by fine polishing (SECM), or the probe was cleaned and re-assembled (SICM).

Prior to imaging experiments, substrates were levelled according to the following procedure. For plane substrates with homogeneously distributed electrochemical activity, i. e. model substrates, a series of PACs towards three individual points surrounding the area of interest was conducted. To start, an initial PAC was recorded. Then, the probe was retracted by 250 μm from the surface and it was moved to the coordinates of the second point. The difference in travel distance of two individual PACs indicates the magnitude of tilt of the substrate between those two coordinates. This procedure was repeated until a tilt of less than 1 $\mu\text{m mm}^{-1}$ was reached. In the case of real samples, i. e. BDD or LIB graphite electrodes, with a distinct topography and/or heterogeneously distributed electrochemical activity, PACs were not sufficient to ensure proper levelling. Therefore, additionally line scans were conducted between the PAC coordinates.

References

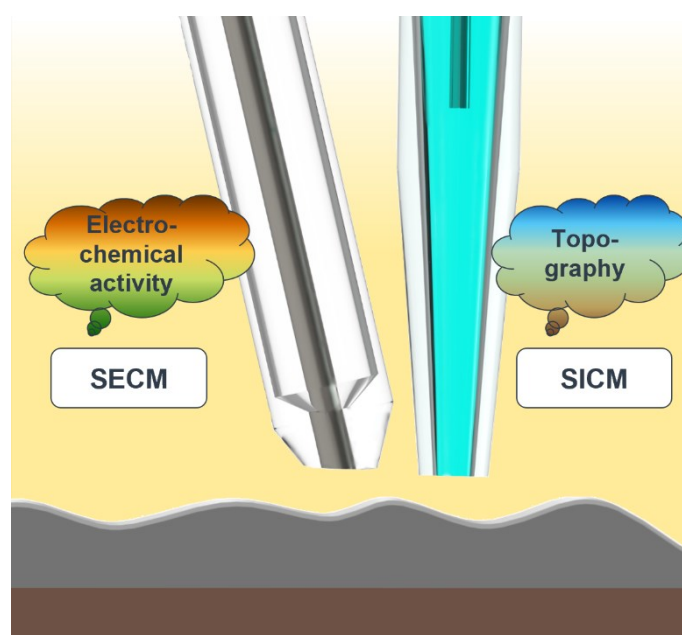
- [1] C. G. Zoski, *Electroanal.* 2002, 14, 1041.
- [2] A. J. Bard, M. V. Mirkin, *Scanning Electrochemical Microscopy*, CRC Press, Boca Raton, 2012.
- [3] J. L. Amphlett, G. Denuault, *J. Phys. Chem. B* 1998, 102, 9946.
- [4] R. Cornut, C. Lefrou, *J. Electroanal. Chem. Chemistry* 2007, 608, 59.

4 Results and discussion

4.1 Simultaneous scanning ion conductance and electrochemical microscopy in lithium-ion battery research

Eidenschink Johannes, Matysik Frank-Michael

ChemElectroChem 11 (2024) e202300577.

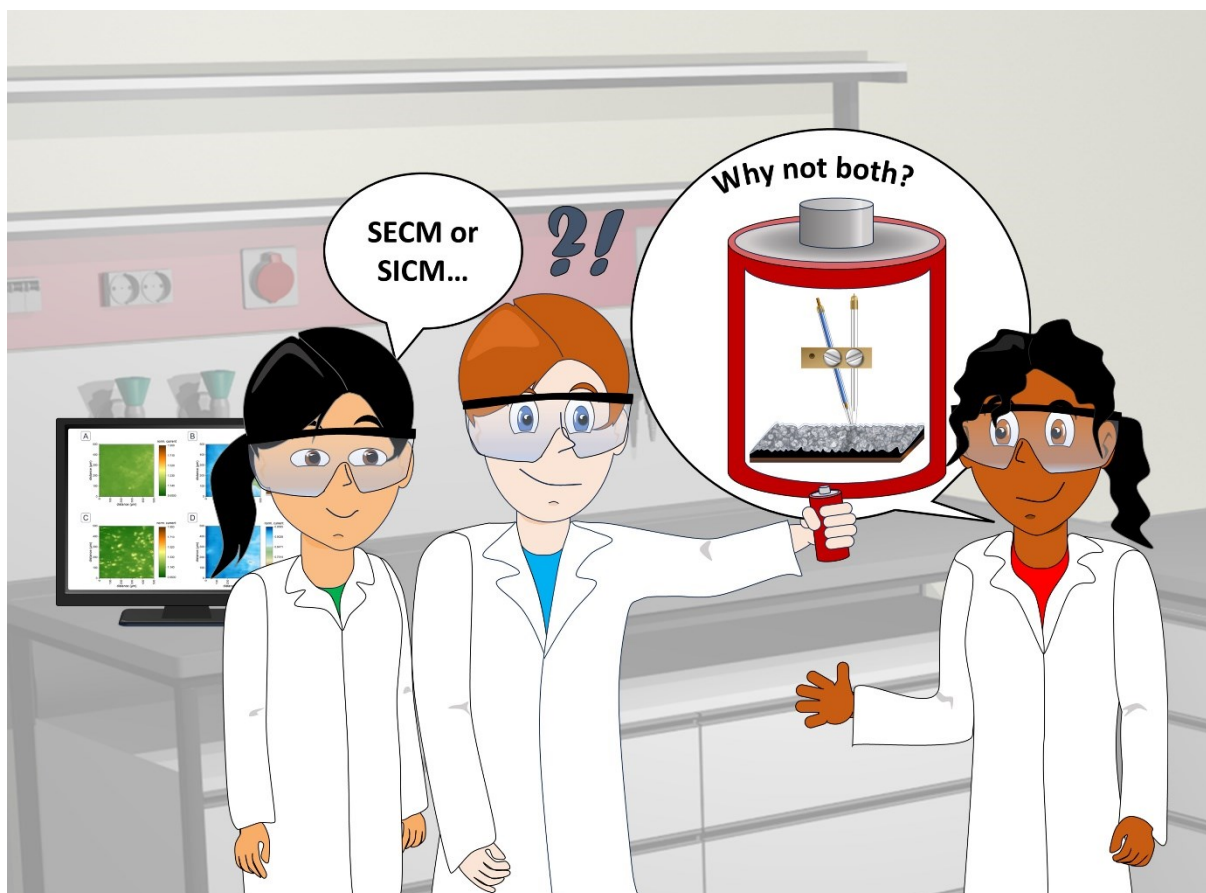


Abstract

Deeper understanding of processes involved in operation of lithium-ion batteries (LIBs) is necessary to further optimize them for future applications. Extensive research was conducted on the formation of a solid electrolyte interphase (SEI) on negative battery electrodes, still leaving several questions unanswered. Scanning probe microscopies (SPMs) enable *in situ* and *operando* investigations and have the potential to explain some phenomena. Scanning electrochemical microscopy (SECM) and scanning ion conductance microscopy (SICM) could be employed in LIB studies. A novel SICM method based on the redox couple ferrocene/ferrocenium is introduced for applications in carbonate solvents widely used in LIBs. Proof of concept measurements were conducted with a micro milled copper circuit board as

model substrate. Furthermore, the proposed SICM approach was hyphenated with feedback mode SECM resulting in the simultaneous mapping of morphology and electrochemical activity. A flexible dual-probe arrangement was developed enabling usage of both SPM techniques at the same time, and furthermore, an easy replacement of both individual probes if needed. The setup was applied in the characterisation of commercial graphite electrodes for LIBs before and after conducting a pre-charging protocol. Changes in electrochemical activity and topography of the graphite electrode were resolved in simultaneously generated SECM/SICM recordings.

Front Cover



The Front Cover art illustrates a common scenario in the laboratory, showcasing a scientist engaged in working with scanning probe techniques. A key consideration arises regarding the choice of the scanning probe microscopy (SPM) technique relevant to the subject. In the context of lithium-ion batteries, both scanning electrochemical microscopy and scanning ion conductance microscopy emerge as viable options. However, the question arises: why limit oneself to a single technique when the possibility exists to employ both simultaneously? Cover design by Dr. Thomas Herl.

4.1.1 Introduction

Lithium-ion batteries (LIBs) are among the most important energy storage devices of our time. [1,2] Their main applications are portable electronic devices and electric vehicles. [3] Typically, a LIB consists of negative electrode, positive electrode, and a separator in between plus the organic electrolyte solution. Because of safety issues related to bare lithium, host materials capable of lithium-ion intercalation are normally used. During charge and discharge processes, lithium-ions are shuttled between these host electrodes, which led to the description of LIBs as “rocking chair” batteries. [4] While charging, the potential of the negative electrode, often graphite in commercial cells, exceeds the electrochemical stability window of the electrolyte. This generally results in the formation of a so-called solid electrolyte interphase (SEI), which mainly consists of insoluble degradation products. [5] The intrinsic properties of the SEI are detrimental for safe and long-term stable operation of batteries. Ideally, it prevents further degradation of the electrolyte solution, while still enabling diffusion of Li^+ . Furthermore, the formation of the SEI is responsible for the initial, irreversible capacity loss of a LIB due to changing the intercalation capacity of the negative electrode. Extensive research has been dedicated to the investigation of SEI formation and corresponding properties, because of its importance regarding long-term cycling stability and battery safety. [6–11] Although LIBs improved immensely since their commercialisation, there is still a lot of potential for improvement of LIB technology, e. g., novel electrode materials, full understanding of processes involved in operation, and replacement of hazardous liquid electrolytes. [1] To further drive innovations in these fields, there is a growing demand for powerful analytical techniques capable of *in situ* or even *in operando* investigations.

Several scanning probe microscopies (SPMs) are well suited for this task. One of the more prominent SPMs applied for investigations in LIB research is scanning electrochemical microscopy (SECM). [12] In this contactless technique, a nano- or micro sized electrode is scanned across the surface of interest. By application of an appropriate potential, a diffusion-limited current is measured resulting from the oxidation / reduction of a redox-active substance, the mediator. In the scope of LIB related research, two commonly used mediators are ferrocene [10,11,13] and 2,5-di-*tert*-butyl-1,4-dimethoxybenzene. [6,13] Since its introduction in the late 1980s, SECM excelled in diverse applications, ranging from biological samples, [14] kinetic characterisation of novel materials [15] to lately studies of battery electrode materials and processes. [6,10] A drawback of stand-alone SECM approaches lies in the interpretation of recorded data. This is because the current signal is not only dependent on the electrochemical activity, but also on the morphology of the investigated substrate. Over the past decade, various solutions were introduced to overcome this limitation. Measuring shear

force on a vibrating SECM probe, [16] application of an alternating current (AC-SECM), [17] or hybridisation with the atomic force microscope [7,9,18] are only a short selection of possibilities which should be mentioned. Not all of them were yet successfully implemented in battery research due to the intrinsic challenges of the subject.

An alternative approach to separate morphological from electrochemical activity information in SECM studies is the hyphenation with a complementary SPM technique called scanning ion conductance microscopy (SICM). This SPM was introduced in 1989 by Hansma *et al.* [19] and became a well-established non-contact method in a variety of research fields ever since. The principle of SICM is typically applied in aqueous solutions. A silver-silver chloride wire is placed in a glass capillary filled with a chloride containing solution. In this approach, a second silver-silver chloride wire is placed in the bulk solution and an ionic current between the two wires could be measured by application of a potential bias. [20] During operation, the current decreases as soon as the tip of the capillary is approaching a surface, i. e. the orifice will be partly blocked. Scanning the probe across the surface enables the generation of highly resolved topographical information about the substrate. In the context of LIB research, to the best knowledge of the authors, few contributions from 2011, [21] 2014, [22] and 2023 [23] including SICM experiments could be found. Lipson *et al.* [21,22] used a lithiated tin wire within an electrolyte-filled capillary in the investigation of lithiation processes on tin thin films and MnO substrates. Takahashi *et al.* [23] evaluated the correlation of ion-concentration profile and surface topography changes on graphite electrodes with a SICM approach based on a lithium-coated copper electrode inside of the capillary. The simultaneous operation of SICM together with SECM was already accomplished in aqueous media, [24] but not yet in non-aqueous, carbonate-based solvents widely used in LIBs. Despite its attractiveness in mapping topographical information and ion-flux, SICM is still underrepresented in this field of research. [2,21–23]

Within this contribution, a simple-to-use SICM method for applications in the context of LIBs is introduced. The method is based on the ferrocene-ferrocenium (Fc/Fc^+) redox couple, which was found to enable a stable SICM signal and could also be used as a redox couple-based reference electrode in carbonate solvents. Its open circuit potential vs. a Li/1 M Li^+ reference electrode was determined at +3.274 V. Furthermore, the proposed SICM method was coupled with feedback mode SECM to simultaneously generate topographic information as well as spatially resolved electrochemical activity characterisation of substrates. The application of our dual-probe SECM/SICM approach was demonstrated in the characterisation of LIB graphite electrodes before and after treatment with a pre-charging protocol.

4.1.2 Results and discussion

Development of a novel SICM method for applications in LIB electrolytes

The goal of this publication is to design a novel SICM method based on using the Fc/Fc⁺ couple as a reference system for two main reasons. Firstly, the combination of a platinum wire with the Fc/Fc⁺ redox couple was already used as a reference electrode in experiments in propylene carbonate [25] and similar approaches on platinum-based reference systems for non-aqueous solvents were already published. [26] Secondly, the mediator of choice for the SECM investigation was Fc, because of its recently reported superior signal stability in organic carbonate-based electrolytes. [9,10,13] Chronoamperometry was conducted at fixed potentials of 3.174, 3.374, and 3.474 V vs. Li/1 M Li⁺ in preliminary studies to evaluate the signal stability of the proposed SICM approach. Results suggested that the measured current generated from the SICM probe is sufficiently stable in the tested potential range. Highest signal stability in the chronoamperometric experiments was achieved by application of a potential difference of 3.374 V vs. Li/1 M Li⁺. The signal decrease with a probe potential of 3.374 V was less than 4% for a period of 15 min compared to 4.5% at 3.174 V, and 6.3% at 3.474 V. Thus, this potential bias was chosen for further experiments.

Afterwards, the reproducibility of the SICM method was tested. For that purpose, five consecutive probe approach curves (PACs) with a current target of 85% of bulk current towards the same position on a model substrate were conducted. As such, a copper circuit board with micro milled channels was used. In Figure 4.1.1, the results are shown as normalized current, given by the ratio of the tip current at the respective position divided by bulk current. To start, the SICM probe tip was positioned at a distance of approximately 110 μm above the sample surface. It was found that the course as well as the ending point of the approach curves was highly reproducible with only minor deviations of less than 100 nm in the total travel distance.

Final steps in the SICM method development were imaging experiments mapping the topography of the model substrate. The channels in the copper circuit board were micro milled and they had a width of 200 μm, as shown in Figure 4.1.2A. After approaching the SICM probe to a distance of 5 μm, correlating to a signal of 70% of bulk current, a topographical map was recorded (Figure 4.1.2B). Above the channels the distance from probe tip to substrate was greater resulting in higher currents (blue) than above the copper surface (brown).

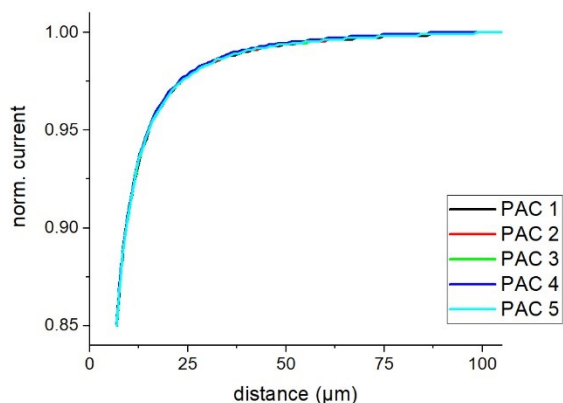


Figure 4.1.1. Signal reproducibility of the SICM method shown by five consecutive probe approach curves towards the surface of the model substrate. Measurements recorded in 1.5 mM Fc in 0.1 M LiPF₆ solution (EC:EMC 30/70). The probe consisted of a Pt wire inserted into a glass capillary (opening diameter 30 μm, total tip diameter 90 μm) filled with 1.5 mM Fc/Fc⁺ solution. PAC parameters: Probe potential was 3.374 V vs. Li/1 M Li⁺, quiet time of 15 s, maximum approach speed was 10 μm s⁻¹.

Even small details in the channels (X 1200/Y 600) were visible in the SICM image, and the channels could be clearly resolved in the current map. The signal changes were attributed to blockage of the SICM probe's orifice above the copper surface, or the almost unobstructed capillary opening above the micro milled channels. Thus, the applicability of the proposed SICM method in carbonate-based solvents was shown.

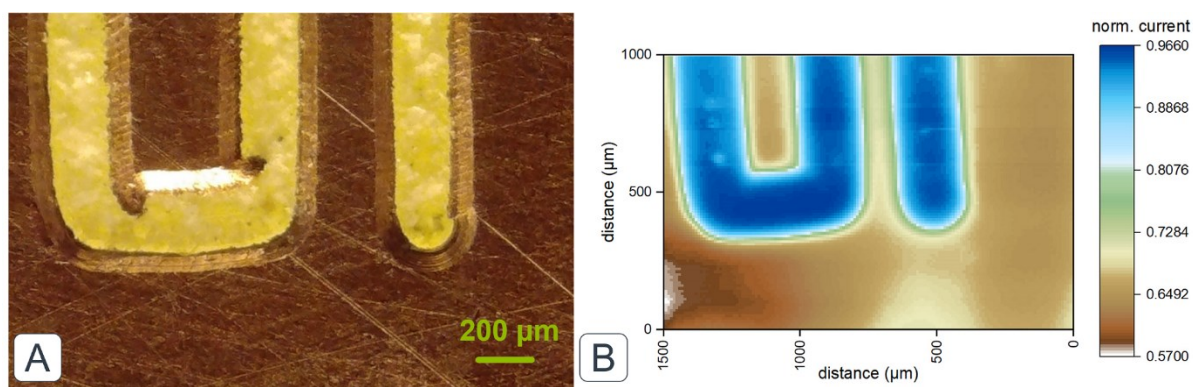


Figure 4.1.2. Model substrate used in the development of the SICM method. A) Micrograph of the model substrate. A copper circuit board with micro milled channels (width = 200 μm) was used. B) SICM image of the circuit board measured in 1.5 mM Fc in 0.1 M LiPF₆ solution (EC:EMC 30/70). The probe was a Pt wire inserted into a glass capillary (opening diameter 30 μm, total tip diameter 150 μm) filled with 1.5 mM Fc/Fc⁺ solution. Probe potential was 0.1 V, quiet time of 15 s, height corresponding to 70% of bulk current, movement speed was 200 μm s⁻¹.

Simultaneous SECM/SICM characterisation of a LIB graphite electrode

With more complex investigations in mind, e. g., SEI formation and characterisation, stand-alone SICM measurements are suited to track morphological changes of the electrode material. The formation of an SEI is generally linked with changes in the electrochemical activity. Therefore, the possibility to map the topographical as well as the electrochemical changes of the surface is highly attractive. In the next step, the proposed SICM method was combined with feedback mode SECM to generate complementary information on the substrate characteristics. Successively measuring with both methods is possible but more reliable information would be achieved by simultaneous measurements. This is due to the fact that exchanging probes would inevitably lead to a small misplacement of the probe tip resulting in measuring at a different position on the sample surface. Thus, only a hybrid approach with simultaneous usage of both SPM techniques is adequate.

The most important part for the approach towards hybrid SECM/SICM with two individual probes was to design a satisfactory probe holder. It should be resistant against the used carbonate-based solvent, the positioning of both probe tips should be as close as possible, and the signal response of both techniques should not be changed significantly because of the probe arrangement. The in-house built holding system, which is shown in more detail in the Experimental section, was found to be sufficient regarding those requirements. A tilted position of one of the two probes at a 15-degree angle was determined to be the sweet spot in lowest possible change of signal response and close positioning of both probe tips. In preliminary experiments, the influence of a tilted position on the behaviour of the probe was determined. PACs and imaging in feedback mode SECM revealed poor performance of a flatly polished probe mounted in the tilted position. Therefore, the SECM probe was also polished at a 15-degree angle resulting in a parallel orientation towards the sample surface. This adjustment theoretically amounts to an increase of the electrode's surface area of 3.5%, and a slight distortion of the tip shape. The resulting performance decrease was acceptable. Prior to measuring surface characteristics of the sample, the arrangement of SICM and SECM probes was carefully adjusted and controlled with the help of a digital microscope camera. The performance of both SPM was then tested with PACs, and eventually, the adjustment was repeated. Further experiments were started only after the behaviour of both probes during PACs was sufficient. For SECM, a probe potential of 3.574 V was chosen based on cyclic voltammetry and the redox potential of the used mediator Fc, which was determined at 3.274 V vs. Li/1 M Li⁺ in the applied experimental setup. In SICM, a potential bias of 3.374 V vs. Li/1 M Li⁺ was applied based on the signal stability measurements described in the previous section.

The sample material of choice for showcasing the strengths of the non-aqueous SICM method in hyphenation with feedback mode SECM were typical graphite electrodes for LIBs. Samples were characterised as received, with no additional surface treatment. Prior to SECM/SICM measurements, microscopic images were taken of a part of the graphite electrode and the surface roughness was determined. A representative microscopic image and a false colour image are shown in Figure 4.1.3. Particles were found to have sizes in the micrometre range. The surface area roughness was determined from four randomly selected regions on the sample, with an area of $216 \times 289 \mu\text{m}$ each. The core roughness depth S_k according to ISO 25178 [27] was measured at $2.3 \mu\text{m}$, and the maximum height S_z was $9 \mu\text{m}$ in the investigated areas.

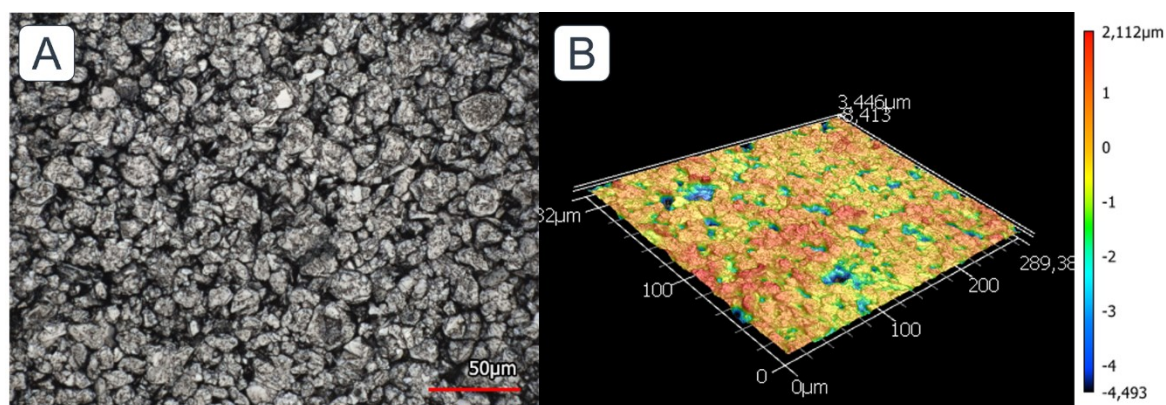


Figure 4.1.3. Graphite electrode for LIBs which was used for investigation with the dual-probe setup. A) Micrograph of the graphite electrode surface. B) False colour image highlighting the graphite surface roughness.

Following the careful adjustment of SECM and SICM probe in the positioning unit of the SECM setup, a PAC was started to approach the graphite surface. An example of such a PAC is shown in Figure 4.1.4A, which was recorded at the position (X 0/Y 0) of later imaging experiments. On one hand, the current signal of the SECM probe increased with less distance to the surface, indicating positive feedback of the uncovered graphite electrode. The SICM signal, on the other hand, decreased with the probe assembly getting closer to the substrate, because of the increasing blocking of the tip orifice. Several preliminary PACs and images were recorded until a suitable, representative imaging area was found. Subsequently, the SECM/SICM imaging experiment was started. To be able to show the identical area mapped with both SPM techniques, it was a necessity to scan a larger area of $500 \times 1000 \mu\text{m}$. From those larger matrices, corresponding areas for SECM and SICM were extracted. The areas were selected based on the measured distance between the active tip elements from optical

microscopy, and by the comparison of surface details. Matching current maps from SECM and SICM signals before pre-charging of the graphite electrode are shown in Figure 4.1.5A and 4.1.5B. From the SECM image (Figure 4.1.5A), a rather homogeneous distribution of electrochemical activity was observed with small variations depicting particles of the electrode material. Furthermore, a slight signal increase was measured in the middle right part of the imaged area, which could either mean higher electrochemical activity or a reduced distance between tip and sample surface. It was explained by the findings in the SICM current map (Figure 4.1.5B), where a matching signal decrease, i. e., an elevation of the surface, was recorded in the identical area. Signal variations resulting from electrode particles in both SPM modes matched well with the size determination from laser scanning microscopy results. In literature, it is generally assumed that the electrochemical activity of pristine graphite electrodes is homogeneous. [6,11]

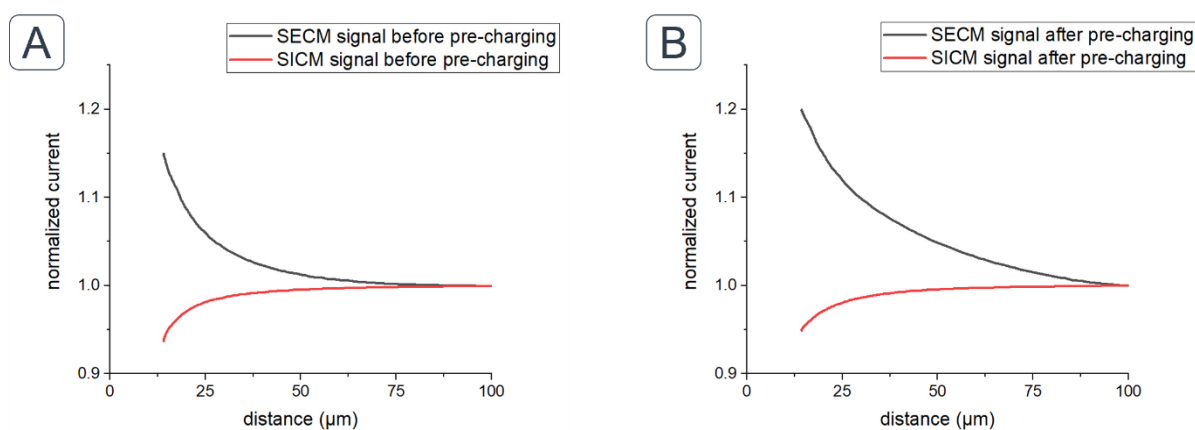


Figure 4.1.4. Simultaneous SECM/SICM PACs towards the surface of a Customcells graphite electrode before (A) and after (B) the pre-charging protocol recorded in 1.5 mM Fc in 0.1 M LiPF₆ solution (EC:EMC 30/70). SECM probe was a Pt UME ($r = 6.25 \mu\text{m}$, $R_g = 7$), which was polished at a 15-degree angle and mounted in a tilted position at 15°. SICM probe consisted of a Pt wire inserted into a glass capillary (opening diameter 20 μm , total diameter 100 μm) filled with 1.5 mM Fc/Fc⁺ solution. Probe potentials were 3.574 V (SECM) or 3.374 V vs. Li/1 M Li⁺ (SICM), quiet time of 15 s, max. approach speed was 10 $\mu\text{m s}^{-1}$.

To induce changes in surface characteristics, initial steps towards the formation of a SEI, and repeated Li⁺ (de-)intercalation, a pre-charging protocol was applied to the graphite sample after the initial characterisation and mapping of a suitable, representative area by SECM/SICM. During pre-charging, the SECM/SICM probe assembly was retracted from the sample surface to exclude any possible interferences. The protocol consisted of an initial scan from 3.274 to 1.274 V vs. Li/1 M Li⁺, followed by cycling between 1.274 to 0.04 V vs. Li/1 M Li⁺ for two cycles. Both steps were conducted at a scan rate of 1 mV s⁻¹. Similar conditions had previously

been applied in the investigation of graphite electrode samples. [9–11] Passivation of the electrode surface, i. e., reduced electrochemical activity due to the formation of a SEI, is the expected outcome of the pre-charging. The topography, on the other hand, is believed to change minimally, since the SEI thickness is generally accepted to be in the nanometre range. [5,8]

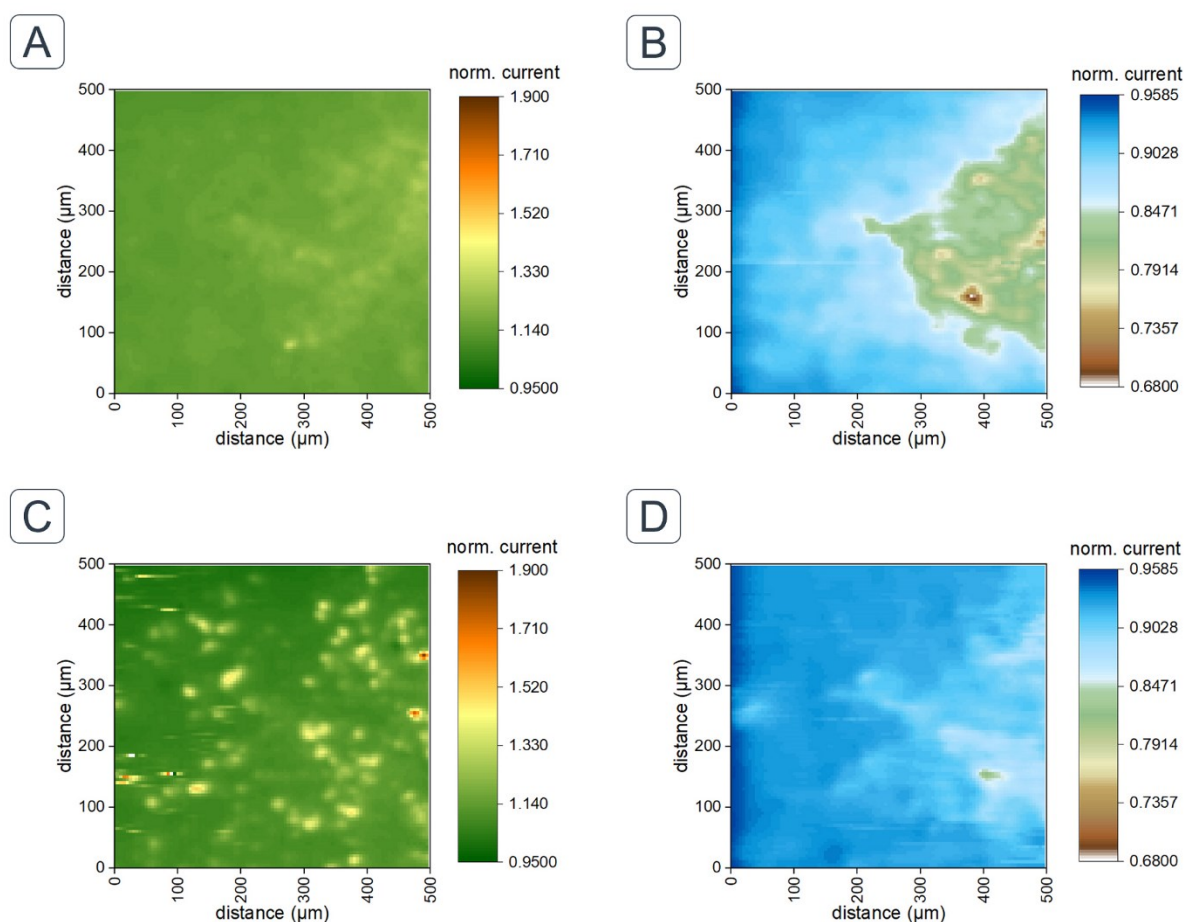


Figure 4.1.5. Simultaneous SECM/SICM images from the surface of a Customcells graphite electrode before (A+B) and after (C+D) the pre-charging protocol recorded in 1.5 mM Fc in 0.1 M LiPF₆ solution (EC:EMC 30/70). SECM probe was a Pt UME ($r = 6.25 \mu\text{m}$, $R_g = 7$), which was polished at a 15-degree angle and mounted in a tilted position at 15°. SICM probe consisted of a Pt wire inserted into a glass capillary (opening diameter 20 μm , total tip diameter 100 μm) filled with 1.5 mM Fc/Fc⁺ solution. Probe potentials were 3.574 V (SECM) or 3.374 V vs. Li/1 M Li⁺ (SICM), quiet time of 15 s, movement speed was 50 $\mu\text{m s}^{-1}$.

After this pre-charging process, the SECM/SICM probe assembly was moved to the starting position of the PAC before (Figure 4.1.4A), and a new approach curve was initiated. The SECM/SICM PACs after pre-charging are shown in Figure 4.1.4B. Interestingly, this second PAC terminated at a total travel distance of 9 μm less than the previous one. Most likely, this

height difference resulted from solvent uptake. Bülter *et al.* [28] reported swelling of graphite electrodes because of swelling of the binder used in the graphite composite formulation. Another intriguing finding was the fact that the SICM PAC, on the one hand, did not show significant changes, but on the other hand, the course of the SECM curve was altered in a different way than anticipated. A signal decrease resulting from formation of an electronically insulating SEI was expected, but the opposite was measured. In Figure 4.1.5C and 4.1.5D, SECM and SICM current maps from the same region as in 4.1.5A and 4.1.5B are shown. The distribution of electrochemical activity (Figure 4.1.5C) changed considerably, indicating several local hot spots randomly distributed in the investigated area. Similar results were also observed elsewhere. Bülter *et al.* [6] attributed these local jumps of activity to temporal dissolving of parts of the SEI, terming this phenomenon as short-term events. Zeng *et al.* [11] observed locally high electrochemical activity spots as well in their studies of graphite composite electrodes. They concluded that lithiated graphite was exposed locally as a result of the initially unstable nature of the SEI. Also, other possible explanations are discussed in literature, including speculation on electron tunnelling towards Fc^+ through the SEI, when Fc was present during formation. [29] The majority of the investigated area exhibited typical behaviour correlated with SEI formation, i. e. a decrease in electrochemical activity. Interestingly, the topography of the graphite electrode sample changed between the imaging experiments before and after pre-charging. The elevation on the right side of the imaged area was found to be less pronounced after the SEI formation. In combination with the detected height difference of 9 μm in the PACs before and after pre-charging, it was presumed that these changes in morphology are related to a physical swelling of the surface. Studies by Bülter *et al.* [28] were dedicated to the swelling of pristine graphite composites resulting from solvent uptake. It was found that binder additives in the graphite composite could swell immensely after immersion of the electrode in electrolyte solution, and similar dimensions of sample swelling were observed in their experiments.

4.1.3 Conclusion

Within this contribution we have introduced a simple and straightforward SICM method based on the Fc/Fc^+ redox couple, and a reference electrode for usage in LIB electrolyte. Furthermore, we have designed a probe holding system for working with two scanning probe microscopies at the same time. We have employed the setup in the investigation of a LIB graphite electrode treated with a pre-charging protocol by measuring SECM and SICM simultaneously.

The Fc/Fc^+ SICM probes have been tested regarding their signal stability and reproducibility with a micro milled copper circuit board as model substrate. The signal has been found to be most stable at a potential offset of 0.1 V vs. the Fc/Fc^+ reference electrode (corresponding to 3.374 V vs. $\text{Li}/1 \text{ M Li}^+$). PACs have been highly reproducible towards the sample with only minor variations in the total travel distance. Eventually, topographic mapping of the substrate surface has been conducted highlighting the performance of the SICM probes. In further experiments, SICM has been combined with SECM to generate topographical as well as electrochemical activity information of graphite electrodes before and after application of a pre-charging protocol. The findings within these experiments put emphasis on the need of separating the influence of topography and electrochemical activity onto the SECM signal by hyphenation with other scanning probe techniques or other means. This is particularly important in the context of LIB research where typically topography and electrochemical activity of the active electrode material change simultaneously.

The proposed dual-probe approach on SECM/SICM is highly versatile, also enabling hyphenated use of other SPM probes, due to its modular nature. Furthermore, in contrast to a theta-capillary approach, an exchange of defective individual probes is possible. Last, but not least, it is simple to use, with the adjustment of the probe tips being the most complicated step in the setup installation. Then again, the displacement between the active areas of the probe tips limits the application of the dual-probe approach in the achievable resolution. Nanoscale investigations would only be feasible by significant reduction of probe sizes, which in turn would result in highly fragile probes and problems in the tip adjustment. In this regard, an approach with several SPM functions in a single probe would be more straightforward. Nevertheless, the presented SECM/SICM method has the potential to deliver new insights into several LIB related topics. Especially the investigation of industrial type of electrode material with distinct surface topography, as the employed Customcells graphite electrode, is a promising research area. Moreover, studies on novel, promising electrode materials which exhibit significant volume changes during lithium (de-)intercalation, e. g. Si-based electrodes, [30] could benefit from simultaneous SECM/SICM mappings.

4.1.4 Experimental section

Chemicals and materials

Dimethyl carbonate (DMC, anhydrous, $\geq 99\%$), ethyl methyl carbonate (EMC, 99%), ethylene carbonate (EC, anhydrous, 99%), ferrocene (Fc, 98%), ferrocenium hexafluorophosphate (FcPF_6 , 97%), and lithium hexafluorophosphate (LiPF_6 , battery grade, $\geq 99.99\%$) were purchased from Sigma–Aldrich (St. Louis, USA). Platinum wire ($r = 6.25 \mu\text{m}$, 99.99%) and platinum wire ($r = 0.25 \text{ mm}$, 99.99%) were purchased from Advent Research Materials (Oxford, UK) and Goodfellow (Huntingdon, UK), respectively. LIB graphite electrodes (Product ID 11124) were purchased from Customcells (Itzehoe, Germany). Lapping film sheets with particle sizes ranging from 0.1 to $5 \mu\text{m}$ were purchased from Precision Surfaces International (Houston, USA).

All experiments were conducted in a solution of 1.5 mM Fc dissolved in a mixture of EC:EMC (30:70 by wt.) containing 0.1 M LiPF_6 . SICM probes and reference electrodes were prepared with a mixture containing 1.5 mM Fc, 1.5 mM FcPF_6 , and 0.1 M LiPF_6 dissolved in EC:EMC (30:70 by wt.). DMC was used to rinse probes and the electrochemical cell between measurement sessions.

SECM and SICM probe fabrication

SECM probes were fabricated from soda-lime glass capillaries and platinum wire ($r = 6.25 \mu\text{m}$, 99.99%). The tips of the probes were treated with a custom-made polishing device equipped with lapping film sheets with particle sizes ranging from 0.1 to 5 microns. Regular SECM measurements were performed with a flat probe tip. For SECM/SICM hybrid measurements, the tip of the SECM probe was polished at a 15-degree angle countering the effect of the tilted position in the dual-probe holder. SICM probes were fabricated from soda-lime glass capillaries. Opening diameters of 10 to $30 \mu\text{m}$ were achieved by defined polishing of the tip. The capillaries were then filled with electrolyte solution (EC:EMC 30:70 by wt., 0.1 M LiPF_6 , 1.5 mM Fc, 1.5 Mm FcPF_6), and a platinum wire ($r = 0.25 \text{ mm}$, 99.99%) was inserted. A detailed description of the probe fabrication can be found in the supporting information, section SI-1.

Experimental setup

Experiments and procedures were conducted in an Argon-filled glovebox. Furthermore, the SECM setup was placed on a dampening mat inside a custom-made Faraday cage.

Measurements were conducted with a SECM 920 C system from CH Instruments (Austin, USA) equipped with an electrochemical cell made from polytetrafluoroethylene. Working electrode channel 1 was connected to the SECM probe or to the graphite sample during the pre-charging protocol, respectively. Channel 2 was connected to the SICM probe. As a reference electrode, a platinum wire inserted into a glass tube with a ceramic frit and filled with electrolyte solution (EC:EMC 30:70 by wt., 0.1 M LiPF₆, 1.5 mM Fc, 1.5 mM FcPF₆) was used. Auxiliary electrode was a platinum wire. These reference and auxiliary electrodes were utilized in all experimental procedures. Potentials stated within this work were measured with this electrode setup and recalculated to a Li/1 M Li⁺ reference system based on the open circuit potential of the Fc/Fc⁺ reference of +3.274 V vs. Li/1 M Li⁺. A schematic and more instrumental details of the setup are supplied in the supporting information, section SI-2.

Hybrid SECM/SICM measurements were possible due to the use of two probes at once. This was achieved by an in-house built dual-probe holding system shown in Figure 4.1.6. The probe holder was made from polyether ether ketone. Two probes could be mounted and installed in the SECM setup at once. In this approach, one probe is installed at a 15-degree angle, which allowed the positioning of both tips in close proximity to each other. The SECM probe was installed in the tilted position and therefore also polished at a 15-degree angle as described before. The distance between the active tip parts (micro disk electrode and capillary orifice) was estimated to be approximately 250 μm by inspection with an optical microscope. The probe holding system is described in more detail in the supporting information, section SI-3.

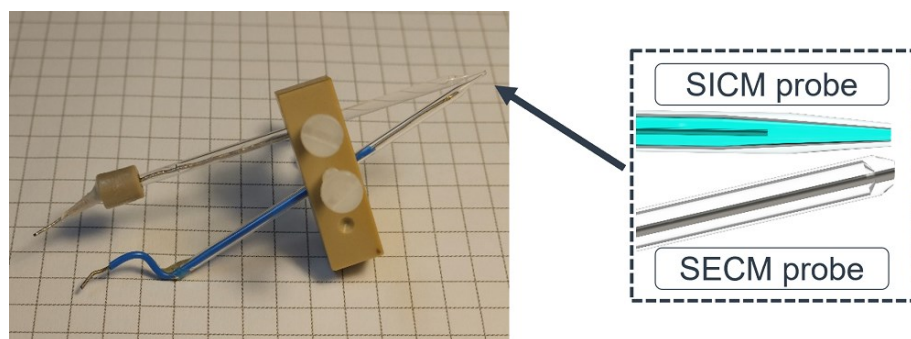


Figure 4.1.6. SECM/SICM dual-probe assembly utilized in the experiments. Photograph of the in-house built dual-probe holder with installed SECM and SICM probes and scheme highlighting the probe tip positioning. The distance between the SECM probe micro disk electrode and the opening of the SICM capillary is approximately 250 μm.

Two different samples were investigated. As a model substrate in the development of the SICM method, a micro milled copper circuit board was used. Channels with a width of 200 μm were milled into the substrate's surface. Hybrid SECM/SICM measurements were performed with LIB graphite electrodes from Customcells. Samples with a diameter of 4 mm were obtained from a larger foil using a punching iron. For measurements, the small sample was placed on a sample holder made from polyether ether ketone and installed in the electrochemical cell. Microscopic images and surface roughness parameters of the graphite electrode samples were obtained from a VK-X3000 3D laser scanning microscope from Keyence (Neu-Isenburg, Germany).

Experimental procedures

For experiments, the samples were installed in the electrochemical cell, which was filled with 5 mL of mediator solution (1.5 mM Fc and 0.1 M LiPF_6 in EC:EMC). Within a measurement session, solvent evaporation, essentially the EMC component, takes place. For the typical duration of a session, the changes were in an acceptable range. The slight signal increase of bulk current resulting from the concentration increase of Fc was considered in the results. Levelling was achieved by subsequent probe approach and probe scan curves (PSC) until the substrate tilting was sufficiently corrected for imaging experiments.

Initially, a suitable potential bias of the SICM probe was determined with chronoamperometric measurements. Potential biases of 3.174 V, 3.374 V, and 3.474 V were applied to the SICM electrode, and the current signal was recorded for 15 min. In the proof-of-concept SICM experiments, PACs and images were recorded with a potential of 3.374 V. Quiet time before start of current recording was 15 s. PACs were conducted with a maximum approach speed of 10 $\mu\text{m s}^{-1}$. Images were recorded with a scan speed of 200 $\mu\text{m s}^{-1}$, pixel size was 10 μm , and an area of 1000 \times 1500 μm was covered. The SICM probe tip had an opening diameter of 30 μm and a total tip diameter of 150 μm . During imaging, the SICM tip was positioned at a constant height, corresponding to a normalized tip current of 0.7 at the starting point of the measurement.

Prior to the hybrid measurements, the SECM/SICM dual-probe assembly was carefully adjusted under a digital microscope camera. The correct adjustment was verified by PACs towards the sample surface until a satisfactory signal change in both SPM techniques was achieved. In the simultaneous SECM/SICM experiments, PACs and images were recorded with a probe potential of 3.374 V (SICM) or 3.574 V (SECM), respectively. Quiet time before start of current recording was 15 s. PACs were conducted with a maximum approach speed

of $10 \mu\text{m s}^{-1}$. Images were recorded with a scan speed of $100 \mu\text{m s}^{-1}$, pixel size was $5 \mu\text{m}$ and an area of $500 \times 1000 \mu\text{m}$ was covered. The SICM probe tip had an opening diameter of $20 \mu\text{m}$ and a total tip diameter of $100 \mu\text{m}$. The SECM tip had a total tip diameter of approximately $90 \mu\text{m}$ and a micro disk diameter of $12.5 \mu\text{m}$. During imaging, the probe tips were positioned at a height of approximately $7 \mu\text{m}$ above the surface at the imaging starting point.

After the initial morphology and electrochemical activity mapping of the pristine sample, the connection of WE1 was changed from the SECM probe to the graphite electrode and the pre-charging protocol was started. This procedure applied to the graphite electrode samples was adapted and modified from similar experimental conditions reported in literature. [9–11] It consisted of a linear potential sweep from 3.274 to 1.274 V with a scan rate of 1 mV s^{-1} followed by cycling in the potential range of 1.274 to 0.040 V with a scan rate of 1 mV s^{-1} for two full cycles.

Subsequently, following the completion of the pre-charging protocol, WE1 was connected to the SECM probe again and hybrid SECM/SICM measurements with identical parameters than before pre-charging were conducted.

4.1.5 Supporting information

SI-1 SECM and SICM probe fabrication

SECM and SICM probes were fabricated from soda-lime glass (inner diameter 1.15 mm) from Hilgenberg (Malsberg, Germany). Glass capillaries were pulled in a butane flame from the base material and controlled with a digital microscope camera. Capillaries with inner tip diameters of approx. 100 μm were used for further fabrication steps.

In the case of a SECM probe, a 1 cm piece of platinum wire ($r = 6.25 \mu\text{m}$, 99.99% purity) from Advent Research Materials (Oxford, UK) was soldered to a jumper wire (cross-section 0.2 mm², outer diameter 1.1 mm). The wire was then carefully inserted into the glass capillary until approx. 1 mm of the platinum protruded from the capillary tip. The similar outer diameter of the jumper wire insulation and the inner diameter of soda-lime glass resulted in mechanical stability of the probe. The glass at the capillary tip of the probe was molten resulting in an insulating glass layer around the platinum wire. Afterwards, the probe was installed in a laboratory-made polishing device. Essentially, the device consists of a rotating disk with a mounted lapping film sheet of 0.3 μm particle size from Precision Surfaces International (Houston, USA) and a probe holder with adjustable angle between probe and rotating polishing disk. An angle of 15° was set and the probe was carefully polished, resulting in a mirror finish disk-like ultramicroelectrode with varying R_g values. The tip quality and the R_g value were evaluated with an optical microscope with 100x magnification. Finally, the SECM probe was tested regarding its electrochemical behaviour by recording CVs in 1.5 mM Fc solution (0.1 M LiPF₆, EC:EMC 30:70 by wt.).

The fabrication of a SICM probe started with re-sealing the tip of a pulled soda-lime glass capillary in a butane flame. Then, the capillary was installed in the laboratory-constructed polishing device with an angle of 0° set between the polishing disk (0.3 μm particle size) and the capillary. The polishing procedure was stopped, after a small opening at the tip was polished free, with opening diameters in the range of 10 to 30 μm . Furthermore, the total tip diameter was reduced, by tilting the capillary and carefully polishing while rotating the capillary. Eventually, capillaries with total tip diameters of approx. 100 μm and circular shape were achieved as determined by inspection under an optical microscope. Residues of the polishing lapping sheets in the capillary opening were removed by repeated flushing, first with water, then with acetone. After drying for at least one hour, the capillary was introduced into the glovebox. It was filled with electrolyte solution (EC:EMC 30:70 by wt., 0.1 M LiPF₆, 1.5 mM Fc, 1.5 mM FcPF₆), a platinum wire with a radius of 0.25 mm (99.99% purity, Goodfellow Oxford UK) was inserted, and it was sealed with a custom-made cap made from polyether ether

ketone. The signal stability of the finished SICM probe was evaluated with chronoamperometric measurements in 1.5 mM Fc solution (0.1 M LiPF₆, EC:EMC 30:70 by wt.).

SI-2 Instrumental setup

All experiments were carried out with a SECM 920C system from CH Instruments (Austin, USA). In Figure 4.1.S1, a schematic depiction of the SECM setup is shown. The computer, bipotentiostat, and positioning control unit are positioned outside of the glovebox. Cable connections to the SECM motors and the electrodes are fed through gas-tight connectors to the inside of the Argon-filled glovebox. Inside the glovebox, the electrochemical setup and the SECM motor unit are placed on a dampening mat within a custom-made Faraday cage to minimize electromagnetic interferences and signal distortions resulting from vibrations. The electrochemical cell was made from polytetrafluoroethylene and it can be filled with approximately 5 mL of solvent. Experimental procedures were conducted with either a three-electrode arrangement (stand-alone SICM and pre-charging), or a four-electrode arrangement (hybrid SECM/SICM measurements). In all cases, a platinum wire was placed in the bulk solution and used as auxiliary electrode. The reference electrode consisted of a platinum wire inserted into a glass tube with a ceramic frit on its lower end. It was filled with electrolyte solution (EC:EMC 30:70 by wt., 0.1 M LiPF₆, 1.5 mM Fc, 1.5 mM FcPF₆) and closed on the upper end with a polytetrafluoroethylene cap. Working electrode channel 1 was connected to the SECM probe in hybrid measurements. During pre-charging it was connected to the Customcells graphite electrode sample, and in the stand-alone SICM measurements it was connected to the SICM probe. The working electrode channel 2 was only used during the simultaneous SECM/SICM measurements and then connected to the SICM probe.

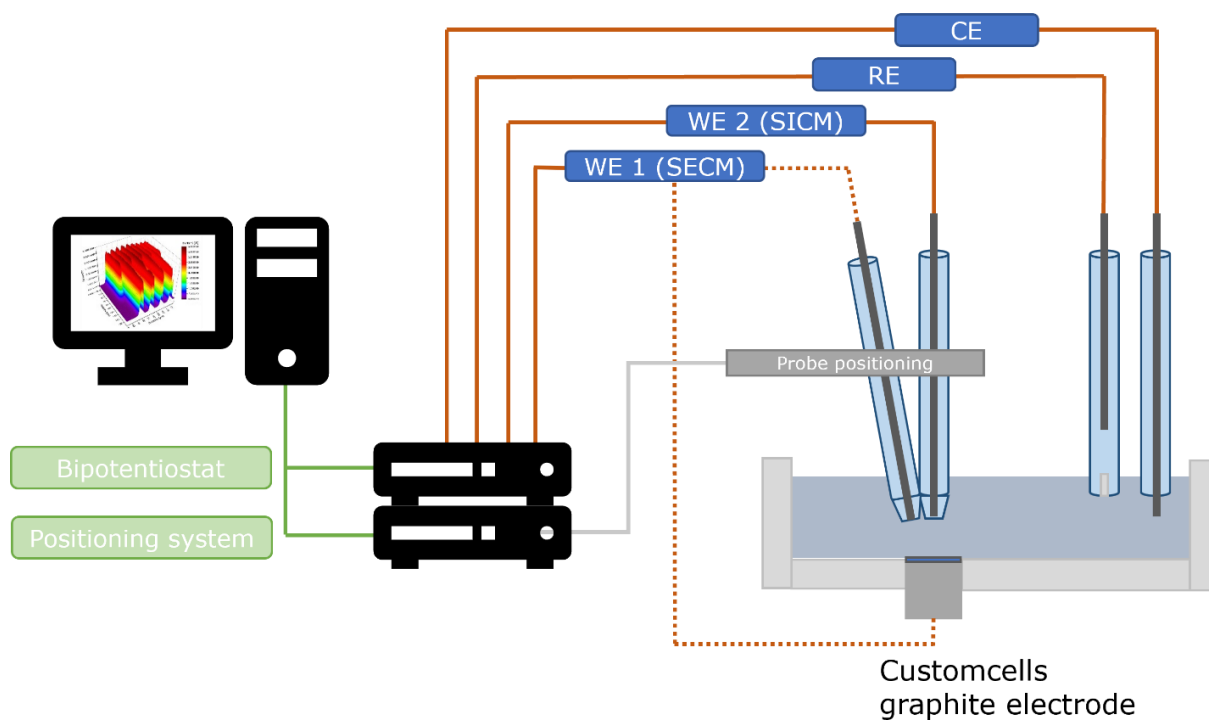


Figure 4.1.S1. Schematic depiction of the SECM setup. Computer, bipotentiostat, and positioning system are outside of the glovebox. Cables are fed through gas-tight connectors to the inside of the Argon-filled glovebox. The electrochemical setup and the SECM motor unit are placed on a dampening plate and installed in a Faraday cage within the glovebox. During SECM/SICM measurements, working electrode channels 1 and 2 are connected to the SECM and SICM probes, respectively. For the pre-charging procedure, working electrode channel 1 is connected to the graphite electrode. Reference electrode was a Fc/Fc^+ based electrode, and counter electrode was a platinum wire.

SI-3 Dual-probe holder blueprints

The dual-probe holding system plays a major role within this publication. It consists of two parts, the main part, and the probe block. The wide side of the main part is mounted to the motor unit of the SECM device. A blueprint is given in Figure 4.1.S2. It is fabricated from polyether ether ketone. On the slim end of the part a magnet is implemented in a small borehole (diameter 7 mm, depth 2 mm), which enables easy installation of the probe block. Afterwards the probe block can be fixated with two M3 screws from the left and right side. In Figure 4.1.S3, the probe block for usage of two SPM probes simultaneously is shown. It also is fabricated from polyether ether ketone with a second magnet in the rear-facing end. One probe is mounted with no tilting, while the hole for the second probe was drilled in a 15°-angle. Both probes are fixated with additional M3 screws from the left and the right side, which also enables a precise arrangement of the probe tips closely next to each other. In the present works, the SICM probe was installed with no tilting and the SECM probe was installed with the 15°-angle tilting.

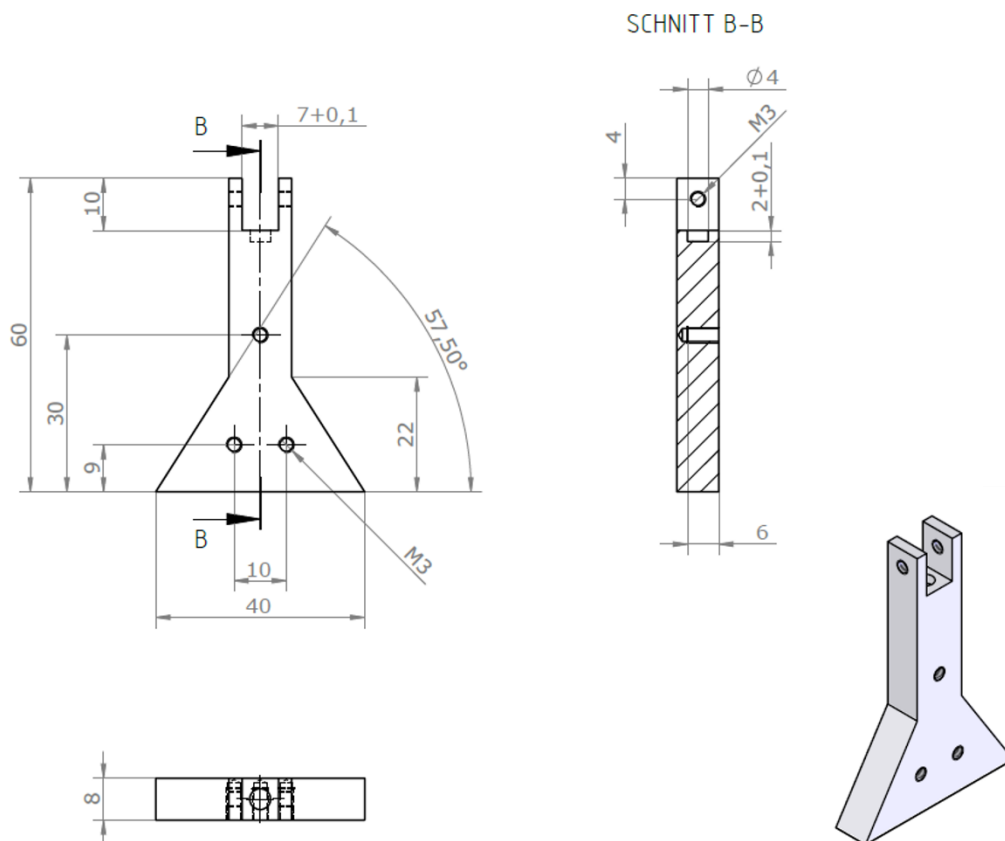


Figure 4.1.S2. Blueprint of the main part of the dual-probe holder made from polyether ether ketone. The main part is mounted on the SECM positioning unit with three M3 screws. The probe block (depicted in Figure 4.1.S3) is inserted in the upper part, hold in place via magnets and fixated with two M3 screws.

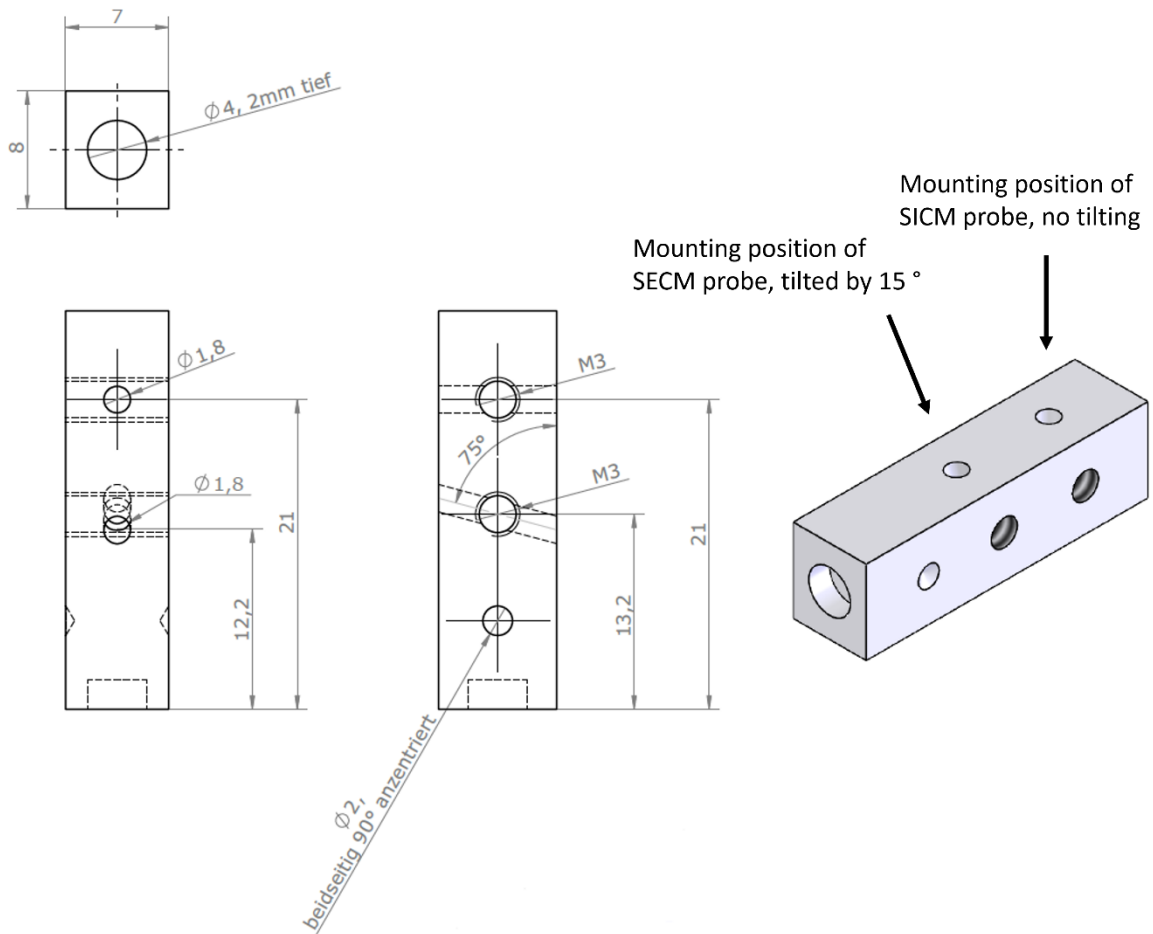


Figure 4.1.S3. Blueprint of the probe block made from polyether ether ketone. The block with installed SECM and SICM probes can be mounted in the front of the main part. It is held in position via magnets in both parts and fixated with two M3 screws. Probes are fixated with two M3 screws each. One probe (SECM) is positioned at a 15° -angle, the other one (SICM) with no tilting.

References

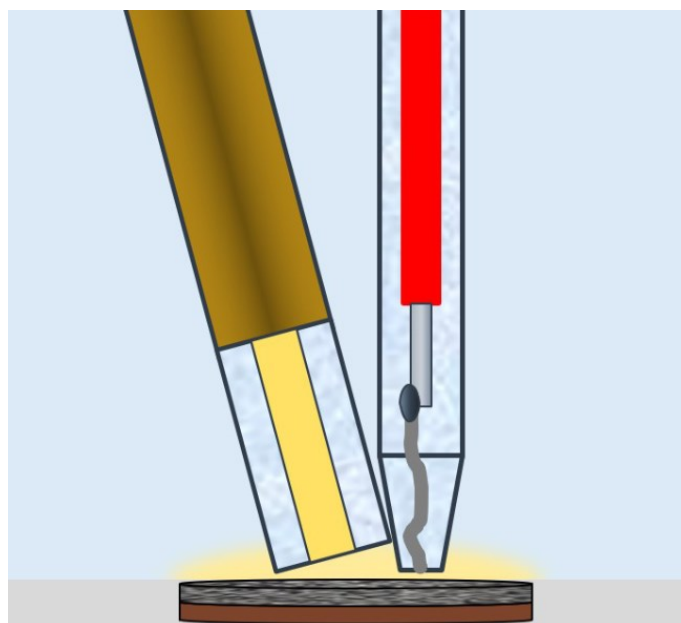
- [1] C. Villevieille, *Adv. Mater. Inter.* 2022, 9, 2101865.
- [2] A. Kumatani, T. Matsue, *Curr. Opin. Electrochem.* 2020, 22, 228.
- [3] R. Kempaiah, G. Vasudevamurthy, A. Subramanian, *Nano Energy* 2019, 65, 103925.
- [4] S. Megahed, B. Scrosati, *J. Power Sources* 1994, 51, 79.
- [5] E. Peled, S. Menkin, *J. Electrochem. Soc.* 2017, 164, A1703–A1719.
- [6] H. Bülter, F. Peters, J. Schwenzel, G. Wittstock, *Angew. Chem. Int. Ed.* 2014, 53, 10531.
- [7] S. Daboss, T. Philipp, K. Palanisamy, J. Flowers, H. S. Stein, C. Kranz, *Electrochim. Acta* 2023, 453, 142345.
- [8] P. Schwager, H. Bülter, I. Plettenberg, G. Wittstock, *Energy Technol.* 2016, 4, 1472.
- [9] G. Zampardi, S. Klink, V. Kuznetsov, T. Erichsen, A. Maljusch, F. La Mantia, W. Schuhmann, E. Ventosa, *ChemElectroChem* 2015, 2, 1607.
- [10] G. Zampardi, F. La Mantia, W. Schuhmann, *Electrochem. Commun.* 2015, 58, 1.
- [11] X. Zeng, D. Liu, S. Wang, S. Liu, X. Cai, L. Zhang, R. Zhao, B. Li, F. Kang, *ACS Appl. Mater. Interfaces* 2020, 12, 37047.
- [12] A. J. Bard, M. V. Mirkin, *Scanning electrochemical microscopy*, CRC Press, Boca Raton, 2012.
- [13] F. M. Weber, I. Kohlhaas, E. Figgemeier, *Molecules* 2022, 27, 1737.
- [14] a) T. Raith, A. Kröninger, M. J. Mickert, H. H. Gorris, F.-M. Matysik, *Talanta* 2020, 214, 120844; b) D. Zhan, X. Li, A. B. Nepomnyashchii, M. A. Alpuche-Aviles, F.-R. F. Fan, A. J. Bard, *J. Electroanal. Chem.* 2013, 688, 61.
- [15] M. Zelenský, J. Fischer, S. Baluchová, L. Klimša, J. Kopeček, M. Vondráček, L. Fekete, J. Eidenschink, F.-M. Matysik, S. Mandal, et al., *Carbon* 2023, 203, 363.
- [16] A. Hengstenberg, C. Kranz, W. Schuhmann, *Chem. Eur. J.* 2000, 6, 1547.
- [17] D. Liu, X. Zeng, S. Liu, S. Wang, F. Kang, B. Li, *ChemElectroChem* 2019, 6, 4854.
- [18] a) C. Kranz, G. Friedbacher, B. Mizaikoff, A. Lugstein, J. Smoliner, E. Bertagnolli, *Anal. Chem.* 2001, 73, 2491; b) K. Mahankali, N. K. Thangavel, L. M. Reddy Arava, *Nano Lett.* 2019, 19, 5229.
- [19] P. K. Hansma, B. Drake, O. Marti, S. A. Gould, C. B. Prater, *Science* 1989, 243, 641.
- [20] C. Zhu, K. Huang, N. P. Siepser, L. A. Baker, *Chem. Rev.* 2021, 121, 11726.
- [21] A. L. Lipson, R. S. Ginder, M. C. Hersam, *Adv. Mater.* 2011, 23, 5613.

- [22] A. L. Lipson, K. Puntambekar, D. J. Comstock, X. Meng, M. L. Geier, J. W. Elam, M. C. Hersam, *Chem. Mater.* 2014, 26, 935.
- [23] Y. Takahashi, D. Takamatsu, Y. Korchev, T. Fukuma, *JACS Au* 2023, 3, 1089.
- [24] a) S. Wert, S. Baluchová, K. Schwarzová-Pecková, S. Sedláková, A. Taylor, F.-M. Matsyk, *Monatsh. Chem.* 2020, 151, 1249; b) Y. Takahashi, A. I. Shevchuk, P. Novak, Y. Murakami, H. Shiku, Y. E. Korchev, T. Matsue, *J. Am. Chem. Soc.* 2010, 132, 10118.
- [25] G. Inzelt, A. Lewenstam, F. Scholz, *Handbook of reference electrodes*, Springer, New York, 2013.
- [26] a) T. N. P. Truong, H. Randriamahazaka, J. Ghilane, *Electrochem. Commun.* 2016, 73, 5; b) D. Sarbapalli, A. Mishra, J. Rodríguez-López, *Anal. Chem.* 2021, 93, 14048.
- [27] DIN EN ISO 25178–1 : 2016-12, Geometrische Produktspezifikation (GPS) – Oberflächenbeschaffenheit: Flächenhaft – Teil 1: Angabe von Oberflächenbeschaffenheit (ISO 25178-1 : 2016); Deutsche Fassung EN_ISO_25178-1: 2016, Beuth Verlag, Berlin, 2016.
- [28] H. Bültel, F. Peters, J. Schwenzel, G. Wittstock, *J. Electrochem. Soc.* 2016, 163, A27–A34.
- [29] M. Tang, J. Newman, *J. Electrochem. Soc.* 2012, 159, A1922–A1927.
- [30] a) P. Bärmann, B. Krueger, S. Casino, M. Winter, T. Placke, G. Wittstock, *ACS Appl. Mater. Inter.* 2020, 12, 55903; b) T. Tarnev, P. Wilde, A. Dopilka, W. Schuhmann, C. K. Chan, E. Ventosa, *ChemElectroChem* 2020, 7, 665.

4.2 Development of an *in situ* mediator dosing concept for scanning electrochemical microscopy in lithium-ion battery research

Eidenschink Johannes, Matysik Frank-Michael
ChemElectroChem 11 (2024) e202400311.

Unpublished data was added to this chapter as section 4.2.6.



Abstract

In scanning electrochemical microscopy (SECM), the addition of a redox active species plays an essential role. Those deliberately added mediators may alter results in SECM studies. In investigations of lithium-ion battery (LIB) materials, especially of the positive electrode, the oxidation potentials of commonly used mediator substances such as ferrocene are located within the operation potential of the electrode. Thus, they possibly interfere with the regular charge/discharge processes. *In situ* studies are therefore in need of approaches reducing or eliminating the use of mediators. Within this publication, a novel mediator dosing (MD) concept is introduced. A capillary was closely positioned at the tip of the scanning probe. By gravity flow, stable flow rates of mediator solution of up to $32.4 \pm 0.6 \mu\text{L h}^{-1}$ were achieved. These low

amounts were found to be sufficient to form a ferrocene zone at the probe tip enabling feedback mode SECM measurements with comparable quality to measurements directly in ferrocene solution. Proof of concept experiments were conducted by investigation of a thin-film electrode with a micro-structured surface. Furthermore, the MD concept was applied in imaging experiments of a commercially available LIB graphite electrode.

4.2.1 Introduction

In recent years, lithium-ion batteries (LIBs) gained more and more importance due to their countless applications, for example electromobility and energy storage. [1–3] This type of secondary cell generally consists of two electrodes, positive and negative, a separating, porous membrane, and electrolyte. [4]

Much effort was and still is dedicated to further optimization of those basic components regarding battery life, operation safety, and energy density. [5] Commercial LIBs mainly utilize state-of-the-art materials capable of intercalating lithium ions during charge/discharge cycles. The most widely applied material as negative electrode is graphite due to low cost, low toxicity, and long cycle life. [2,6] A common material for the positive electrode is LiCoO_2 , but the demand for higher energy densities has driven the development of materials operating at higher potentials such as lithium nickel manganese cobalt oxides (NMC). [3]

The operation of a LIB includes repeated insertion of lithium into the host materials and redissolution. Therefore, LIBs are also called “rocking-chair batteries”. [7] The potentials reached during those cycles may exceed the electrochemical stability window of the electrolyte, resulting in its degradation and the formation of interphases between electrode and electrolyte. [1] In the case of the negative electrode, the newly formed interphase is called solid electrolyte interphase (SEI). [8] It inhibits further degradation of the electrolyte and is therefore a prerequisite for safe and stable operation of a LIB. For positive electrodes, the formation of an interphase and its nature is still controversial and a hot topic in LIB research. [9] Sophisticated analytical techniques are needed to drive further improvements in LIBs. Scanning probe microscopies (SPMs) are a family of microscopic techniques which can be applied in LIB research *in situ* and even *in operando*. [10,11]

Amongst others, scanning electrochemical microscopy (SECM) [12] is part of that group. An ultramicroelectrode (UME), often a platinum disk, is used as probe. By application of a suitable potential, a usually deliberately added redox-active substance, the so-called mediator, is either oxidized or reduced. The resulting tip current delivers information about the electrochemical activity as well as the topography of a substrate’s surface. [13] In the scope of LIBs, an extensive number of studies were conducted including SECM as characterisation technique. [14] Topics range from SEI formation on different electrode materials, [15,16] swelling of composite electrodes, [11] hyphenation of SPMs, [17,18] to, more rarely, the study of positive electrode materials. [19] Most works consider possible interfering effects [20] due to the deliberately added mediator in some way or another. In the study of Zampardi *et al.* [18] on the SEI formation on glassy carbon, the formation protocol is conducted in pure electrolyte without added mediator, followed by an exchange of solutions to mediator-containing

electrolyte. The same approach of an electrolyte change between procedures was used in several other LIB investigations with SECM. [15,21] As careful as this exchange may take place, changes in the surface properties can't be fully ruled out. Another approach is to operate the investigated battery electrode in solution with the mediator already present during cycling. This method was applied in the studies of Zeng *et al.* [22] in their investigation of temporal changes of the SEI after various numbers of charge/discharge cycles. Similarly, the mediator was also present during the formation protocols in other publications. [16,17,23] Although the redox potentials of commonly used mediators ferrocene (Fc) [16-18,22,24] and 2,5-di-*tert*-butyl-1,4-dimethoxybenzene [11,15,24] lie outside of the regular operating potentials of negative electrodes, their influence on the complex formation processes of the SEI should not be neglected as they can potentially alter SEI properties. [25] For investigations of positive electrode materials, the interference of mediators is more severe, as supported by Zampardi *et al.* [19] in their study of the positive electrode/electrolyte interface in LIBs.

In the scope of this contribution, an alternative approach to minimize mediator interferences is introduced. By highly localized dosage of mediator solution at the SECM probe tip, the overall mediator concentration in the battery cell is drastically reduced. The gravity flow of mediator solution in the proposed setup is controlled by adjusting a height difference between inlet and outlet solvent levels of a dosing capillary. Proof-of-concept measurements with a micro-structured thin-film electrode as model substrate were conducted. As a possible application, feedback mode SECM images of a commercial LIB graphite electrode were recorded under MD conditions and compared to images recorded directly in mediator-containing electrolyte.

4.2.2 Results and discussion

The novel approach on feedback mode SECM with minimized mediator usage was designed with several requirements in mind. First, the data quality should be as close to regular SECM measurements in mediator solution as possible. Second, the amount of deliberately added mediator should be kept at a minimum. Third, the overall setup should be as simple as possible, i. e. no complicated probe fabrication. Those requirements were met by utilization of a dosing capillary mounted together with a regular SECM probe in a previously described dual-probe holder. [17]

Similar approaches utilizing the dosage of solutions in the context of SPM measurements could be found in literature. Two recent examples should be mentioned here. Asserghine *et al.* [26] employed a micro sized pipette installed in the probe positioning system of a SECM device to dose defined volumina of an oxygen containing solution. In their approach comparable to the microjet electrode [27] and pioneering works by Engstrom [28] the solution is dosed by the pipette and the signal collection is achieved by the substrate, which was termed as pumped-micropipette delivery/substrate collection mode (Pumped-MD/SC) of SECM. This novel variation of the MD/SC mode of SECM [29] was then used in the investigation of the oxygen reduction reaction during the corrosion of a model system of copper-rich aluminium alloys. The second approach which is related to the MD concept was used in the study of the SEI formation conducted by Muñoz Torrero *et al.* [30] In their research a redox-mediated scanning droplet cell [31] was used to deliver a series of different solutions in a fixed position on the sample surface. This setup enabled the SEI formation with no mediator present followed by investigation of the passivation properties using Fc.

Determination of gravity-driven flow rates at various height differences

Gravity flow in the context of capillary-based setups was introduced by Matysik *et al.* [32] in 1993. In their original works the adjustment of the height difference between the liquid levels in inlet and outlet reservoirs resulted in well-defined introduction of sample solution into a fused-silica capillary. This capillary flow injection analysis (CFIA) system was then applied in the determination of trace metals in tear samples. The obtained gravity flow was found to be highly reproducible and stable for extended time periods. To determine the amount of mediator introduced into the bulk solution by the MD approach, chronoamperometric experiments with varying height differences were performed. Measurements were conducted in triplicates for each height difference. An exemplary i-t curve is shown in Figure 4.2.1A. After a certain time,

the mediator solution inside the dosing capillary reaches the outlet end and subsequently the platinum macro electrode, resulting in an increasing current signal from the oxidation of Fc. The average times until the oxidation signals were detected are summarized in Table 4.2.1. By application of a height difference of 5 cm, in average, a time interval of 12.9 ± 0.2 min passed until the Fc solution reached the macro electrode. Doubling the height difference to 10 cm resulted in a decrease of the time interval to an average of 7.2 ± 0.1 min. At the maximum height difference of 15 cm achievable in the design of the MD concept, an average signal time of 5.1 ± 0.1 min was determined. With the help of equation 4.2.1, the flow rates could be calculated.

$$flow\ rate = \frac{V_{capillary}}{t_{Fc\ signal}} = \frac{\pi \cdot r_{capillary}^2 \cdot l_{capillary}}{t_{Fc\ signal}} \quad (4.2.1)$$

with $V_{capillary}$: volume of dosing capillary; $t_{Fc\ signal}$: time interval until oxidation signal of Fc was detected; $r_{capillary}$: inner radius of the capillary; $l_{capillary}$: total length of the dosing capillary.

Flow rates were determined to be in the range of 12.8 ± 0.2 (Δ height = 5 cm) up to 32.4 ± 0.6 $\mu\text{L h}^{-1}$ (Δ height = 15 cm). Mathematical fitting of the applied height differences with the corresponding flow rates revealed a linear dependence as shown in the graph in Figure 4.2.1B. By considering the volume of the bulk solution in the electrochemical cell ($V_{cell} = 5$ mL) a more practical parameter was calculated, the temporal change of Fc concentration. Operating the MD setup at a height difference of 15 cm would result in a change of the Fc concentration in the bulk solution of 9.7 $\mu\text{M h}^{-1}$. At a typical measurement session of 6 hours only approximately 200 μL of mediator solution are introduced into the electrochemical cell, less than 4% of the volume of the bulk solution. Since the mediator dosage could be stopped at any time, for example during the charge/discharge of a battery electrode, real values of introduced mediator would be lower. The dosage could be easily stopped by repositioning the capillary inlet out of the mediator solution. Overall, the gravity-driven dosage of mediator solution by applying a height difference between the solvent levels in the inlet and outlet reservoirs (Δ height) of a capillary was found to deliver smooth and stable flow rates and resulted in a minimized introduction of mediator solution into SECM experiments. The comparatively low flow rates couldn't be reproduced in measurements where the dosing was achieved via a syringe pump. Furthermore, the pulsating action of the syringe pump had a distorting effect on SECM images. Therefore, further experiments were solely conducted with the gravity-driven approach. A height difference of 15 cm was chosen, since it showed a good compromise between amount of introduced mediator and achievable SECM data quality.

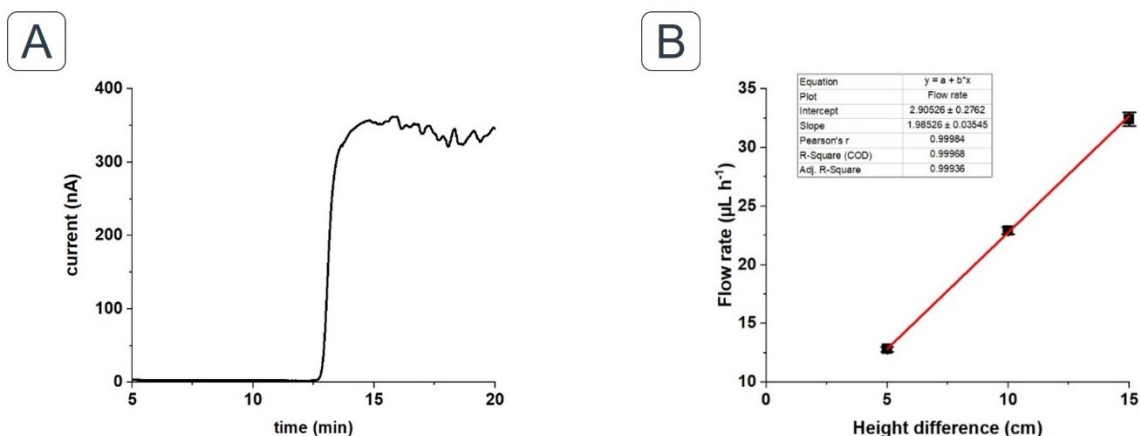


Figure 4.2.1. Determination of flow rates resulting from a height difference between inlet and outlet of the dosing capillary. A) Exemplary amperometric i-t curve recorded with a height difference of 5 cm. B) Dependency on the flow rate from the applied height difference. The outlet of the dosing capillary (OD = 360 μm , ID = 100 μm , length = 35 cm) was positioned closely to the surface of a platinum macro electrode which was used as working electrode. Experiments were conducted in 0.1 M LiPF_6 solution (EC:EMC 30/70), three measurements per height difference. Working electrode potential was 3.574 V vs. Li/1 M Li^+ .

Table 4.2.1. Measured Fc signal times (average of three individual measurements each) in the mediator dosing setup in chronoamperometric experiments at the respective height differences (Δ height). Determined flow rates and resulting dynamic concentration changes in the electrolyte solution based on a volume of 5 mL in the electrochemical cell.

	Δ height = 5 cm	Δ height = 10 cm	Δ height = 15 cm
$\text{time}_{\text{Fc signal}} / \text{min}$	12.9 ± 0.2	7.2 ± 0.1	5.1 ± 0.1
$\text{flow rate} / \mu\text{L h}^{-1}$	12.8 ± 0.2	22.9 ± 0.3	32.4 ± 0.6
$\Delta \text{conc.}_{\text{Fc}} / \mu\text{M h}^{-1}$	3.8 ± 0.1	6.9 ± 0.1	9.7 ± 0.2

Proof-of-concept measurements with a Micrux thin-film electrode as model substrate

After clarifying the flow rates and deciding on a suitable height difference in the mediator dosing setup, measurements with a model substrate were conducted to showcase the performance of the approach. A thin-film electrode with an interdigitated electrode structure (Micrux IDRA1) was chosen for that purpose. First, a series of probe approach curves (PACs) towards conductive and non-conductive parts of the sample surface was performed in order to evaluate the reproducibility and the accordance with theoretical fits for negative [33] and positive [34] feedback PACs. In Figure 4.2.2A, five consecutive PACs under MD conditions over a non-conductive part of the model substrate's surface are shown together with the theoretical, negative feedback PAC calculated according to Cornut *et al.* [33]. The mathematical approximation was obtained for an R_g value of 5.1. Experimental PACs were found to be highly reproducible with minor distance variations of up to 200 nm. A systematic deviation from the theoretical feedback model for negative feedback was found for normalized distances smaller than four. This phenomenon can be explained by the proximity of the dosing capillary to the SECM probe. The practically applicable value for R_g is therefore greater than with a simple probe. Figure 4.2.2B depicts five sequential PACs recorded with the MD setup towards a conductive part of the substrate surface. The mathematic approximation for a purely positive feedback PAC was generated according to Amphlett *et al.* [34] for an R_g value of 5.1. Again, PACs exhibited high reproducibility under MD conditions with deviations up to 500 nm. Experimental data is described very well by the theoretical fit.

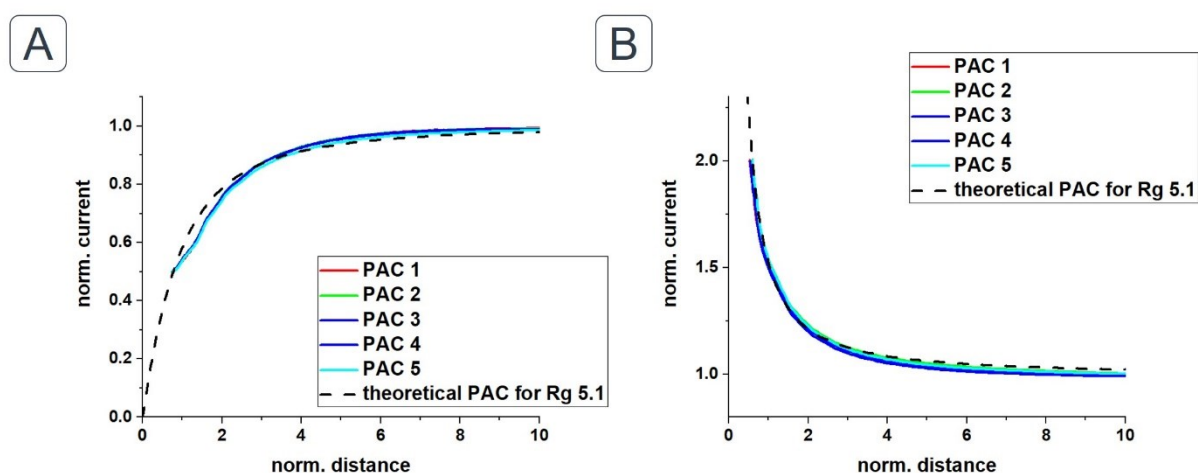


Figure 4.2.2. Consecutive PACs towards the surface of a Micrux thin-film electrode used as a model substrate. A) Five PACs towards a non-conductive part of the thin film electrode surface. B) Five PACs towards a conductive part of the thin film electrode. Measurements were recorded in 0.1 M TBAPF₆ solution (EC:DMC 30/70). Fc solution (1.5 mM in 0.1 M TBAPF₆ EC:DMC 30/70) was dosed via a fused-silica capillary (OD = 360 μ m, ID = 75 μ m, length = 35 cm) by application of a height difference of 15 cm. SECM probe was a platinum UME ($r = 6.25$ μ m, $R_g = 5$). Probe potential was 3.424 V, quiet time of 15 s, maximum approach speed was 2.5 μ m s⁻¹.

After appropriate levelling of the model substrate by a series of PACs and line scans, imaging experiments were started at the highlighted area of the model substrate shown in Figure 4.2.3A. The recorded SECM image in Fc solution can be found in Figure 4.2.3B. Details of the interdigitated electrode structure of the thin-film electrode were well resolved, the electrode bands with a width of 10 μm and a distance between two bands of 10 μm were well visible. The identical area was then imaged by application of the MD setup in electrolyte containing no Fc. Again, the distinct features of the model substrate could be resolved with high quality, conductive and non-conductive parts could be easily differentiated and the gaps between the electrode bands were finely resolved. Overall, the image quality was found to be on par with the image generated in Fc solution. Measured currents were lower in the MD approach, but the contrast given by the ratio of highest and lowest current was identical.

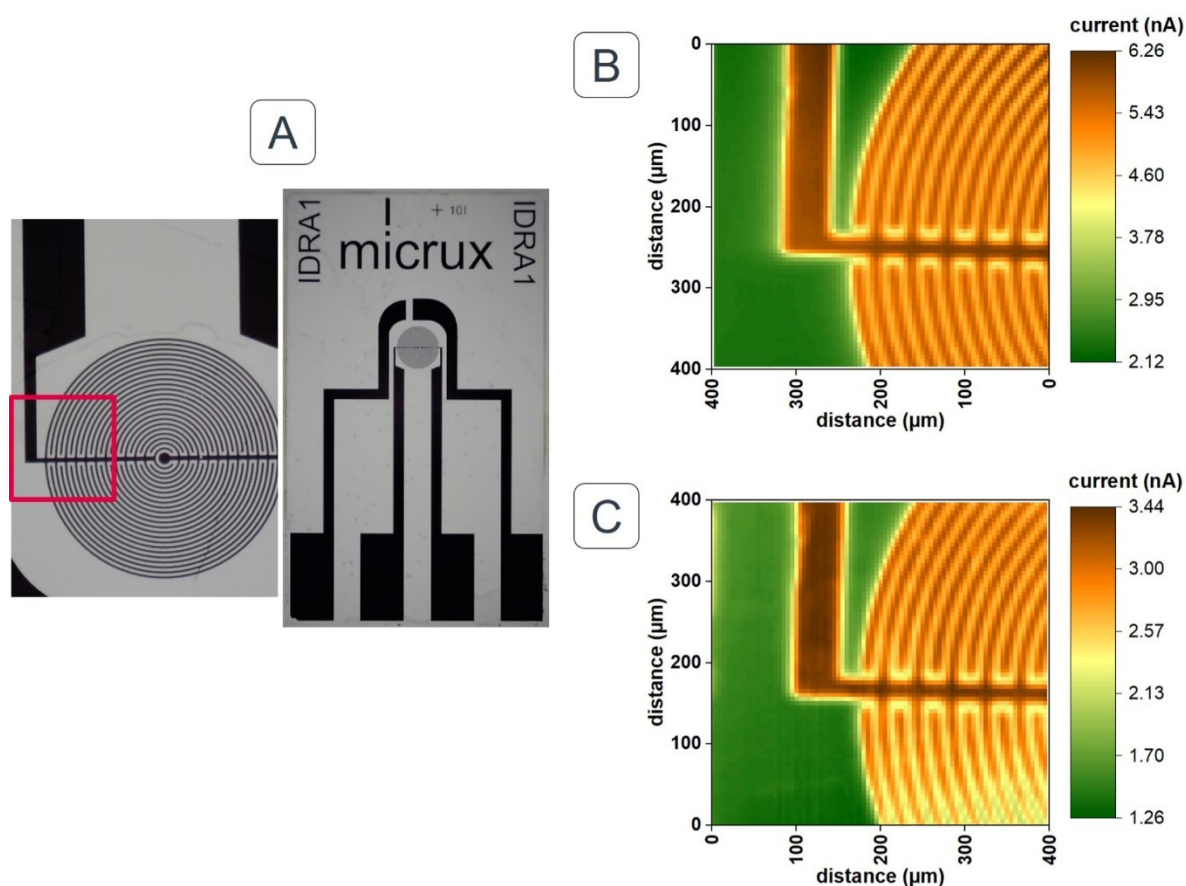


Figure 4.2.3. Model substrate experiments with a Micrux thin-film electrode. A) Microscopic images of a Micrux chip with interdigitated electrode area (10 μm bands with 10 μm spacing). The area imaged in SECM measurements is highlighted in red. B) SECM image recorded in 1.5 mM Fc in 0.1 M LiPF_6 solution (EC:DMC 30/70). C) SECM image recorded in 0.1 M LiPF_6 solution (EC:DMC 30/70). Fc solution (1.5 mM in 0.1 M LiPF_6 EC:DMC 30/70) was dosed via a fused-silica capillary (OD = 360 μm , ID = 100 μm , length = 35 cm) by application of a height difference of 15 cm. SECM probe was a platinum UME ($r = 6.25 \mu\text{m}$, $R_g = 5$). Probe potential was 3.574 V, quiet time of 15 s, movement speed was 100 $\mu\text{m s}^{-1}$.

Investigation of a Customcells LIB graphite electrode

Proof-of-concept studies with a model substrate revealed comparable data quality generated under MD conditions. Further studies were then conducted with a typical battery electrode material to put emphasis on the applicability of the newly developed MD approach. As such, a commercially available LIB graphite electrode from Customcells was chosen. Samples were investigated as received with no further treatment of the surface. Initially, the surface of the graphite electrode was characterised by means of optical microscopy and scanning ion conductance microscopy (SICM), which is another SPM able to map a sample's topography at micro- and nanoscale in a non-contact measurement. [35] In Figure 4.2.4A and B, a microscopic image and a false colour image of the sample are shown. The particles had typical sizes at the micrometre scale. Surface roughness parameters were measured according to ISO 25178 [36] from four randomly chosen areas with a size of $216 \times 289 \mu\text{m}$ each. A core surface roughness S_k of $2.3 \mu\text{m}$ and a maximum height of $9 \mu\text{m}$ were determined for the sample. The SICM image shown in Figure 4.2.4C is coherent with the findings from optical microscopy and furthermore reveals a slight curvature of graphite samples. In the investigated area of $500 \times 500 \mu\text{m}$, a plateau could be found in the middle of the image, which was also found in a series of similar measurements conducted on the same batch of electrode samples.

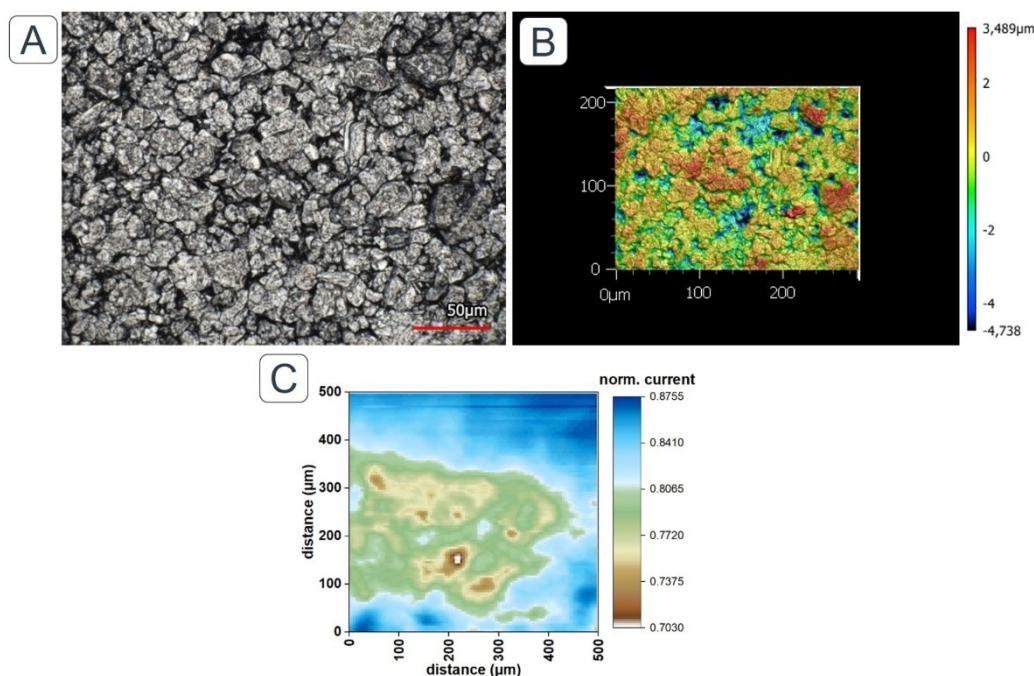


Figure 4.2.4. Customcells graphite electrode for LIBs which was used for investigation with the mediator dosing setup. A) Microscopic image of the graphite electrode surface showing particle size. B) False colour image highlighting the graphite surface roughness. C) SICM image highlighting the topography of the graphite sample. Image was recorded in 0.1 M LiPF_6 solution (EC:EMC 30/70). Probe potential was 3.374 V, quiet time of 15 s, movement speed was $100 \mu\text{m s}^{-1}$.

Eventually, the graphite electrode was investigated by means of feedback mode SECM. After the careful adjustment of dosing capillary and SECM probe, the sample was levelled by a series of PACs and line scans in electrolyte containing no mediator and local dosing of Fc. Subsequently, a SECM image was recorded over a suitable spot of the sample. The image recorded under MD conditions is shown in Figure 4.2.5B. Overall, positive feedback was observed in the investigated area with the exemption of a nonconductive spot at the coordinates (X 370/Y 450). Other local variations of the measurement signal can be explained by the distinct surface topography of the sample, as described before by the results from optical microscopy and SICM. Homogeneous distribution of electrochemical activity is generally assumed for pristine graphite electrodes in literature. [15,22] Following the completion of the SECM image, the solution in the electrochemical cell was exchanged with electrolyte containing 1.5 mM Fc (0.1 M LiPF₆ in EC:EMC 30/70). Subsequently, a SECM image of the identical area at the same starting height was recorded. Distinct surface features, as the non-conductive spot (X 370/Y 450) verified that the position was not changed during the exchange of solutions. Slight differences in the image details could be found. These changes can be explained by the study of Bülter *et al.* [11] who investigated the swelling of graphite composite electrodes in contact with electrolyte. It was found that immense physical swelling of binding agents could occur resulting in a volume expansion of the whole graphite electrode. Furthermore, the process of the solvent swap between measurements could have had a distorting effect. In total, surface details were resolved in excellent image quality by the MD approach while significantly reducing the introduction of mediator into the system.

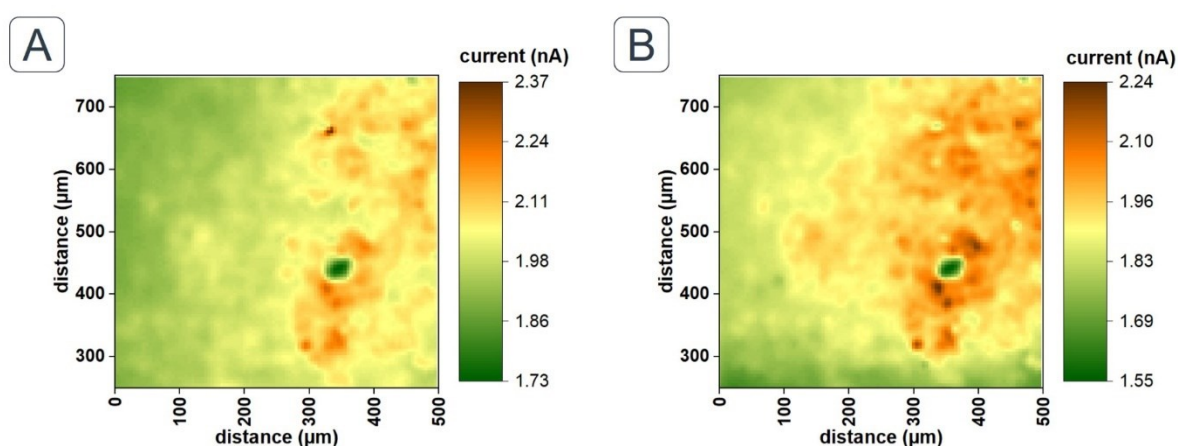


Figure 4.2.5. SECM images of a Customcells graphite electrode. A) SECM image recorded in 1.5 mM Fc in 0.1 M LiPF₆ solution (EC:EMC 30/70). B) SECM image of the graphite electrode recorded in 0.1 M LiPF₆ solution (EC:EMC 30/70). Mediator solution (1.5 mM Fc, 0.1 M LiPF₆, EC:EMC 30/70) was dosed via a fused-silica capillary (OD = 360 μm, ID = 100 μm, length = 35 cm) by application of a height difference of 15 cm. SECM probe was a platinum UME ($r = 6.25 \mu\text{m}$, $R_g = 7$). Probe potential was 3.574 V, quiet time of 15 s, movement speed was $100 \mu\text{m s}^{-1}$.

4.2.3 Conclusion

In this publication, a novel concept on localized dosing of mediator solution in the context of feedback mode SECM was introduced for applications in LIB research. A dosing capillary was used to deliver small amounts of mediator solution driven by application of a height difference between capillary inlet and outlet. The capillary outlet could be positioned precisely near the tip of a regular SECM probe by installation in a custom-made dual-probe holder which was previously utilized in the hyphenation of SECM and SICM. [17]

First experiments were performed to determine the flow rates of mediator solution at various height differences. Chronoamperometric measurements revealed flow rates in the range of 12.8 up to 32.4 $\mu\text{L h}^{-1}$ resulting from height differences of 5, 10, or 15 cm. Within that range a maximum of mediator concentration change of 9.7 $\mu\text{M h}^{-1}$ was determined considering the electrolyte volume in the electrochemical cell ($V_{\text{cell}} = 5 \text{ mL}$). Afterwards, the performance of the newly developed concept was tested with a thin-film electrode as model substrate. Negative and positive feedback PACs towards the surface of the sample revealed remarkable reproducibility as well as good accordance with theoretical approximations for both cases of feedback. The distance deviations between PACs of a set were found to be below 500 nm. Furthermore, the micro-structured electrode area of the model substrate could be finely resolved under MD conditions with image quality comparable to measurements conducted directly in mediator solution. To further test the applicability of the MD approach in feedback mode SECM experiments, a real-world sample was investigated. The LIB graphite composite electrode could be imaged well, again, with quality on par with regular SECM measurements. Surface details resulting from the graphite particles were well visible.

The introduced MD concept was found to meet all the initial requirements, namely minimized mediator use, comparable data quality, and avoidance of complicated probe designs. Possible applications could be *in situ* studies of interphase formation on negative and positive LIB electrodes, while reducing mediator interference during charge/discharge processes to a minimum. Another advantage even for *in operando* setups is the possibility to stop mediator dosage at any given time for example during battery cycling. Furthermore, the setup is not limited to LIB applications. It could be applied in SECM studies of sensitive samples where the usage of typical redox mediators may alter the results, for example in studies of biological cells.

4.2.4 Experimental section

Chemicals and materials

The following chemicals were purchased from Sigma-Aldrich (St. Louis, USA): dimethyl carbonate (DMC, anhydrous, $\geq 99\%$), ethyl methyl carbonate (EMC, 99%), ethylene carbonate (EC, anhydrous, 99%), ferrocene (Fc, 98%), ferrocenium hexafluorophosphate (FcPF₆, 97%), lithium hexafluorophosphate (LiPF₆, battery grade, $\geq 99.99\%$), and tetrabutylammonium hexafluorophosphate (TBAPF₆, $\geq 99\%$). Platinum wires with radii of 6.25 μm (99.99%) and 0.5 mm (99.99%) were purchased from Advent Research Materials (Oxford, UK). Platinum wire with a radius of 0.25 mm (99.99%) was purchased from Goodfellow (Huntingdon, UK). Graphite electrodes for LIBs (Product ID 11124) were acquired from Customcells (Itzehoe, Germany). Thin-film electrodes (Type IDRA1) were purchased from Micrux Technologies (Gijón, Spain). Fused-silica capillaries with an outer diameter of 360 μm and inner diameters of 75 and 100 μm were supplied by Polymicro Technologies (Phoenix, USA). Soda-lime glass tubes with an inner diameter of 1.1 mm were purchased from Technische Glaswerke Ilmenau (Ilmenau, Germany). Lapping film sheets with particle sizes ranging from 0.3 to 30 μm were purchased from Precision Surfaces International (Houston, USA). Two-component adhesive (Epoxy resin L + Hardener S) were acquired from R&G Faserverbundwerkstoffe (Waldenbuch, Germany).

SICM probes were filled with a mixture containing 1.5 mM Fc, 1.5 mM FcPF₆, and 0.1 M LiPF₆ dissolved in EC:EMC 30/70. Fc/Fc⁺ based reference electrodes [37] were prepared with 1.5 mM Fc, 1.5 mM FcPF₆, and 0.1 M LiPF₆ dissolved in either EC:EMC 30/70 or EC:DMC 30/70. DMC was used to rinse and clean SPM probes and the electrochemical cell.

SPM probe and dosing capillary fabrication

SPM probes were prepared from soda-lime glass, which was pulled to pipettes with opening diameters of approximately 100 μm in a butane flame. In the case of a SECM probe, a platinum wire ($r = 6.25 \mu\text{m}$) soldered to a piece of jumper wire was carefully inserted into a glass pipette until it was protruding circa 1 mm from the tip. Afterwards the platinum wire was sealed in the glass tip and subsequently exposed again by polishing in a custom-made polishing device. Resulting SECM probes had a mirror-finish disk electrode and R_g values of ca. 5 – 7. SICM probes were manufactured according to the previously published instructions. [17] A glass capillary with a tip opening diameter in the range of 10 – 30 μm was filled with electrolyte

solution, and a platinum wire ($r = 0.25$ mm) was inserted. Fused-silica capillaries with inner diameters of 75 or 100 μm were used as dosing capillaries. A piece with a length of 35 cm was cut from the base material with a ceramic cutter. Afterwards, approximately 0.5 cm of the polyimide coating was removed from both sides. Tips were polished with the polishing device and lapping film sheets with particle sizes of 30 μm (first step, coarse polishing) and 1 μm (second step, fine polishing) to a clean, flat finish. Subsequently, a glass hull enabling the installation in the dual-probe holder was glued to the capillary.

A more detailed description of the SPM probe and dosing capillary fabrication steps is supplied in the supporting information, section SI-1.

Experimental setup

All experiments, sample preparation steps and parts of the SPM probe and dosing capillary fabrication were carried out in an Argon-filled glovebox. Within the glovebox, the electrochemical setup and the positioning motor unit were placed on a dampening mat located inside a laboratory-constructed Faraday cage.

A commercial SECM 920C system from CH Instruments (Austin, USA) was used in combination with electrochemical cells made from polytetrafluoroethylene. The working electrode channel was either connected to the SPM probe in SECM experiments or to a platinum macro-electrode in the flow rate determination. The auxiliary electrode was a platinum wire. A Fc/Fc^+ based reference electrode, briefly a platinum wire immersed in Fc/Fc^+ containing electrolyte, was utilized in most measurements. All potentials within this publication are recalculated to a $\text{Li}/1$ M Li^+ reference system based on the open circuit potential of the Fc/Fc^+ reference of +3.274 V vs. $\text{Li}/1$ M Li^+ .

The dosing of mediator solution was enabled by usage of a laboratory-constructed dual-probe holder. [17] It is possible to mount two probes at once, where one probe is installed in upright position while the second one is tilted by a 15° -angle. In Figure 4.2.6, the mediator dosing setup is illustrated. A capillary is used to locally dose a 1.5 mM Fc solution in close proximity to the SECM probe tip. The capillary was pre-flushed with Fc solution by application of a pressure pulse via the septum of the inlet vial while the assembly was positioned far away from the substrate. A height difference between inlet and outlet (Δ height) results in a defined, gravity-driven flow of the solution forming a Fc zone near the platinum disk electrode. Tips of SECM probe and dosing capillary were carefully aligned under a digital microscope camera. The scan direction for the high frequency axis during imaging experiments is shown in Figure 4.2.6B, the pipette was ahead of the SECM probe.

Two different substrates were utilized in the evaluation of the mediator dosing concept. A thin-film electrode with an interdigitated electrode structure was used as model substrate. The structure consisted of a circular arrangement of electrode bands with a width and distance of 10 μm , each. Furthermore, SECM experiments were conducted on a commercially available LIB graphite electrode as realistic substrate. Additionally, the electrode material was characterised with a VK-X 3000 3D laser scanning microscope from Keyence (Neu-Isenburg, Germany).

The experimental setup is described in more detail in the supporting information, section SI-2.

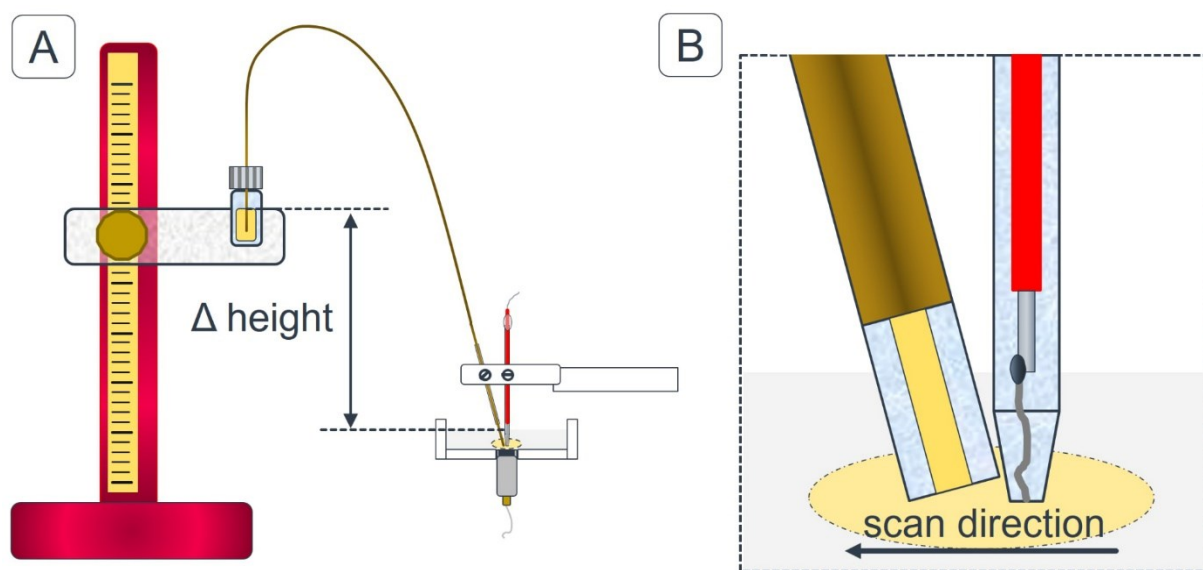


Figure 4.2.6. Schemes of mediator dosing setup and highlighted view of the capillary-probe tip assembly. A) The inlet vial filled with ferrocene solution is mounted at an adjustable height difference (Δ height) to the outlet of the dosing capillary resulting in a gravity-driven flow of the mediator solution. B) Dosing capillary and SECM probe are closely aligned at their tips. A ferrocene zone is formed in close proximity to the platinum disk electrode.

Experimental procedures

Initially, the flow rates of mediator solution resulting from Δ height of 5, 10, and 15 cm between inlet and outlet of the dosing capillary were determined. Therefore, a platinum disk electrode with an electrode diameter of 3 mm was mounted in the bottom of the electrochemical cell and the cell was filled with 5 mL of 0.1 M LiPF_6 solution (EC:EMC 30/70). Then, a mediator dosing assembly (SECM probe + dosing capillary) was approached under mediator flow (Δ height = 15 cm) towards the surface by measuring a PAC. Parameters were: probe potential = 3.574 V vs. Li/1 M Li^+ , quiet time = 15 s, maximum approach speed = 10 $\mu\text{m s}^{-1}$, feedback target = 200%. The auxiliary electrode was a platinum wire, the reference was a

Fc/Fc⁺ based reference electrode. After approaching the surface, the working electrode connection was switched from the SECM probe to the bottom-mounted platinum electrode. Two inlet vials were inserted in the adjustable height stand, one filled with mediator solution (Vial 1, 1.5 mM Fc in 0.1 M LiPF₆ EC:EMC 30/70) and one filled with pure electrolyte (Vial 2, 0.1 M LiPF₆ in EC:EMC 30/70). The height difference was adjusted to 5 cm, the inlet side of the capillary was positioned in vial 2, and an i-t curve was started (electrode potential = 3.574 V vs. Li/1 M Li⁺). After 30 s, the capillary inlet was moved into vial 1 resulting in the flow of mediator solution towards the platinum electrode. The time until the oxidation signal of Fc could be detected was used together with the capillary dimensions to calculate the corresponding flow rate. For each Δ height, the experiment was conducted three times.

To showcase the performance of the mediator dosing setup, a thin-film electrode with an interdigitated electrode structure (Micrux type IDRA1) was investigated. The substrate was mounted in the electrochemical cell, which was subsequently filled with 5 mL of a 1.5 mM Fc solution (0.1 M LiPF₆ or 0.1 M TBAPF₆ in EC:DMC). Then, a dosing capillary and a SECM probe were installed and aligned in the dual-probe holder under inspection with a digital microscope camera. Levelling of the substrate was achieved by a series of PACs at three different positions surrounding the area of interest. A reference image in Fc solution was recorded after which the solution in the electrochemical cell was exchanged with pure electrolyte. A vial was filled with 1.5 mM of Fc solution and installed together with the capillary inlet at a corresponding Δ height of 15 cm. The reproducibility under mediator dosing conditions was then evaluated by five consecutive PACs towards the glass surface of the thin-film electrode (negative feedback) and another set of five PACs towards the conductive platinum electrode surface (positive feedback). Furthermore, to compare the image quality received in Fc bulk solution with the mediator dosing setup, SECM images of the same electrode structure were recorded under both experimental conditions. PACs were recorded in 0.1 M TBAPF₆ (EC:DMC 30/70), probe potential was 3.424 V vs. Li/1 M Li⁺, maximum approach speed was 2.5 $\mu\text{m s}^{-1}$, and a quiet time of 15 s before current recording was chosen. The probe movement is slowed down close to reaching the feedback target. In the measurement set of negative feedback PACs, at a norm. distance of 1 (feedback current of approx. 54%), the average movement speed was 0.36 $\mu\text{m s}^{-1}$. Further away, at a norm. distance of 1.5 (feedback current of approx. 65%), the average speed was 1.26 $\mu\text{m s}^{-1}$. The auxiliary electrode was a platinum wire, and an Ag/AgCl wire was used as quasi-reference. The SECM images were obtained with a platinum wire as auxiliary electrode, and a Fc/Fc⁺ based reference electrode. Probe potential was 3.574 V vs. Li/1 M Li⁺, scan speed of 100 $\mu\text{m s}^{-1}$, pixel size of 5 μm , and the quiet time was 15 s. Mediator dosing images were recorded in 0.1 M LiPF₆ (EC:DMC 30/70).

Eventually, a commercially available LIB graphite electrode (Customcells product ID 11124) was evaluated comparing imaging in Fc solution and under mediator dosing conditions. After mounting the substrate and filling the electrochemical cell with 5 mL of electrolyte solution (0.1 M LiPF₆ in EC:EMC 30/70), the sample was levelled by a series of PACs at three different positions on the surface. Next, a SECM image was recorded by application of the mediator dosing setup, followed by exchanging the measurement solution with Fc containing electrolyte (1.5 mM Fc in 0.1 M LiPF₆ in EC:EMC 30/70). Subsequently, a SECM image of the same area was generated. Mediator dosing was achieved by applying a Δ height of 15 cm between inlet and outlet reservoirs connected with a fused-silica capillary with an inner diameter of 100 μm and a length of 35 cm. The experimental parameters were identical in both cases. Auxiliary electrode was a platinum wire, and a Fc/Fc⁺ based reference electrode was utilized. A probe potential of 3.574 V vs. Li/1 M Li⁺ was applied, probe movement speed was 100 $\mu\text{m s}^{-1}$, pixel size was 5 μm , and a quiet time of 15 s was used before current recording. The SECM probe was a platinum UME ($r = 6.25 \mu\text{m}$) with a R_g value of 7.

4.2.5 Supporting information

SI-1 SPM probes and dosing capillary fabrication

SECM and SICM probes were produced from soda-lime glass tubes with an inner diameter of 1.1 mm (Technische Glaswerke Ilmenau, Ilmenau, Germany). Glass tubes with a length of approximately 10 cm were heated and pulled in a butane flame to form the base material of the SPM probes. Resulting capillaries were inspected with a digital microscope camera and probes with opening diameters in the range of 100 μm were selected for further steps.

For SECM probes, approx. 1 cm of the insulation from a piece of jumper wire was removed on both sides (cross-section 0.2 mm², insulating layer outer diameter 1.1 mm) and 1 cm of platinum wire ($r = 6.25 \mu\text{m}$, 99.99% purity) from Advent Research Materials (Oxford, UK) was soldered onto one end. Then, the assembly was carefully inserted into the glass capillary until the platinum wire protruded about 1 mm from the capillary tip. Mechanical stability was ensured by the matching dimensions of the glass tube inner diameter and the diameter of the insulation of the jumper wire. The tip was molten again in a butane flame resulting in an insulating glass layer enclosing the platinum wire. A laboratory-constructed polishing device consisting of a rotating disk with adjustable rotating speed and a probe holder was used for re-exposing the platinum and defining the tip dimensions of the probe. It was equipped with a lapping film sheet with a particle size of 0.3 μm from Precision Surfaces International (Houston, USA). The procedure resulted in a mirror finish, disk-shape platinum ultramicroelectrode with variable R_g values, which is the ratio of the radii of the insulating glass layer and the platinum disk. Overall quality and the R_g value of a probe were estimated from optical microscopy at 100x magnification. In the case of the mediator dosing, probes with smaller diameters were found to be preferable. Therefore, probes with R_g values of 5 to 7 were used in experiments. Before usage in the mediator dosing setup the electrochemical performance of probes was tested by cyclic voltammetry in a 1.5 mM Fc solution (0.1 M LiPF₆, EC:EMC 30/70).

The fabrication of SICM probes was done according to the previously published instructions. [17] Briefly, capillary tips were re-sealed in the butane flame, and, subsequently, the tips were treated with the polishing device resulting in opening diameters of 10 to 30 μm . After cleaning, the probe was filled with 1.5 mM Fc/Fc⁺ solution (0.1 M LiPF₆ in EC:EMC 30/70), a platinum wire with a diameter of 0.5 mm was inserted, and the top was sealed with a custom-made cap.

Fused-silica capillaries with an outer diameter of 360 μm and inner diameters of 75 or 100 μm from Polymicro Technologies (Phoenix, USA) were used as dosing capillaries. Pieces with a length of approx. 35 cm were cut by using a ceramic cutter. From each side, ca. 0.5 cm of the

polyimide coating was removed by burning in a butane flame followed by carefully cleaning away the residues with isopropanol. Afterwards, the tips of the capillary were polished to a clean, flat finish. Polishing was conducted in the polishing device under constant flushing of the capillary with de-ionized water. Lapping film sheets with a particle size of 30 μm (first step, coarse polishing) and 1 μm (second step, fine polishing) were used. Then, it was cleaned from polishing residues with isopropanol, followed by air-drying for at least one hour. For mounting into the dual-probe holder, the finished capillary was inserted into a soda-lime glass tube with a pulled tip (inner diameter ca. 500 μm) and glued in place with two-component adhesive (Epoxy resin L + Hardener S) from R&G Faserverbundwerkstoffe (Waldenbuch, Germany). After curing, the assembly was transferred into the glovebox.

SI-2 Experimental setup

Experimental procedures were conducted with a SECM 920C system from CH Instruments (Austin, USA). The main parts of the instrumental setup are schematically shown in Figure 4.2.S1. Bipotentiostat, positioning system, and a PC were placed close to an Argon-filled glovebox. Electric connections and control cables were fed through with gas-tight connections. Inside the glovebox, the electrochemical setup, and the motor unit were placed on a dampening mat within a custom-made Faraday cage. The height adjustable stand used for mediator dosing experiments was positioned next to the dampening mat.

The electrochemical setup consisted of two electrochemical cells made from polytetrafluoroethylene with a total volume of 5 mL and either with or without a hole in the bottom for the installation of substrates. The experiments including a Micrux thin-film electrode as substrate were conducted in the cell without a hole, the investigation of Customcells LIB graphite electrodes were done in the second cell. A three-electrode arrangement was employed in all experimental procedures. The working electrode channel was connected to a SPM probe (SECM or SICM, respectively). A platinum wire was used as counter electrode. Most measurements were carried out with a Fc/Fc^+ based reference electrode consisting of a glass tube with ceramic frit, an inserted platinum wire, and an electrolyte solution (1.5 mM Fc , 1.5 mM FcPF_6 , 0.1 M LiPF_6 , EC:EMC 30/70). PACs in TBAPF_6 based electrolyte were recorded with an Ag/AgCl wire as quasi-reference.

To be able to have a local delivery of mediator solution near the SECM probe tip a gravity-driven approach was chosen. Main advantages are the simplicity of the setup and constant flow rates with low fluctuation. The mediator dosing setup consisted of an adjustable height stand, a vial with mediator solution, and a dosing capillary. By application of height

difference (Δ height) between the solvent levels in compartments of capillary inlet and outlet a gravity-driven flow of the mediator solution is achieved. On the inlet side, the capillary was fixed within the vial by a rubber septum with a canula for pressure equilibration. On the outlet side, it was positioned in close proximity to the SECM tip by careful alignment under a digital microscope camera. Probe and dosing capillary were mounted in a laboratory-constructed dual-probe holder which was previously described in more detail. [17] The SECM probe was installed in the upright position, the dosing capillary was installed at a tilted position with a 15° -angle.

Two different substrates were investigated with the mediator dosing setup. First, a thin-film electrode from Micrux Technologies (Gijón, Spain) of the type IDRA1. The electrode had a circular, interdigitated electrode structure with a band width and a band distance of $10\ \mu\text{m}$, respectively. Second, LIB graphite electrodes (Product ID 11124) supplied by Customcells (Itzehoe, Germany). Pieces with a diameter of 4 mm were produced with a punching iron and mounted in laboratory-constructed sample holders made from polyether ether ketone.

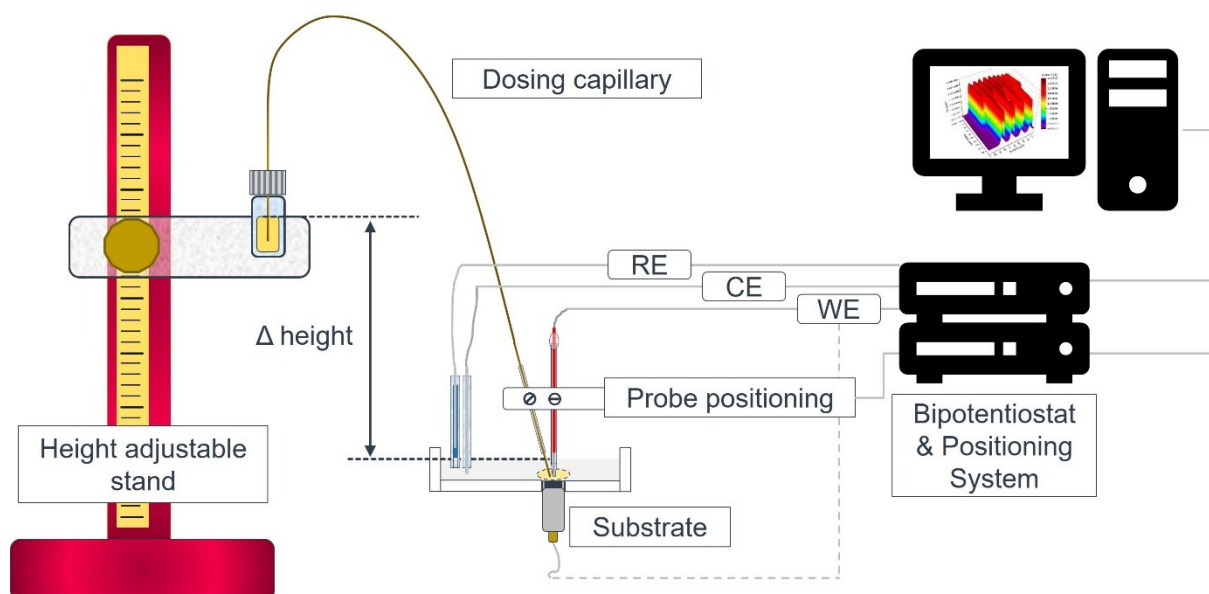


Figure 4.2.S1. Schematic depiction of the experimental setup. The adjustable height stand and the electrochemical cell are installed within a Faraday cage in an Argon-filled glovebox. Furthermore, the electrochemical cell and the SECM motor unit are placed on a dampening plate. Electrical connections and control cables for the positioning are fed through gas-tight connections. The inlet vial filled with ferrocene solution is mounted at an adjustable height difference (Δ height) to the outlet of the dosing capillary resulting in a gravity-driven flow of the mediator solution. During measurements, the working electrode channel is connected to the SECM probe. For the pre-charging procedure, the connection is changed to the substrate. Reference electrode was a Fc/Fc^+ based electrode, and counter electrode was a platinum wire.

4.2.6 Unpublished data

In addition to the experimental data shown in the main article, another series of measurements was conducted to give a first estimation on the influence of Fc present during the pre-charging of an LIB graphite electrode. The study of Tang *et al.* [25] suggested a possible corrosive effect of ferrocenium, which is formed during the pre-charging on the counter electrode, on the formed SEI. Customcells graphite electrodes were first levelled by repeated PACs and line scans either in Fc solution or under MD conditions. Subsequently, a pre-charging protocol adapted from similar procedures in literature [16,18,22] was applied. The procedure consisted of a cyclic voltammetry protocol with three cycles starting from 3.774 V vs. Li/1 M Li⁺ down to 0.074 V at a scan rate of 5 mV s⁻¹. In Figure 4.2.U1, the corresponding cyclic voltammograms recorded in solutions containing either no Fc (blue), Fc residues from previous MD imaging experiments (red), or 1.5 mM of Fc (black) are shown. Distinct differences could be found, the most prominent being the shifting of the peaks between 2 to 1 V vs. Li/1 M Li⁺, which could be attributed to the degradation of the solvent. Differences in the course of the cyclic voltammograms suggested some interference due to the mediator presence.

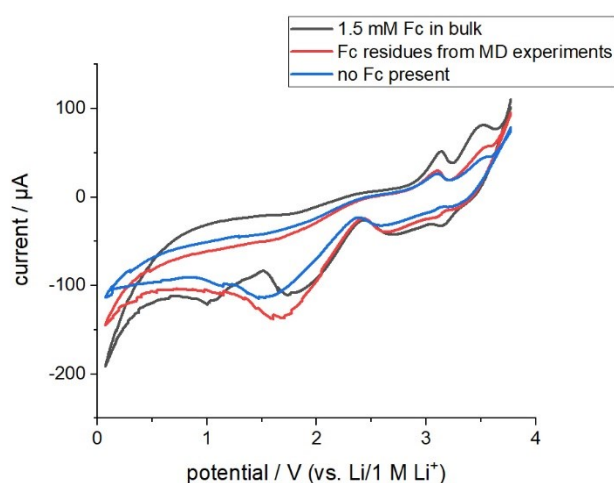


Figure 4.2.U1. Pre-charging procedure applied to Customcell graphite electrodes. CVs recorded in 1.5 mM Fc in 0.1 M LiPF₆ solution (EC:EMC 30/70, black line), in 0.1 M LiPF₆ solution (EC:EMC 30/70) containing Fc residues from MD measurements (red line), or in 0.1 M LiPF₆ solution (EC:EMC 30/70, blue line). CV parameters: scan speed 5 mV s⁻¹, quiet time 15 s, 3 cycles. The third cycle of each measurement is shown. Reference electrode was Pt in 1.5 mM Fc/Fc⁺ solution, counter electrode was a Pt wire.

In Figure 4.2.U2, four feedback mode SECM images are shown recorded from the surface of graphite electrode samples. Figure 4.2.U2A and B depict images recorded before the application of the pre-charging protocol. After their completion, the SECM probe was retracted from the surface, the sample was connected to the working electrode channel, and the pre-

charging was started. Subsequently, the working electrode was connected to the SECM probe and the graphite surface was approached with a PAC. In both cases, Fc solution and MD, a difference of approximately 10 μm in approach distance could be detected. Most probably this was due to the physical swelling of the binding agent as already investigated by Bülter *et al.* [11] Images in Figure 4.2.U2C and D were recorded in the identical locations as before pre-charging. After the pre-charging SECM images reveal overall passivation of the electrode, as shown by reduced electrochemical activity. Still, spots with high electrochemical activity could be found.

In these preliminary SECM experiments, no significant differences in surface passivation could be resolved between applying the pre-charging in Fc solution compared to the treatment under reduced mediator introduction by the MD concept. The recorded CVs from the pre-charging suggest differences in the formation, as shown by a shift of the solvent degradation signal. Ultimately, further studies are needed to give a definite answer on the degree of influence of Fc present during the SEI formation.

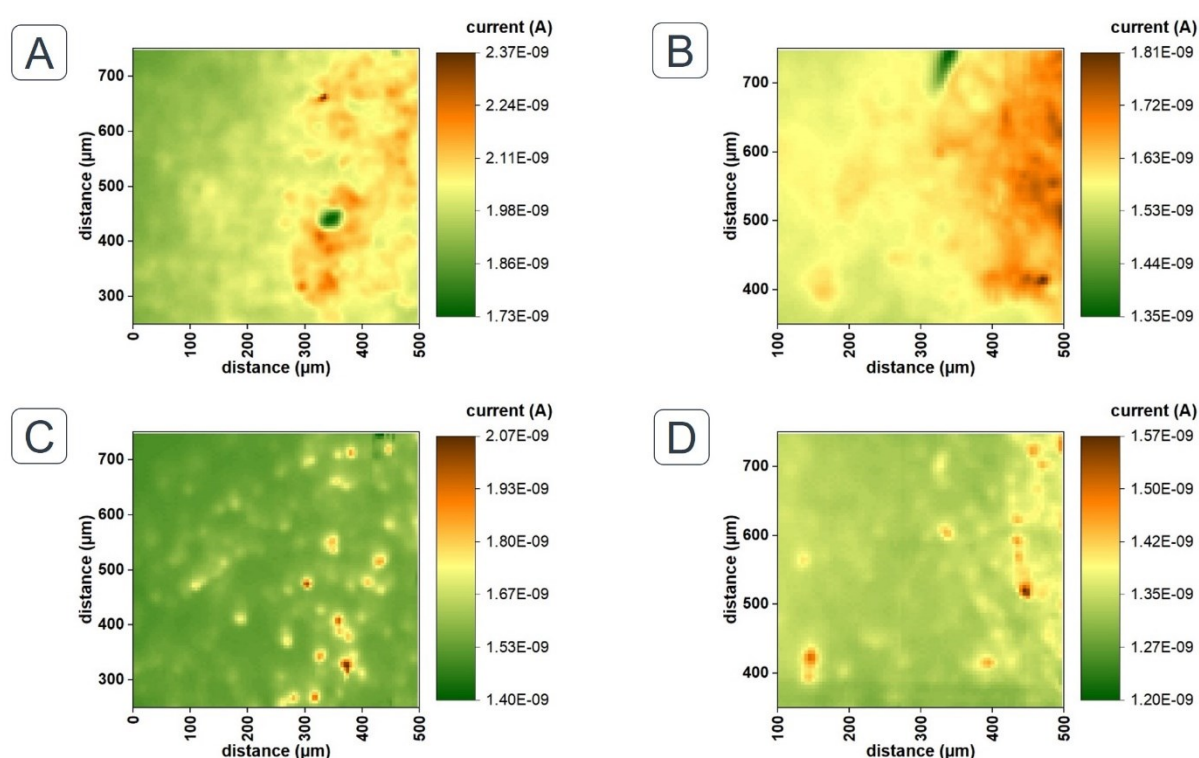


Figure 4.2.U2. SECM images of a Customcells graphite electrode for LIBs. A) Image recorded with Fc in solution before application of pre-charging protocol. B) Image recorded with the mediator dosing setup before pre-charging protocol. C) Image recorded with Fc in solution after pre-charging protocol. D) Image recorded with the MD setup after pre-charging protocol. SECM probe was a platinum UMEs ($r = 6.25 \mu\text{m}$, $R_g = 7$). The Fc solution (1.5 mM in 0.1 M LiPF₆ EC:EMC 30/70) was dosed via a fused-silica capillary (OD = 360 μm , ID = 100 μm , length = 35 cm) and a height difference of 15 cm between in- and outlet. Measurements were conducted in either 1.5 mM Fc in 0.1 M LiPF₆ solution (EC:EMC 30/70) or in 0.1 M LiPF₆ (EC:EMC 30/70, MD experiments).

References

- [1] C. Villevieille, *Adv. Mater. Inter.* 2022, 9, 2101865.
- [2] H. Adenusi, G. A. Chass, S. Passerini, K. V. Tian, G. Chen, *Adv. Energy Mater.* 2023, 13.
- [3] A. Mishra, D. Sarbapalli, O. Rodríguez, J. Rodríguez-López, *Annu. Rev. Anal. Chem.* 2023, 16, 93.
- [4] G. Zubi, R. Dufo-López, M. Carvalho, G. Pasaoglu, *Renewable Sustainable Energy Rev.* 2018, 89, 292.
- [5] V. A. Nikitina, *Curr. Opin. Electrochem.* 2021, 29, 100768.
- [6] L. Danis, S. M. Gateman, C. Kuss, S. B. Schougaard, J. Mauzeroll, *ChemElectroChem* 2017, 4, 6.
- [7] S. Megahed, B. Scrosati, *J. Power Sources* 1994, 51, 79.
- [8] E. Peled, S. Menkin, *J. Electrochem. Soc.* 2017, 164, A1703-A1719.
- [9] G. Zampardi, F. La Mantia, *Batteries Supercaps* 2020, 3, 672.
- [10] a) P. Schwager, H. Bülter, I. Plettenberg, G. Wittstock, *Energy Technol.* 2016, 4, 1472;
b) E. Ventosa, P. Wilde, A.-H. Zinn, M. Trautmann, A. Ludwig, W. Schuhmann, *Chem. Commun.* 2016, 52, 6825.
- [11] H. Bülter, F. Peters, J. Schwenzel, G. Wittstock, *J. Electrochem. Soc.* 2016, 163, A27-A34.
- [12] A. J. Bard, F. R. F. Fan, J. Kwak, O. Lev, *Anal. Chem.* 1989, 61, 132.
- [13] A. J. Bard in *Scanning Electrochemical Microscopy*, Vol. 2 (Eds.: A. J. Bard, M. V. Mirkin), CRC Press, Boca Raton, 2012, pp. 1-15.
- [14] R. He, L. Zhou, R. Tenent, M. Zhou, *Mater. Chem. Front.* 2023, 7, 662.
- [15] H. Bülter, F. Peters, J. Schwenzel, G. Wittstock, *Angew. Chem. Int. Ed.* 2014, 53, 10531.
- [16] G. Zampardi, F. La Mantia, W. Schuhmann, *RSC Adv.* 2015, 5, 31166.
- [17] J. Eidenschink, F.-M. Matysik, *ChemElectroChem* 2024, 11, e202300577.
- [18] G. Zampardi, S. Klink, V. Kuznetsov, T. Erichsen, A. Maljusch, F. La Mantia, W. Schuhmann, E. Ventosa, *ChemElectroChem* 2015, 2, 1607.
- [19] G. Zampardi, R. Trocoli, W. Schuhmann, F. La Mantia, *Phys. Chem. Chem. Phys.* 2017, 19, 28381.
- [20] D. Polcari, P. Dauphin-Ducharme, J. Mauzeroll, *Chem. Rev.* 2016, 116, 13234.

- [21] a) C. S. Santos, A. Botz, A. S. Bandarenka, E. Ventosa, W. Schuhmann, *Angew. Chem. Int. Ed.* 2022, 61, e202202744; b) N. Jiyane, E. García-Quismondo, E. Ventosa, W. Schuhmann, C. S. Santos, *Batteries Supercaps* 2023, 6, e202300126.
- [22] X. Zeng, D. Liu, S. Wang, S. Liu, X. Cai, L. Zhang, R. Zhao, B. Li, F. Kang, *ACS Appl. Mater. Inter.* 2020, 12, 37047.
- [23] B. Krueger, L. Balboa, J. F. Dohmann, M. Winter, P. Bieker, G. Wittstock, *ChemElectroChem* 2020, 7, 3590.
- [24] F. M. Weber, I. Kohlhaas, E. Figgemeier, *Molecules* 2022, 27, 1737.
- [25] M. Tang, J. Newman, *J. Electrochem. Soc.* 2012, 159, A1922-A1927.
- [26] A. Asserghine, S. Juillard, J. Ducrot, V. Vivier, C. M. Sánchez-Sánchez, *Electrochim. Acta* 2023, 441, 141775.
- [27] J. V. Macpherson, S. Marcar, P. R. Unwin, *Anal. Chem.* 1994, 66, 2175.
- [28] R. C. Engstrom, *Anal. Chem.* 1984, 56, 890.
- [29] C.-L. Lin, J. Rodríguez-López, A. J. Bard, *Anal. Chem.* 2009, 81, 8868.
- [30] D. Muñoz-Torrero, C. Santana Santos, E. García-Quismondo, S. Dieckhöfer, T. Erichsen, J. Palma, W. Schuhmann, E. Ventosa, *RSC Adv.* 2023, 13, 15521.
- [31] A. W. Hassel, M. M. Lohrengel, *Electrochim. Acta* 1997, 42, 3327.
- [32] F. M. Matysik, G. Werner, *Analyst* 1993, 118, 1523.
- [33] R. Cornut, C. Lefrou, *J. Electroanal. Chem.* 2007, 608, 59.
- [34] J. L. Amphlett, G. Denuault, *J. Phys. Chem. B* 1998, 102, 9946.
- [35] a) P. K. Hansma, B. Drake, O. Marti, S. A. Gould, C. B. Prater, *Science* 1989, 243, 641; b) C. Zhu, K. Huang, N. P. Siepser, L. A. Baker, *Chem. Rev.* 2021, 121, 11726.
- [36] DIN EN ISO 25178-1:2016-12, Geometrische Produktspezifikation_(GPS)_-Oberflächenbeschaffenheit: Flächenhaft_- Teil_1: Angabe von Oberflächenbeschaffenheit (ISO_25178-1:2016); Deutsche Fassung EN_ISO_25178-1:2016, 2016, Beuth Verlag, Berlin.
- [37] K. Izutsu in *Handbook of Reference Electrodes* (Eds.: G. Inzelt, A. Lewenstam, F. Scholz), Springer, Berlin, 2013, pp. 145-188.

4.3 Characterisation of as-grown and chemically-mechanically polished boron-doped diamond electrodes by means of feedback mode scanning electrochemical microscopy

Some of the results shown in this section were published as part of:

Zelenský M, Fischer J, Baluchová S, Klimša L, Kopeček J, Vondráček M, Fekete L, Eidenschink J, Matysik F-M, Mandal S, Williams OA, Hromadová M, Mortet V, Schwarzová-Pecková K, Taylor A.

Carbon 203 (2023) 363-376.

Abstract

Boron-doped diamond (BDD) electrodes feature a combination of unique properties including a large potential window, chemical inertness, and tuneable electrochemical properties. One way of altering and improving BDD performance is by pre-treatment of the surface, for example by means of chemically-mechanically polishing (cmp) the substrate. To be able to fully understand the underlying principle and characterise the induced changes, various analytical techniques are needed. Scanning electrochemical microscopy (SECM) is exceptional in its ability to map the electrochemical activity of surfaces. Within this study, we applied the feedback mode of SECM in the characterisation of two different sets of BDD electrodes, with and without pre-treatment by cmp of the BDD film. Furthermore, films synthesised at various boron doping levels between 500 and 8000 ppm were used. Several redox mediators were tested for their applicability, whereas ferrocene methanol delivered best results. SECM imaging experiments revealed inhomogeneity of electrochemical activity on as-grown BDD films, while cmp BDD electrodes were found to have a much more homogeneous distribution. Furthermore, heterogeneous electron transfer rate constants (k_0) were determined from probe approach curves (PACs). For the BDD₄₀₀₀ ag sample an average k_0 of 0.209 cm s⁻¹ was determined, while for a BDD₄₀₀₀ cmp electrode the average k_0 was 0.319 cm s⁻¹.

4.3.1 Introduction

Boron-doped diamond (BDD) films represent a promising electrode material usable in a multitude of applications, ranging from electroanalysis, energy storage, microfluidics to water treatment. [1–5] This is due to their highly attractive properties including superior chemical and mechanical stability, low background currents, biocompatibility, and a wide potential window. [3]

Typically, BDD layers are synthesized by chemical vapour deposition (CVD) on top of a suitable substrate. [4] Briefly, a boron-containing substance, often trimethylborane, is introduced into the gas phase within a reaction chamber filled with hydrogen and methane. The chemical reaction is then started either via a microwave enhanced plasma or a hot filament. [5,6] Resulting film properties are highly dependent of the B/C ratio in the gas phase, which enables the possibility to tune the electrochemical performance. [3,7] The BDD electrode can be semi-conductive or possess metal-like conductivity, where a threshold in boron content of roughly $1 - 3 \times 10^{20}$ atoms cm^{-3} is widely accepted. [1,8,9] Further important parameters of BDD films are the content of sp^2 carbon, often considered as an impurity, crystallographic orientation, morphology, and surface termination. [5,10–12] After synthesis, BDD is normally H-terminated, which leads to a hydrophobic surface. Anodic pre-treatment induces O-termination resulting in a more hydrophilic character. [7,13] A way of improving the performance of BDD electrodes was introduced by Thomas *et al.* [14] in 2014 in the form of a chemical-mechanical polishing (cmp) method. Shortly summarized, an alkaline silica colloid solution is used to polish the surface of a BDD film. Significant reduction of surface roughness and faster heterogeneous electron transfer (HET) kinetics were reported as outcome. [15]

To study the influence of the individual parameters, like boron doping level or surface termination, as well as their complex interplay on the BDD electrode properties asks for powerful analytical methods. A variety of techniques has already been employed in BDD research. Electrochemical methods including cyclic voltammetry (CV) and electrochemical impedance spectroscopy (EIS) were used in evaluating the electrochemical performance and HET kinetics. [6,10,12,13,16,17] Grain size and orientation were determined by electron backscatter diffraction (EBSD). [1,10] Raman spectroscopy (+ mapping) and X-ray photoelectron spectroscopy (XPS) have been applied in estimating boron content of BDD films. [7,9,10,14,18,19] Morphology and surface roughness of BDD electrodes was determined by scanning electron microscopy (SEM) and other electron microscopic techniques. Furthermore, members of the family of scanning probe microscopies (SPMs) were utilized in studying BDD electrodes. Atomic force microscopy was used in several studies to locally probe the morphologic details of BDD on the micro- and nanoscale. [7,10,14,19–22] Patten *et al.* [23]

investigated active sites for inner-sphere, outer-sphere, and complex electrochemical reactions by means of scanning electrochemical cell microscopy.

Another SPM which is suitable for investigations of BDD is scanning electrochemical microscopy (SECM). This technique utilizes a micro or even nanometre sized electrode to probe the local electrochemical activity and the topography of a substrate. [24] Since its introduction in the 90s [25], SECM became a widely applied technique with investigations ranging from enzymatic samples, [26] lithium-ion battery (LIB) materials [27] to probing electrocatalytic activities. [28] In the context of BDD research, SECM was widely applied as well. Holt *et al.* [22] probed the local heterogeneity of electrochemical activity of H-terminated BDD substrates with varying boron doping level by means of the substrate generation/tip collection (SG/TC) mode of SECM. Their study revealed, that dependent of boron doping level parts of the electrode surface remained electrochemically inactive. In further studies conducted by Neufeld *et al.* [29], the feedback and SG/TC modes of SECM were successfully applied to determine HET rate constants for individual positions on the surface. They were able to show high variation of k_0 values across the BDD electrode surface with several redox mediators. More recently, Liu *et al.* [1] correlated electrochemical activity with the grain orientation of a BDD substrate. They were able to overlay an orientation map generated by EBSD with a feedback mode SECM image and determined that high electrochemical activity was recorded on (111) crystallographic orientation. Furthermore, porous BDD samples [12,30] and the generation of reactive oxygen species on BDD electrodes [31] were investigated by utilizing SECM.

Within this study, we examined BDD electrodes with varying boron doping level and investigated the effect of pre-treatment by cmp. Feedback mode SECM was used in combination with several other analytical techniques. [10] In first experiments, four common redox mediators were evaluated regarding their performance in SECM experiments on the BDD substrates. Then, comparative measurements on both sets of BDD electrodes were conducted and discussed together with the findings of other techniques. Eventually, highly localized k_0 values were determined according to the method introduced by Wei *et al.* [32] from SECM data recorded on BDD₂₀₀₀ as-grown (ag) and cmp samples. SECM determined k_0 values were compared with k_0 values accessed from CV data according to the Nicholson method. [33]

4.3.2 Results and discussion

BDD electrodes were characterised by a range of analytical techniques by cooperation partners. Raman spectroscopy as well as XPS was utilized to determine the boron content in the ag and cmp BDD films. Contents in the range of $0.58 - 4.4 \times 10^{21}$ atoms cm^{-3} were estimated, for brevity samples are still indicated according to their boron doping level, e. g. BDD₅₀₀ for an electrode with a BDD film deposited at 500 ppm. Surface roughness and topography were evaluated by means of AFM and SEM. Cmp electrodes were found to be much smoother with surface roughness in the nanometre range. Furthermore, higher boron doping level was correlated to smaller grain size. EBSD was used to map grain orientation on a BDD₂₀₀₀ cmp electrode and led to the conclusion, that grain orientations were not randomly distributed. The electrochemical performance of ag and cmp electrodes was compared by several electrochemical methods including CV, EIS, and square wave voltammetry. HET kinetics and sensitivity in dopamine detection were improved by cmp of electrodes. Eventually, feedback mode SECM was employed to probe localized differences in the electrochemical activity of both sets of BDD substrates.

Testing the suitability of various redox mediators for feedback mode SECM in BDD studies

The first sub-series of experiments was dedicated to evaluate the performance of four commonly used redox mediators in the feedback mode of SECM. Ferrocene methanol (FcMeOH), hexacyanoferrate(II), hexacyanoferrate(III), and hexaammineruthenium(III) were investigated. Suitable probe potentials for SECM measurements were chosen based on cyclic voltammograms recorded with a 12.5 μm platinum UME in the respective mediator solution. For FcMeOH, a probe potential of +0.3 V (vs. Ag/AgCl/3 M KCl) was determined, measurements in hexacyanoferrate(II) were conducted with a probe potential of +0.5 V, hexacyanoferrate(III) was reduced at +0.1 V, and experiments with hexaammineruthenium(III) were performed with a working electrode potential of -0.2 V. To evaluate the imaging performance, identical areas on two samples, BDD₄₀₀₀ ag and cmp, were imaged in all four mediator solutions. Figure 4.3.1 shows SECM images of a representative area on the surface of the BDD₄₀₀₀ ag substrate. With exception of the respective probe potential, the series of images was recorded with equal parameters. The SECM current map recorded in FcMeOH solution is shown in Figure 4.3.1A depicting non-uniform electrochemical activity in the investigated area. Spots with high electrochemical activity, indicated by orange colour, as well as less and even inactive areas, illustrated by green

colour, could be resolved with good contrast. The image generated in hexacyanoferrate(II) (Figure 4.3.1B) resolved much less detail in comparison. Furthermore, the recorded current signals were lower. Some spots with higher activity were still visible, but most of the surface details were not resolved anymore. In hexacyanoferrate(III) (Figure 4.3.1C), the resolution was better compared to hexacyanoferrate(II) but worse than FcMeOH. The SECM image recorded in hexaammineruthenium(III) shown in Figure 4.3.1D resolved surface details very well with high contrast. The differences in performance could be explained by the surface sensitivity of the mediators. While inner-sphere redox probes, hexacyanoferrate(II) and (III), are highly sensitive to the electrode morphology, outer-sphere markers, FcMeOH and hexaammineruthenium(III), are less influenced by the surface morphology. [10]

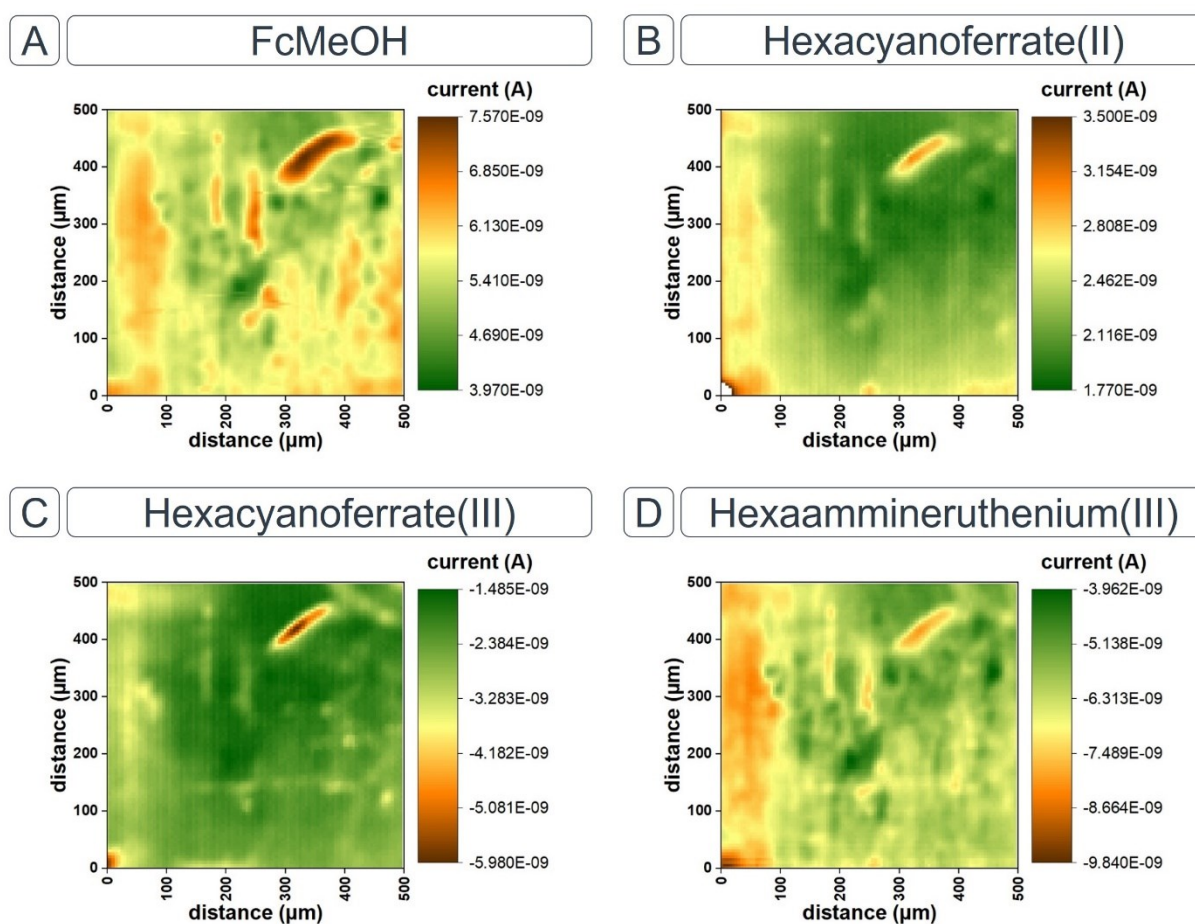


Figure 4.3.1. SECM images of the surface of a BDD₄₀₀₀ ag substrate recorded in four redox mediators, FcMeOH (A), hexacyanoferrate(II) (B), hexacyanoferrate(III) (C), and hexaammineruthenium(III) (D). Probe potentials were +0.3 V (FcMeOH), +0.5 V (hexacyanoferrate(II)), +0.1 V (hexacyanoferrate(III)), or -0.2 V (hexaammineruthenium(III)). Probe scan rate was 200 μm s⁻¹, quiet time of 15 s. An area of 500×500 μm was covered with a pixel size of 5 μm. Measurements were conducted in constant-height mode at a fixed height corresponding to a feedback current of 150%. Probe was a platinum UME (r = 12.5 μm, R_g ~10), reference was an Ag/AgCl/3 M KCl electrode, and auxiliary electrode was a platinum wire.

Another series of SECM images was recorded of a cmp BDD₄₀₀₀ sample. Again, an identical area was mapped in all four mediator solutions as shown in Figure 4.3.2. The surface exhibited a more homogenous distribution of the electrochemical activity. In FcMeOH (Figure 4.3.2A), fine details were resolved well. Images recorded in inner-sphere redox probes, hexacyanoferrate(II) and (III), are depicted in Figure 4.3.2B and C. Although the surface characteristics of the cmp substrate were visible, the recorded currents remained lower than in FcMeOH. During measuring in hexaammineruthenium(III), signal instabilities occurred resulting in poor image quality and low contrast as shown in Figure 4.3.2D. Overall, usage of FcMeOH resulted in the highest image quality and signal stability compared to the other three mediators. The comparative study of both sets of BDD electrodes was therefore conducted in FcMeOH solution.

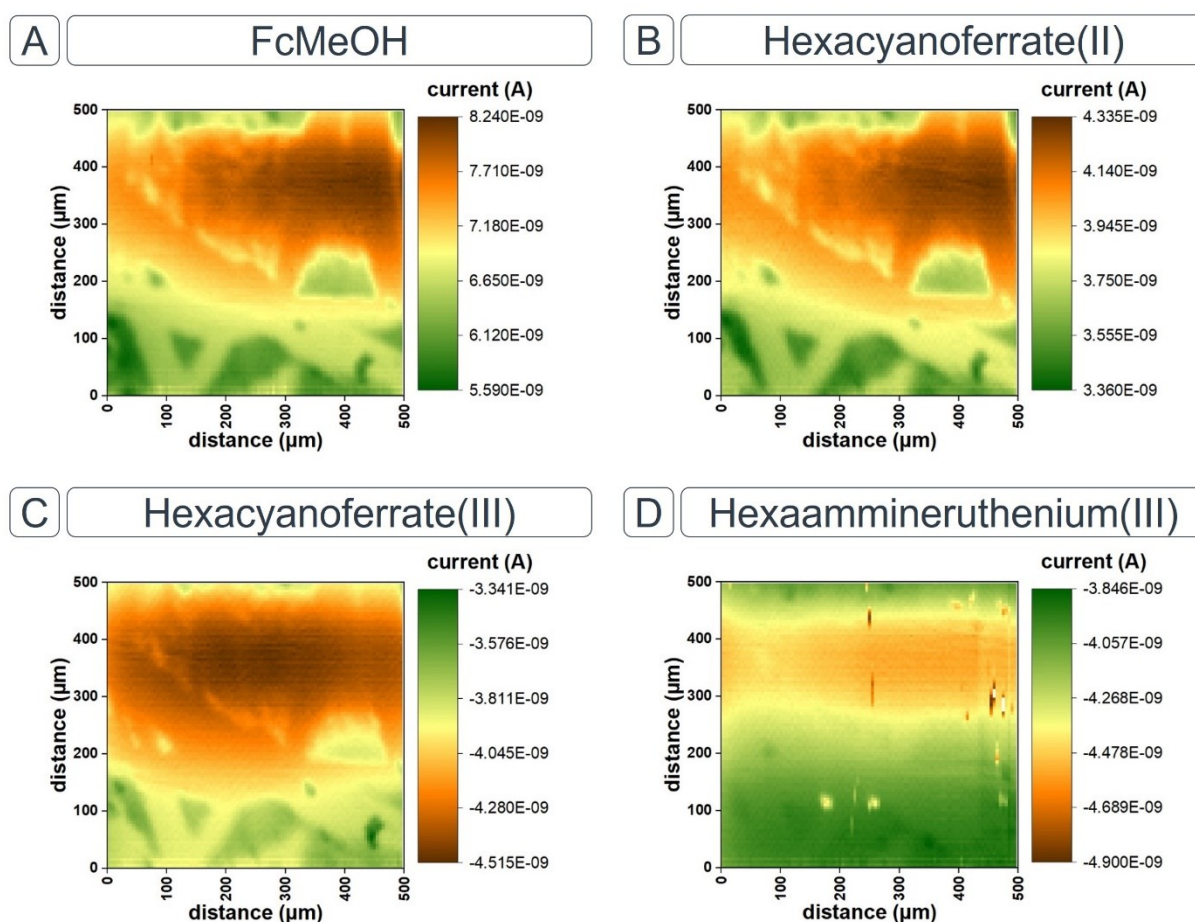


Figure 4.3.2. SECM images of the surface of a BDD₄₀₀₀ cmp substrate recorded in four redox mediators, FcMeOH (A), hexacyanoferrate(II) (B), hexacyanoferrate(III) (C), and hexaammineruthenium(III) (D). Probe potentials were +0.3 V (FcMeOH), +0.5 V (hexacyanoferrate(II)), +0.1 V (hexacyanoferrate(III)), or -0.2 V (hexaammineruthenium(III)). Probe scan rate was 200 $\mu\text{m s}^{-1}$, quiet time of 15 s. An area of 500 \times 500 μm was covered with a pixel size of 5 μm . Measurements were conducted in constant-height mode at a fixed height corresponding to a feedback current of 150%. Probe was a platinum UME ($r = 12.5 \mu\text{m}$, $R_g \sim 10$), reference was an Ag/AgCl/3 M KCl electrode, and auxiliary electrode was a platinum wire.

Comparative investigation of as-grown and chemically-mechanically polished BDD electrodes

Since the current signal in SECM is not only dependent of the electrochemical activity but also of the topography of a sample, information regarding surface topography and roughness are needed. Therefore, four BDD substrates (BDD₅₀₀ ag and cmp, BDD₂₀₀₀ ag and cmp) were investigated by means of optical microscopy. In Figure 4.3.3A-D, false colour images are shown highlighting the surface roughness of BDD layers. Ag BDD samples were found to have a rougher surface compared to the cmp samples. Still, the roughness of all four samples was found to be less than 1 μm . Smoothing of the surface by the cmp protocol is also visible in roughness profiles depicted in Figure 4.3.4A-D. Overall, the trend is coherent with literature, surface roughness decreases with increasing boron content [3] and the cmp procedure further smoothens the BDD layer. [14,15] Similar results were obtained by cooperation partners in AFM and SEM measurements. [10] It was concluded that the topographical influence on the SECM current signal was negligible because of low surface roughness and high planarity of BDD layers.

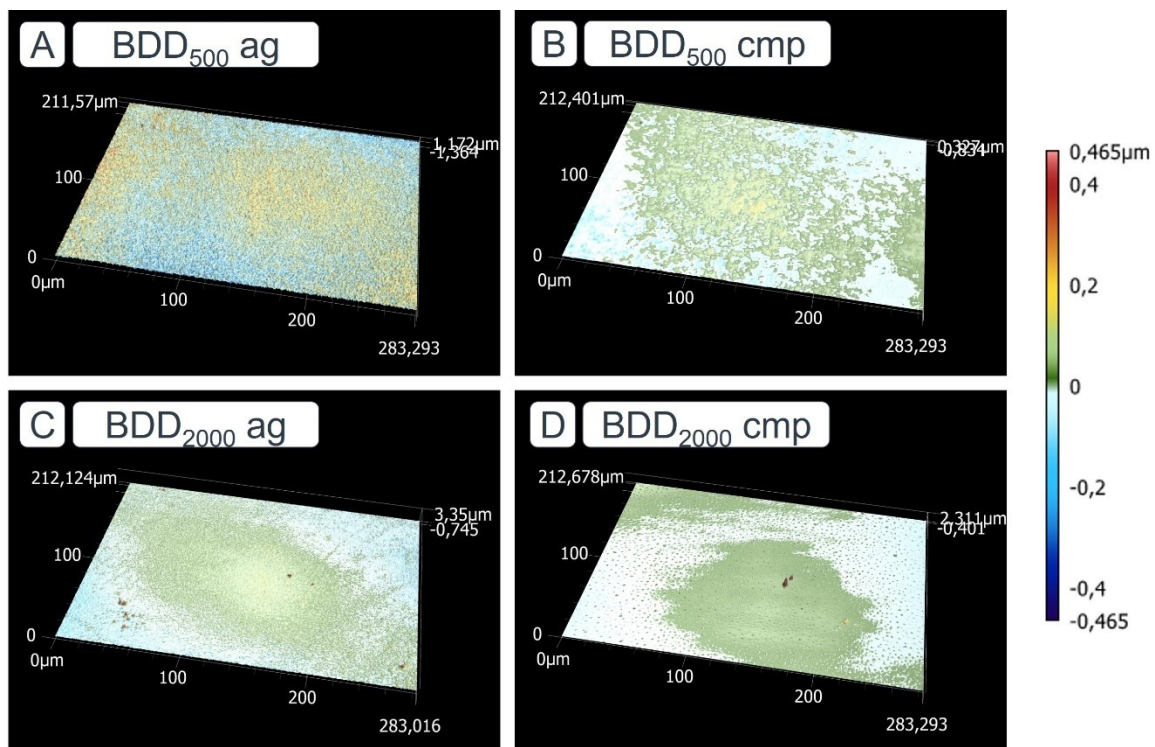


Figure 4.3.3. Microscopic false colour images of four BDD substrates, BDD₅₀₀ ag (A) and cmp (B), and BDD₂₀₀₀ ag (C) and cmp (D). Areas of 211×283 μm were scanned.

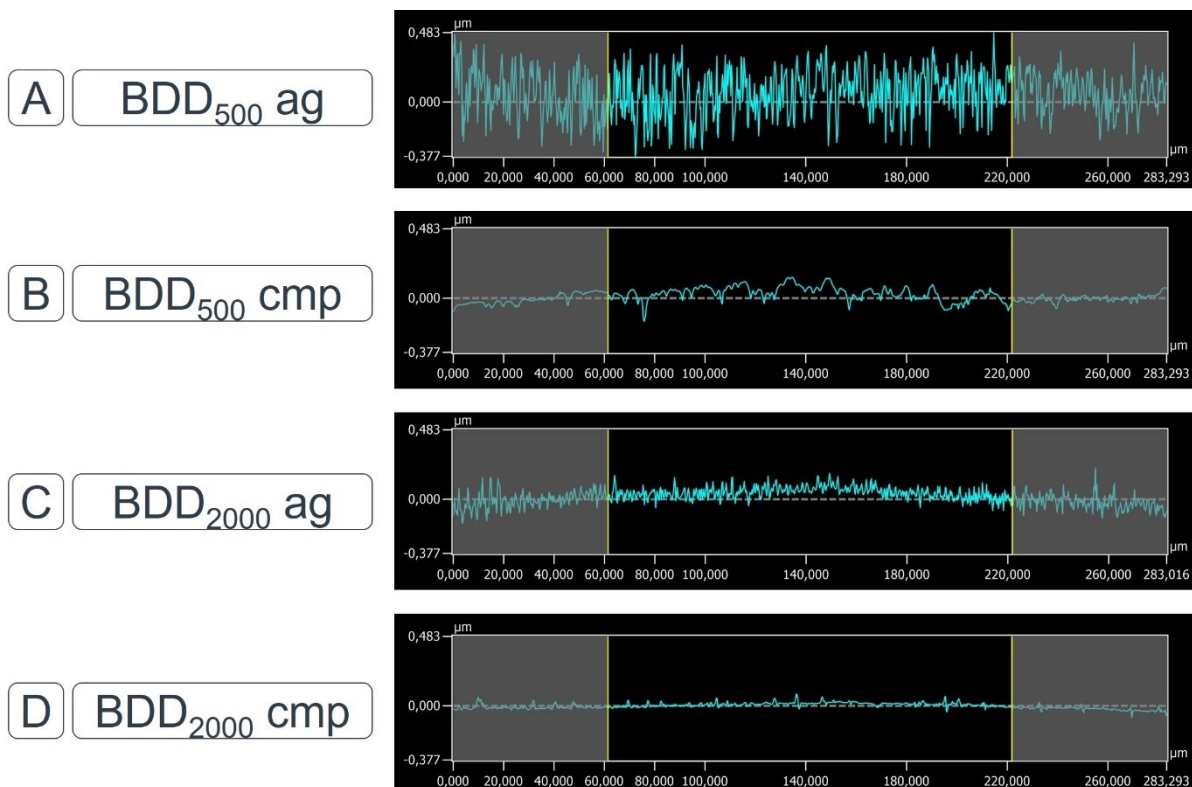


Figure 4.3.4. Roughness profiles of four BDD substrates, BDD₅₀₀ ag (A) and cmp (B), and BDD₂₀₀₀ ag (C) and cmp (D). A line scan with a length of 283 μm was evaluated per sample.

Following the topographical investigation of BDD substrates, SECM experiments were conducted on a selection of samples from both sets. Before imaging of samples is possible, substrates need to be levelled. This is typically achieved with a series of PACs when the electrochemical activity of the substrate is homogenous. Since the activity of BDD films is normally heterogeneously distributed, [20] PACs and probe scan curves (PSCs) were utilized in levelling the samples. Several PACs towards the surface of a BDD₈₀₀₀ ag sample are shown in Figure 4.3.5 together with model PACs for ideal positive [34] and negative [35] feedback. The theoretical PAC for positive feedback was calculated for an R_g of 10 according to the method from Amphlett *et al.* [34], for purely negative feedback the approach of Cornut *et al.* [35] was applied. The experimental data differs significantly from both theoretical approximations. On ag samples not only positive feedback was observed, as assumed for conductive surfaces, but also negative feedback indicating non-conductive areas. This observation was made solely on ag samples, on cmp electrodes only positive feedback was measured. In Figure 4.3.6, comparative SECM images of representative areas on several BDD substrates are shown. For comparability, measured currents were normalised by division of measured current by bulk current. Normalised currents above 1 can be translated as positive feedback, while currents below 1 reveal negative feedback. The same colour scale is used for

all samples. The BDD₅₀₀ ag substrate SECM image can be found in Figure 4.3.6A. Most of the electrode surface exhibited negative feedback, indicating a largely non-conductive surface. Only a small percentage of the image shows spots of positive feedback indicated by orange colour. In comparison, the image recorded of the surface of the BDD₅₀₀ cmp sample (Figure 4.3.6B) indicated much higher electrochemical activity but still with local variations. SECM images of samples with a higher boron doping level of 2000 ppm are depicted in Figure 4.3.6C (ag) and D (cmp). Overall, the electrochemical activity of the BDD₂₀₀₀ ag was much higher than the BDD₅₀₀ ag substrate, yet with heterogeneous distribution. The cmp substrate already exhibited almost completely homogeneous electrochemical activity across the investigated area. Altogether, the trend is also shown in the SECM images of the BDD₈₀₀₀ substrates depicted in Figure 4.3.6E (ag) and F (cmp). The ag substrate had a high number of active spots, nevertheless non-conductive areas can be found as also shown in one of the PACs (green line) depicted in Figure 4.3.5. Again, the pre-treated sample exhibited almost constant electrochemical activity across the surface. In conclusion, the electrode treatment by cmp enhanced the electrochemical performance of BDD films. With lower doped samples (BDD₅₀₀) the increase was found to be more pronounced. Complementary techniques utilized by cooperation partners within the original publication further support the beneficial effects of the cmp protocol. [10]

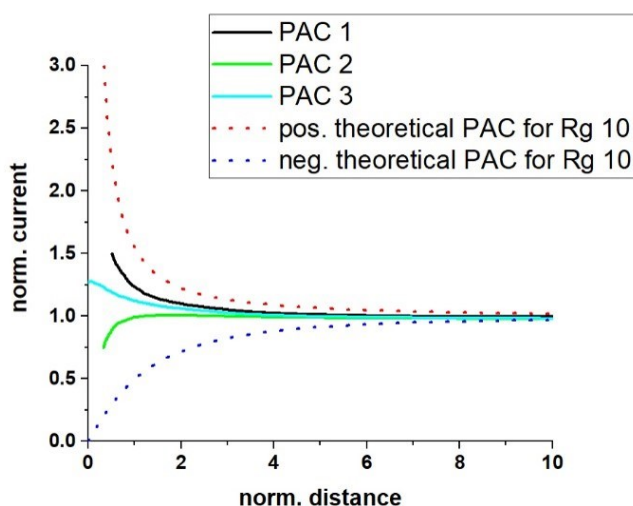


Figure 4.3.5. Series of PACs towards the surface of a BDD₈₀₀₀ ag substrate. Experimental PACs were recorded in 1.5 mM FcMeOH solution with 1 M KNO₃ as supporting electrolyte. Maximum approach speed was 2.5 $\mu\text{m s}^{-1}$, probe potential was +0.3 V, quiet time of 15 s, and a feedback target of 150% relative to steady-state bulk current was used. A platinum UME ($r = 12.5 \mu\text{m}$, $R_g \sim 10$) was used, reference was an Ag/AgCl/3 M KCl electrode, auxiliary electrode was a platinum wire. Theoretical models for positive and negative feedback [34,35] are shown as dotted lines.

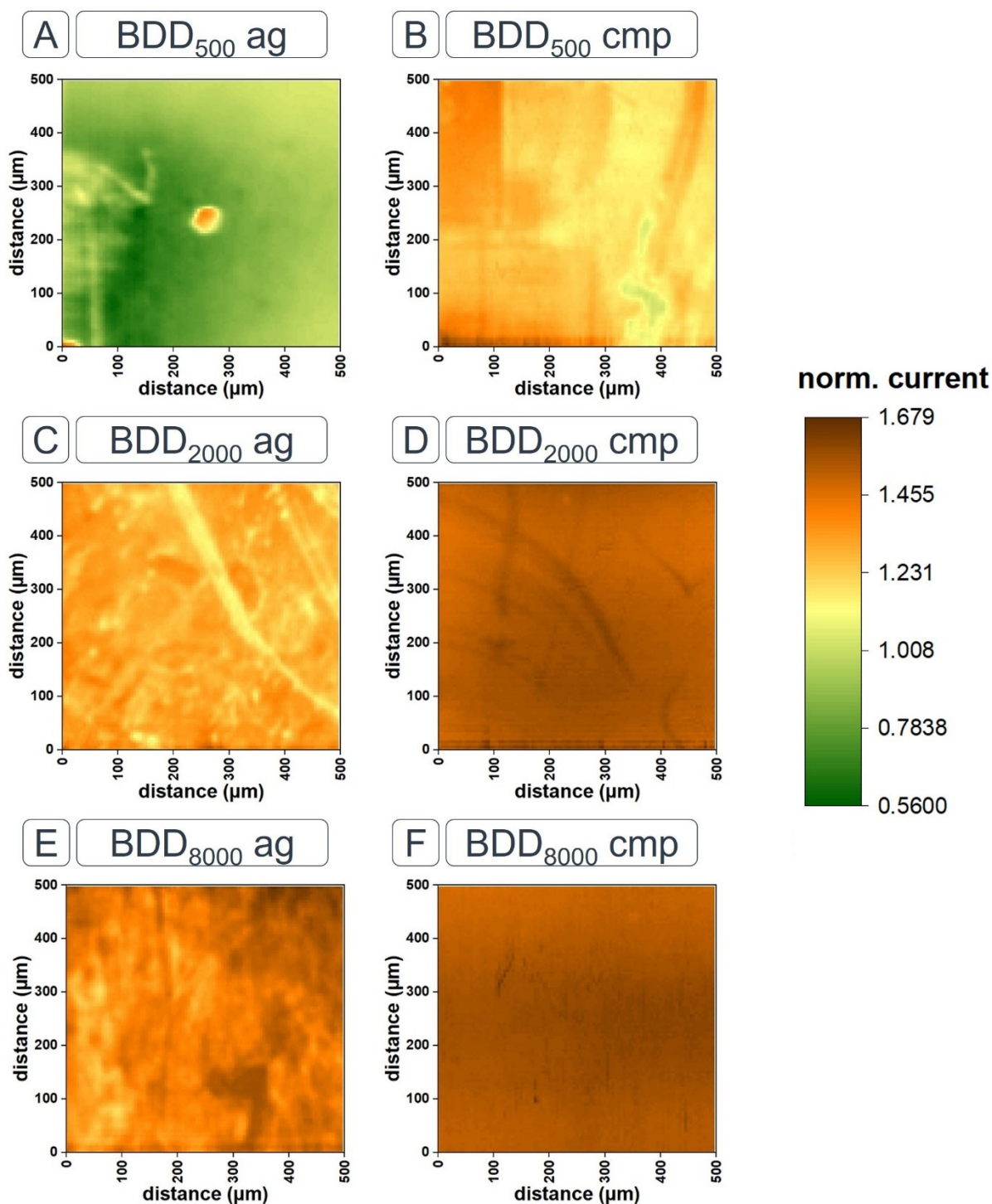


Figure 4.3.6. Comparison of SECM images recorded of the surface of various BDD substrates, BDD₅₀₀ ag (A) and cmp (B), BDD₂₀₀₀ ag (C) and cmp (D), BDD₈₀₀₀ ag (E) and cmp (F). Images were recorded in 1.5 mM FcMeOH solution with 1 M KNO₃ as supporting electrolyte. Scan rate was 200 μm s⁻¹, probe potential was +0.3 V, and quiet time of 15 s. Constant-height mode at a fixed height corresponding to a feedback target of 150% was used. A platinum UME ($r = 6.25 \mu\text{m}$, $R_g \sim 10$) was used, reference was an Ag/AgCl/3 M KCl electrode, auxiliary electrode was a platinum wire.

Determination of HET kinetics from SECM data

Eventually, HET rate constants k_0 were determined for a pair of BDD substrates with a boron doping level of 4000 ppm and compared to k_0 values obtained from CV data according to the Nicholson method. [10,33] While the CV method results in an average rate constant for the whole electrode surface, SECM approaches [16,29,32,36] deliver values for individual spots of an electrode, which renders them much more suitable for investigations of heterogeneous electrode materials. Methods based on SECM were proposed in feedback mode [29,32] as well as in the SG/TC mode. [16,36] For the investigation of ag and cmp BDD electrodes the method proposed by Wei *et al.* [32] was deemed to be the most suitable. Briefly, each PAC towards an individual point generates a k_0 value for that specific location. Per sample, seven individual PACs with differing coordinates on the surface were conducted. For comparability with CV data from cooperation partners, hexaammineruthenium(III) was used as mediator. Calculation of theoretical PACs with k_0 as variable was achieved with equations 4.3.1–4.

$$I_T(L) = \frac{i_T}{i_{T,\infty}} = I_T^{ins}(L) + I_S^{kin}(L, k_0) \left(1 - \frac{I_T^{ins}(L)}{I_T^{cond}(L)} \right) \quad (4.3.1)$$

Where $I_T(L)$ represents the normalised tip current at a distance L from the substrate surface, $I_T^{ins}(L)$ is the normalised tip current towards a purely insulating surface, $I_S^{kin}(L, k_0)$ stands for the normalised current of the substrate resulting from mediator regeneration, and $I_T^{cond}(L)$ represents the normalised tip current for ideal positive feedback. Individual contributions to the total tip current were calculated according to equations 4.3.2–4.

$$I_T^{ins}(L) = \frac{1}{0.40472 + \frac{1.60185}{L} + 0.58819 \exp\left(\frac{-1.41332}{L}\right)} \quad (4.3.2)$$

$$I_S^{kin}(L, k_0) = \frac{0.78377}{L\left(1 + \frac{1}{\kappa L}\right)} + \frac{0.68 + 0.3315 \exp\left(\frac{-1.0672}{L}\right)}{1 + \frac{\left(\frac{11}{\kappa L}\right) + 7.3}{110 - 40L}} \quad (4.3.3)$$

$$I_T^{cond}(L) = 0.72627 + \frac{0.76651}{L} + 0.26015 \exp\left(\frac{-1.41332}{L}\right) \quad (4.3.4)$$

The parameter $\kappa = k_0 r_T / D$ is a dimensionless rate constant, r_T is the radius of the electrode, and D is the diffusion coefficient of the mediator. Equations 4.3.1–4 are valid for $R_g = 10$ and normalised distances $0.1 \leq L \leq 1.5$. The diffusion coefficient used for

hexaammineruthenium(III) in KNO_3 was $5.32 \times 10^{-6} \text{ cm}^2 \text{ s}^{-1}$. [37] Experimental PACs towards BDD_{4000} samples are shown in Figure 4.3.7A towards the ag substrate and in Figure 4.3.7B towards the cmp BDD electrode. Furthermore, PACs for ideal positive feedback are shown as dotted line for comparison. On the ag sample, the maximum reached feedback current varied between 170% up to 330% feedback, while on the cmp sample the reached feedback only varied to a smaller degree between approximately 360% up to 400%. Fitting of experimental data with the theoretical model yields a k_0 value per PAC which are summarized in Table 4.3.1. The range of k_0 values for the ag sample was between 0.113 up to 0.313 cm s^{-1} , while for the cmp substrate rate constants between 0.280 up to 0.382 cm s^{-1} were determined. On average, k_0 values of 0.209 cm s^{-1} on the ag BDD and 0.319 cm s^{-1} on the cmp sample were obtained from SECM data in contrast to 0.057 cm s^{-1} (BDD_{4000} ag) and 0.164 cm s^{-1} (BDD_{4000} cmp) determined from CV data. In both methods, faster kinetics were determined for the cmp BDD and less variance in the SECM determined values further prove lower heterogeneity of the electrochemical activity on the BDD surface.

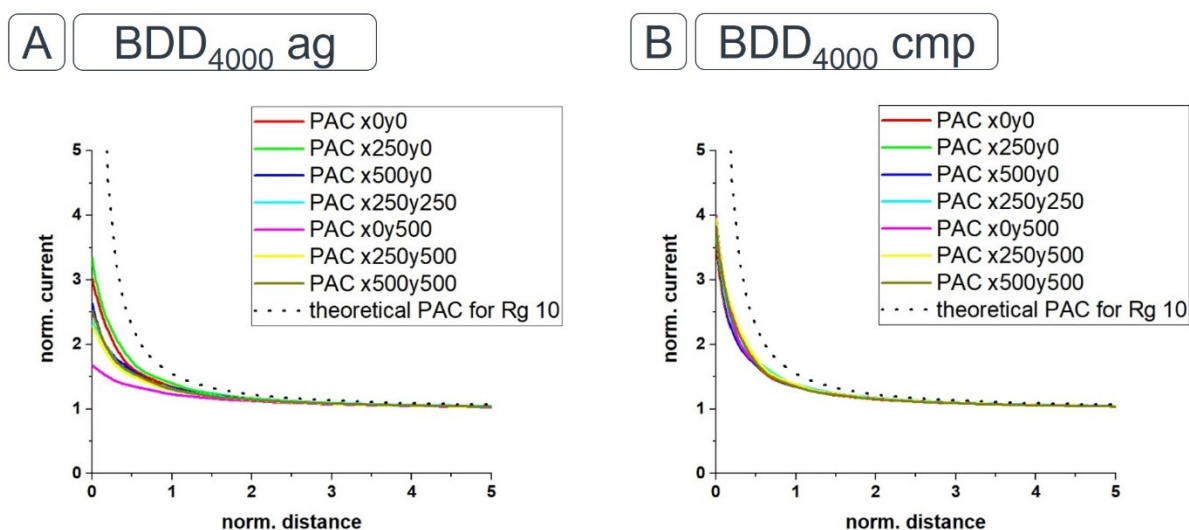


Figure 4.3.7. Series of PACs towards the surface of two BDD_{4000} substrates, BDD_{4000} ag (A) and cmp (B). PACs were recorded in 1.5 mM hexaammineruthenium(III) solution with 1 M KNO_3 as supporting electrolyte. Maximum approach speed was $0.5 \mu\text{m s}^{-1}$, probe potential was -0.3 V , feedback current target of 500%, and quiet time of 15 s. A platinum UME ($r = 6.25 \mu\text{m}$, $R_g \sim 10$) was used as probe, reference was an $\text{Ag}/\text{AgCl}/3 \text{ M KCl}$ electrode, and auxiliary was a platinum wire.

Table 4.3.1. Determined HET rate constants k_0 from PACs and CV of BDD₄₀₀₀ ag and cmp samples according to the methods by Wei *et al.* [32] and Nicholson. [33]

Sample	Coordinates	k_0 (cm s ⁻¹)	k_0 range (cm s ⁻¹)	k_0 from CV data [10] (cm s ⁻¹)
BDD₄₀₀₀ ag	X 0/Y 0	0.270		
	X 250/Y 0	0.313		
	X 500/Y 0	0.203		
	X 250/Y 250	0.193	0.113 – 0.313	0.057
	X 0/Y 500	0.113		
	X 250/Y 500	0.175		
	X 500/Y 500	0.194		
BDD₄₀₀₀ cmp	X 0/Y 0	0.280		
	X 250/Y 0	0.287		
	X 500/Y 0	0.288		
	X 250/Y 250	0.322	0.280 – 0.382	0.164
	X 0/Y 500	0.326		
	X 250/Y 500	0.382		
	X 500/Y 500	0.345		

4.3.3 Conclusion

Within this project, two sets of BDD electrodes, ag and cmp, with boron doping levels between 500 and 8000 ppm were characterised by means of the feedback mode of SECM. Furthermore, several other techniques were utilized by cooperation partners and discussed together with the SECM findings. [10]

In first experiments, four commonly used redox mediators, FcMeOH, hexacyanoferrate(II), hexacyanoferrate(III), and hexaammineruthenium(III) were tested for their suitability in imaging reactivity differences between ag and cmp BDD layers. SECM imaging of BDD₄₀₀₀ ag revealed good image quality for FcMeOH and hexaammineruthenium(III), while usage of hexacyanoferrate(II) and (III) resulted in much less detailed activity maps of the substrate. Quality differences were attributed to the surface sensitivity of used redox markers. While inner-sphere probes, hexacyanoferrate(II) and (III) are highly sensitive to surface morphology, outer-sphere markers are much less sensitive. Imaging of the cmp substrate was successful with FcMeOH, hexacyanoferrate(II), and hexacyanoferrate(III), whereas lower currents were measured in usage of inner-sphere markers. Hexaammineruthenium(III) delivered poor image quality resulting from signal stability issues during measurements. Overall, highest consistency and image quality was achieved in FcMeOH solution.

Next, comparative SECM experiments on both sets of BDD electrodes were conducted in FcMeOH. On ag samples, not only positive feedback characteristic for conductive materials could be detected but also negative feedback indicating non-conductive surface areas. This finding was exclusive for ag substrates, even the lowest doped cmp electrode (BDD₅₀₀ cmp) was found to exhibit only positive feedback in examined areas. Electrochemical activity in general was much more heterogeneously distributed on ag samples. Differences were more drastic on lower doped samples. Higher doped samples of cmp electrodes showed almost homogeneously distributed conductivity across the surface.

Furthermore, HET rate constants k_0 were probed locally by means of SECM using hexaammineruthenium(III) as mediator. While determination from CV data results only in an average value for the whole electrode, the SECM approach yield highly localized values for individual spots on the BDD surface. For the ag BDD₄₀₀₀, k_0 values between 0.113 up to 0.313 cm s⁻¹ were determined with an average of 0.209 cm s⁻¹. PACs towards the surface of the BDD₄₀₀₀ cmp substrate yielded a k_0 range of 0.280 up to 0.382 cm s⁻¹ and an average of 0.319 cm s⁻¹. Less variation and a larger average rate constant further proofed the increased performance of cmp electrodes.

4.3.4 Experimental section

Chemicals and materials

Hexaammineruthenium(III) chloride (99%) was acquired from ABCR (Karlsruhe, Germany). Ferrocene methanol (FcMeOH, 97%) was purchased from Alfa Aesar (Haverhill, USA). Potassium chloride (KCl, $\geq 99.5\%$) was acquired from Carl Roth (Karlsruhe, Germany). Potassium hexacyanoferrate(II) trihydrate ($\geq 99\%$) and potassium hexacyanoferrate(III) ($\geq 99\%$) were purchased from Sigma-Aldrich (St. Louis, USA). Potassium nitrate (KNO_3 , $\geq 99\%$) was acquired from Merck (Darmstadt, Germany).

Lapping film sheets with particle sizes ranging from 0.3 to 30 μm were purchased from Precision Surfaces International (Houston, USA). Platinum wires with radii of 6.25 μm (99.9%), 12.5 μm (99.9%), and 0.5 mm (99.9%) were purchased from Goodfellow (Huntingdon, UK). Silver conductive epoxy adhesive (Article 8331) was acquired from MG Chemicals (Ontario, Canada). Soda-lime glass tubes with an inner diameter of 1.15 mm were supplied by Hilgenberg (Malsberg, Germany). Two-component adhesive (Epoxy resin L + Hardener S) was acquired from R&G Faserverbundwerkstoffe (Waldenbuch, Germany).

All solutions were prepared with ultra-pure water ($>18.2 \text{ M}\Omega \text{ cm}$) supplied by a Milli-Q Advantage A10 system from Merck (Darmstadt, Germany). Mediator solutions consisted of 1.5 mM of respective mediator and 1 M KNO_3 .

SECM probe fabrication and substrate preparation

UME probes suitable for SECM measurements were fabricated from soda-lime glass tubes with an inner diameter of 1.15 mm. Tubes were pulled in a butane flame resulting in pipettes with opening diameters of circa 100 μm . A 1 cm piece of platinum wire (radius either 6.25 or 12.5 μm) was soldered to jumper wire (cross-section 0.2 mm^2 , insulating layer diameter 1.1 mm) and subsequently, the assembly was carefully inserted into a pulled glass pipette. The matching diameters of glass tubes and the insulation layer of the jumper wire led to mechanical stability of the probe. Tips were re-sealed by melting in a butane flame once approximately 1 mm of the platinum wire protruded from the tip opening. Exposition of a platinum micro disk electrode was eventually achieved by defined polishing in a custom-made polishing device equipped with lapping film sheets. Coarse polishing was performed with a grit size of 30 μm , mirror finish of the electrode surface was achieved by fine polishing with a grit size of 0.3 μm . Eventually, the quality of the SECM probe was inspected by optical microscopy

at 100x magnification and its R_g value, i. e. ratio of insulating layer and active electrode radii, was determined. Before utilization in SECM experiments, the electrochemical behaviour was evaluated by cyclic voltammetry in the respective mediator solution.

For installation within the electrochemical cell, BDD electrodes had to be mounted onto laboratory-constructed substrate holders. Holders basically consisted of a brass rod (diameter = 2.5 mm) with a polyvinyl chloride mantle (thickness = 2 mm, total diameter = 6.5 mm). On the flat top of a holder, a small amount of silver conductive epoxy adhesive was applied, followed by the careful positioning of a BDD substrate. The curing time of the conductive adhesive was at least six hours at room temperature. Afterwards, two-component adhesive was applied to the sides of the BDD substrate to prevent exposition of the silver epoxy to the electrolyte solutions. Substrates were suitable for SECM experiments after another curing step of at least 24 hours at ambient conditions.

Experimental setup

SECM experiments were conducted with a commercially available SECM 920C system from CH Instruments (Austin, USA). The electrochemical setup and the positioning motor unit were placed on a dampening mat located within a laboratory-constructed Faraday cage to minimize electromagnetic noise and vibrations. The electrochemical cell was made from polytetrafluoroethylene with a volume of 5 mL. Substrates could be installed in a hole in the bottom of the cell, a tight fit was achieved with small pieces of polytetrafluoroethylene tape. Experiments were conducted in a four-electrode arrangement. Working electrode channel 1 was connected to the SECM probe, working electrode channel 2 was connected to the BDD substrate. A platinum wire was used as auxiliary electrode and an Ag/AgCl/3 M KCl electrode (CH Instruments, Austin, USA) was the reference electrode. All potentials stated are referred to this electrode setup. SECM probes were platinum based UMEs with electrode radii of 6.25 and 12.5 μm and variable R_g values. Two different sets of polycrystalline BDD electrodes from cooperation partners were investigated. BDD layers were deposited on conductive Si wafers with a microwave plasma enhanced CVD AX5010 system from Seki Diamonds Systems (San Jose, USA). Boron doping was achieved by introducing trimethylborane into the gas phase with resulting B/C ratios of 500 up to 8000 ppm (BDD₅₀₀–BDD₈₀₀₀). The first set of BDD electrodes was characterised without any further treatment, “as-grown (ag)”. The second set was modified by chemical-mechanical polishing the BDD layers according to the procedure published by Thomas *et al.* [14] Microscopic images and surface roughness profiles of several BDD substrates were obtained with a VK-X 3000 3D laser scanning microscope from Keyence (Neu-Isenburg, Germany).

Experimental procedures

Four commonly used redox mediators were initially evaluated regarding their performance in feedback mode SECM experiments of BDD electrodes. FcMeOH, hexaammineruthenium(III), hexacyanoferrate(II), and hexacyanoferrate(III) were tested. Solutions with 1.5 mM of the respective mediator and 1 M of KNO_3 as supporting electrode were prepared. A BDD substrate was installed in the bottom of the electrochemical cell, the cell was filled with 5 mL of mediator solution, and it was levelled with a series PACs and PSCs before imaging experiments were started. Suitable probe potentials were determined from cyclic voltammetric measurements in respective mediator solution. For FcMeOH a probe potential of +0.3 V was applied, for hexaammineruthenium(III) the potential was -0.2 V, for hexacyanoferrate(II) it was +0.1 V, and for hexacyanoferrate(III) the probe potential was +0.5 V. Further PAC parameters were: maximum movement speed = $2.5 \mu\text{m s}^{-1}$, quiet time = 15 s, and feedback current target = 150%. After levelling, SECM images were recorded with a probe scan rate of $200 \mu\text{m s}^{-1}$, quiet time of 15 s, image size of $500 \times 500 \mu\text{m}$, and a pixel size of $5 \mu\text{m}$. Imaging was conducted in constant-height mode at a height corresponding to a feedback current of 150% relative to the steady-state current in bulk solution. Two substrates were imaged in all mediator solutions, an ag BDD₄₀₀₀ and a cmp BDD₄₀₀₀ electrode. For evaluating the performance of individual mediators, an identical area per sample was imaged in all four solutions. Experiments were conducted with a platinum UME with an electrode radius of $12.5 \mu\text{m}$ and an R_g value of ~ 10 .

Comparative studies of both sets of BDD electrodes, ag and cmp, with various boron doping levels were conducted in FcMeOH solution (1.5 mM FcMeOH, 1 M KNO_3). A BDD sample was mounted in the electrochemical cell, which was then filled with 5 mL of the FcMeOH solution. Proper levelling was achieved by repeated PACs and PSCs across the BDD surface. PAC parameters were: maximum approach speed = $2.5 \mu\text{m s}^{-1}$, probe potential = +0.3 V, quiet time = 15 s, feedback current target = 150%. Eventually, representative SECM images were recorded of each sample. For comparability between individual specimen, constant-height mode at a height corresponding to a feedback current of 150% was used. Areas of $500 \times 500 \mu\text{m}$ were imaged per with a pixel size of $5 \mu\text{m}$, a quiet time of 15 s before current recording, a probe movement speed of $200 \mu\text{m s}^{-1}$, and a probe potential of +0.3 V. A total of six substrates were imaged this way, BDD₅₀₀, BDD₂₀₀₀, and BDD₈₀₀₀, each in the ag and cmp variant. UME probes with an electrode radius of $6.25 \mu\text{m}$ and R_g values of ~ 10 were used.

In order to evaluate spatially resolved heterogeneous electron transfer kinetics of BDD₄₀₀₀ ag and cmp substrates from SECM data, the method developed by Wei *et al.* [32] was used. The respective substrate was mounted in the electrochemical cell, which was subsequently filled with 5 mL of mediator solution. To be able to compare the obtained heterogeneous electron transfer rate constants k_0 with the results [10] of the cooperation partners, hexaammineruthenium(III) solution (1.5 mM hexaammineruthenium(III), 1 M KNO₃) was used as mediator. After sufficient levelling of a sample, a series of seven individual PACs on different locations were performed. PAC parameters were: probe potential = -0.3 V, maximum approach speed = 0.5 $\mu\text{m s}^{-1}$, quiet time = 15 s, feedback current target = 500%. Part of PAC measurements were manually stopped after the surface was touched by the probe tip. Experimental data was fitted with a theoretical model yielding one k_0 per approached position. The diffusion coefficient for hexaammineruthenium(III) used for calculations of k_0 values was $5.5 \times 10^{-6} \text{ cm}^2 \text{ s}^{-1}$. [37] A platinum UME with an electrode radius of 6.25 μm and an R_g of ~ 10 was used.

References

- [1] Z. Liu, S. Baluchová, Z. Li, Y. Gonzalez-Garcia, C. E. Hall, J. G. Buijnsters, *Acta Mater.* 2024, 266, 119671.
- [2] A. Taylor, P. Ashcheulov, P. Hubík, Z. Weiss, L. Klimša, J. Kopeček, J. Hrabovsky, M. Veis, J. Lorinčík, I. Elantyeve et al., *Diam. Relat. Mater.* 2023, 135, 109837.
- [3] S. Baluchová, A. Daňhel, H. Dejmková, V. Ostatná, M. Fojta, K. Schwarzová-Pecková, *Anal. Chim. Acta* 2019, 1077, 30.
- [4] N. Yang, S. Yu, J. V. Macpherson, Y. Einaga, H. Zhao, G. Zhao, G. M. Swain, X. Jiang, *Chem. Soc. Rev.* 2019, 48, 157.
- [5] K. Muzyka, J. Sun, T. H. Fereja, Y. Lan, W. Zhang, G. Xu, *Anal. Methods* 2019, 11, 397.
- [6] V. Rehacek, I. Hotovy, M. Marton, M. Mikolasek, P. Michniak, A. Vincze, A. Kromka, M. Vojs, *J. Electroanal. Chem.* 2020, 862, 114020.
- [7] K. Schwarzová-Pecková, J. Vosáhlová, J. Barek, I. Šloufová, E. Pavlova, V. Petrák, J. Zavázalová, *Electrochim. Acta* 2017, 243, 170.
- [8] J.-P. Lagrange, A. Deneuve, E. Gheeraert, *Diam. Relat. Mater.* 1998, 7, 1390.
- [9] M. Bernard, A. Deneuve, P. Muret, *Diam. Relat. Mater.* 2004, 13, 282.
- [10] M. Zelenský, J. Fischer, S. Baluchová, L. Klimša, J. Kopeček, M. Vondráček, L. Fekete, J. Eidenschink, F. M. Matysik, S. Mandal et al., *Carbon* 2023, 203, 363.
- [11] T. A. Ivandini, T. Watanabe, T. Matsui, Y. Ootani, S. Iizuka, R. Toyoshima, H. Kodama, H. Kondoh, Y. Tateyama, Y. Einaga, *J. Phys. Chem. C* 2019, 123, 5336.
- [12] S. Baluchová, A. Taylor, V. Mortet, S. Sedláková, L. Klimša, J. Kopeček, O. Hák, K. Schwarzová-Pecková, *Electrochim. Acta* 2019, 327, 135025.
- [13] S. C. B. Oliveira, A. M. Oliveira-Brett, *Electrochim. Acta* 2010, 55, 4599.
- [14] E. L. Thomas, G. W. Nelson, S. Mandal, J. S. Foord, O. A. Williams, *Carbon* 2014, 68, 473.
- [15] J. Ryl, A. Zielinski, L. Burczyk, R. Bogdanowicz, T. Ossowski, K. Darowicki, *Electrochim. Acta* 2017, 242, 268.
- [16] S.-Y. Tan, R. A. Lazenby, K. Bano, J. Zhang, A. M. Bond, J. V. Macpherson, P. R. Unwin, *Phys. Chem. Chem. Phys.* 2017, 19, 8726.
- [17] K. Jüttner, D. Becker, *J. Appl. Electrochem.* 2006, 37, 27.
- [18] a) J. Steeds, A. Gilmore, S. Charles, P. Heard, B. Howarth, J. Butler, *Acta Mater.* 1999, 47, 4025; b) S. Ferro, M. Dal Colle, A. de Battisti, *Carbon* 2005, 43, 1191.

- [19] S. Szunerits, M. Mermoux, A. Crisci, B. Marcus, P. Bouvier, D. Delabouglise, J.-P. Petit, S. Janel, R. Boukherroub, L. Tay, *J Phys. Chem. B* 2006, 110, 23888.
- [20] S. Wang, G. M. Swain, *J. Phys. Chem. C* 2007, 111, 3986.
- [21] N. R. Wilson, S. L. Clewes, M. E. Newton, P. R. Unwin, J. V. Macpherson, *J. Phys. Chem. B* 2006, 110, 5639.
- [22] K. B. Holt, A. J. Bard, Y. Show, G. M. Swain, *J. Phys. Chem. B* 2004, 108, 15117.
- [23] H. V. Patten, S. C. S. Lai, J. V. Macpherson, P. R. Unwin, *Anal. Chem.* 2012, 84, 5427.
- [24] A. J. Bard, M. V. Mirkin, *Scanning electrochemical microscopy*, CRC Press, Boca Raton, 2012.
- [25] a) R. C. Engstrom, C. M. Pharr, *Anal. Chem.* 1989, 61, 1099A-1104A; b) A. J. Bard, F. R. F. Fan, J. Kwak, O. Lev, *Anal. Chem.* 1989, 61, 132.
- [26] T. Raith, A. Kröninger, M. J. Mickert, H. H. Gorris, F.-M. Matysik, *Talanta* 2020, 214, 120844.
- [27] X. Zeng, D. Liu, S. Wang, S. Liu, X. Cai, L. Zhang, R. Zhao, B. Li, F. Kang, *ACS Appl. Mater. Inter.* 2020, 12, 37047.
- [28] C. Iffelsberger, S. Wert, F.-M. Matysik, M. Pumera, *ACS Appl. Mater. Inter.* 2021, 13, 35777.
- [29] A. K. Neufeld, A. P. O'Mullane, *J Solid State Electr.* 2006, 10, 808.
- [30] S. Wert, S. Baluchová, K. Schwarzová-Pecková, S. Sedláková, A. Taylor, F.-M. Matysik, *Monatsh. Chem.* 2020, 151, 1249.
- [31] a) C. Iffelsberger, T. Raith, P. Vatsyayan, V. Vyskočil, F.-M. Matysik, *Electrochim. Acta* 2018, 281, 494; b) J. S. Barroso-Martínez, A. I. B Romo, S. Pudar, S. T. Putnam, E. Bustos, J. Rodríguez-López, *J. Am. Chem. Soc.* 2022, 144, 18896.
- [32] C. Wei, A. J. Bard, M. V. Mirkin, *J. Phys. Chem.* 1995, 99, 16033.
- [33] R. S. Nicholson, *Anal. Chem.* 1965, 37, 1351.
- [34] J. L. Amphlett, G. Denuault, *J. Phys. Chem. B* 1998, 102, 9946.
- [35] R. Cornut, C. Lefrou, *J. Electroanal. Chem.* 2007, 608, 59.
- [36] H. V. Patten, K. E. Meadows, L. A. Hutton, J. G. Iacobini, D. Battistel, K. McKelvey, A. W. Colburn, M. E. Newton, J. V. Macpherson, P. R. Unwin, *Angew. Chem. Int. Ed.* 2012, 51, 7002.
- [37] Y. Wang, J. G. Limon-Petersen, R. G. Compton, *J. Electroanal. Chem.* 2011, 652, 13.

5 Summary

A prerequisite for the first two main projects of the presented dissertation was the ability to operate the SECM setup under inert conditions. Thus, an inert gas box was designed and developed together with the mechanical workshop of the University of Regensburg. It was designed to house the SECM setup as well as enabling manipulations of the electrochemical setup during measurement sessions. A continuous flow of Argon through the box resulted in a permanent excess pressure on the inside. Consequently, an inert atmosphere was ensured even during opening of the glove hole covers for short periods of times.

Within the first main project, a simple and straightforward SICM method for usage in lithium-ion battery (LIB) electrolytes was developed. The method was based on the ferrocene/ferrocenium redox couple, which was also suitable as reference electrode. Measurements on a micro milled copper circuit board as model substrate demonstrated the signal stability and reproducibility of the SICM approach. Probe approach curves (PACs) towards the sample surface were highly reproducible with minor deviations between individual measurements. Moreover, fine details of the sample topography were resolved in imaging experiments. The SICM method was hyphenated to feedback mode SECM with the help of a laboratory-constructed dual-probe holder. It enabled the usage of two individual probes at the same time. The combined SECM/SICM approach was utilized in the study of a commercially available LIB graphite electrode before and after the application of a pre-charging protocol. Measurements revealed changes in the electrochemical activity as well as the topography of the electrode. These findings demonstrated the need for developments capable of separating the topographical and electrochemical influence onto the SECM signal, especially in the context of LIB studies.

The scope of the second main project was to significantly reduce the amount of mediator species within the electrochemical cell, because of its potentially interfering effects on battery chemistry. A novel mediator dosing (MD) concept was designed with the requirements of minimized mediator usage, comparable data quality, and simplicity of the setup. Thus, a dosing capillary installed together with the SECM probe in a dual-probe holder was used to locally dose mediator solution close to the probe tip. A height difference between the inlet and outlet of the capillary was used to generate a gravity-driven flow. In first experiments, the flow rates resulting from various height differences were determined. After choosing a suitable height difference, PACs towards conductive and non-conductive parts of a model substrate were performed and compared to theoretical curves. Measurements demonstrated good accordance with the mathematical approximations and excellent reproducibility. Furthermore, imaging experiments of the model substrate were carried out under MD conditions and

compared to conventional measurements conducted directly in mediator solution. It was found that the quality of MD images was on par with images obtained in mediator solution. Further imaging experiments were performed with a LIB graphite composite electrode. Again, the achieved image quality was comparable to measurements in bulk solution. The proposed MD concept could be beneficial for studies regarding the formation of interphases on negative and positive LIB electrodes during charging/discharging processes, since the interfering influence of added mediator species is reduced to a minimum.

The third project was focused on the SECM characterisation of two sets of boron-doped diamond (BDD) electrodes, as-grown and chemically-mechanically polished (cmp). Moreover, each set consisted of specimen with varying boron doping levels in the range of 500 to 8000 ppm. First experiments were performed, to evaluate four commonly used mediators regarding their suitability to resolve reactivity differences of the BDD substrates. Highest consistency and imaging quality was achieved with usage of ferrocene methanol as mediator. The comparative study revealed that as-grown samples not only exhibited positive feedback typical for conductive materials, but also non-conductive areas, indicated by negative feedback, were found. In contrast, cmp substrates only showed positive feedback. Overall, as-grown samples were found to have a much more heterogeneous electrochemical activity, even at the highest doping level. The electrochemical activity of cmp electrodes was almost homogeneous. Differences between both sets were more drastic on lower doped samples. Further SECM experiments were conducted to locally probe electron transfer kinetics at as-grown and cmp BDD electrodes with 4000 ppm boron doping. A larger average as well as less variation between individual areas was found for the treated sample.

In a side project, the feedback mode of SECM was used to characterise stamping platinum electrodes. By simple application of a non-conductive varnish with a defined shape onto a platinum macro electrode, several microstructures were fabricated. SECM experiments were performed to evaluate the properties of three different structures, a dot-shape, a band-shape, and a circle-shape. The obtained SECM images validated the expected sizes and quality of the microstructures, and furthermore, the stability and insulating properties of the surrounding varnish layer.

In summary, the SECM was improved by instrumental and methodical developments with a focus on LIB research. A simple and straightforward SICM method was introduced and hyphenated to feedback mode SECM. The combined SECM/SICM approach was applied in carbonate-based solvents, typically used in LIBs. Furthermore, a novel concept for reduced usage of mediator during *in situ* and even *in operando* studies of LIBs was established. Measurements with a model substrate and a LIB graphite electrode demonstrated the performance of the MD approach. Besides, SECM was applied in the characterisation of

several electrode materials in the scope of other projects conducted in aqueous media. Two sets of BDD samples, with and without treatment through cmp, were investigated. Additionally, the influence of different boron doping levels was evaluated. Moreover, microstructures stamped on top of platinum macro electrodes were characterised regarding their quality.

6 Zusammenfassung in deutscher Sprache

Eine Voraussetzung für die ersten beiden Hauptprojekte der vorliegenden Dissertation ist die Möglichkeit das SECM unter Inertbedingungen betreiben zu können. Für diesen Zwecks wurde in Kooperation mit der Feinmechanischen Werkstatt der Universität Regensburg eine Inertgasbox aus Plexiglas entwickelt. Sie wurde entworfen, um das existierende SECM-Setup inklusive Faraday-Käfig aufnehmen zu können. Außerdem sollte es weiterhin möglich sein, Veränderungen am elektrochemischen Aufbau vornehmen zu können, auch während des Messbetriebs. Ein kontinuierlicher Argonstrom durch die Box führte zu einem permanenten Überdruck im Inneren. Dadurch war die inerte Atmosphäre auch während des kurzzeitigen Öffnens der Eingriffabdeckungen gewährleistet.

Im Rahmen des ersten Hauptprojekts wurde eine unkomplizierte und leicht anzuwendende SICM-Methode zur Nutzung in Elektrolytlösungen aus Lithium-Ionen-Batterien entwickelt. Die Methode basiert auf der Nutzung des Ferrocen/Ferrocenium-Redoxpaars, welches darüber hinaus geeignet für den Einsatz in einer Referenzelektrode war. Messungen mit einer mikrogefrästen Kupferleiterplatte als Modellsubstrat demonstrierten die Signalstabilität und Reproduzierbarkeit der entwickelten SICM-Technik. Annäherungskurven der Sonde zur Substratoberfläche zeigten eine sehr gute Reproduzierbarkeit einzelner Messungen auf. Weiterhin wurden Details der Oberflächentopografie des Modellsubstrats in Imaging-Experimenten fein aufgelöst dargestellt. Im Anschluss wurde die vorgestellte SICM-Methode mit dem Feedback-Modus des SECM mithilfe eines speziell angefertigten Dual-Sondenhalters kombiniert. Dadurch wurde es ermöglicht, zwei individuelle Sonden gleichzeitig zu verwenden. Der gekoppelte SECM/SICM-Aufbau wurde in der Untersuchung kommerziell erhältlicher LIB-Graphitelektroden, vor und nach der Anwendung eines Vorladungsprotokolls, eingesetzt. Die zugehörigen Messungen zeigten auf, dass sich nicht nur die elektrochemische Aktivität der Probe veränderte, sondern auch ihre Topografie. Diese Ergebnisse betonen die Notwendigkeit von Entwicklungen hinsichtlich der Entkopplung beider Einflüsse auf das Messsignal in der SECM-Thematik, besonders im Kontext von Untersuchungen an Lithium-Ionen-Batterien.

Das Ziel des zweiten Hauptprojekts war es, die Menge an eingesetztem Mediator im elektrochemischen Aufbau signifikant zu verringern, um mögliche Interferenzen auf die Batteriechemie zu unterbinden. Daher wurde ein neuartiges Mediatordosier-Konzept entwickelt im Hinblick auf minimierten Mediatoreinsatz, ausreichende Datenqualität und ein möglichst unkompliziertes Setup. Diese Anforderungen werden erfüllt durch den Einsatz einer Dosierkapillare welche lokal an der Spitze der SECM-Sonde Mediatorlösung zudosiert. Sonde und Kapillare wurden im Dual-Sondenhalter installiert und konnten individuell zueinander ausgerichtet werden. Ein variabler Höhenunterschied zwischen der Eingangs- und

Ausgangsöffnung der Kapillare führte zu einem gravitationsbedingten Fluss der Mediatorlösung. Die resultierenden Fließgeschwindigkeiten wurden in den ersten Experimenten in Abhängigkeit des Höhenunterschieds bestimmt. Nach der Wahl eines geeigneten Höhenunterschieds wurden Annäherungskurven zu leitenden und nichtleitenden Bereichen eines Modellsubstrats durchgeführt und mit theoretischen Kurvenverläufen gegenübergestellt. Die Messungen zeigten eine gute Übereinstimmung mit den mathematischen Modellen und darüber hinaus eine exzellente Reproduzierbarkeit. Im Anschluss wurden Imaging-Experimente am Modellsubstrat unter MD-Bedingungen durchgeführt und mit konventionellen Messungen in Mediatorlösung verglichen. Die erreichte Bildqualität unter MD-Bedingungen war gleichwertig mit konventionellen Messungen. Außerdem wurden weitere Messungen an LIB-Graphitelektroden durchgeführt, mit dem Ergebnis, dass auch hier die erreichte Bildqualität vergleichbar war. Das vorgestellte MD-Konzept kann für Untersuchungen an Grenzflächen, welche im Betrieb von Lithium-Ionen-Batterien auf negativen und positiven Elektroden entstehen, von Vorteil sein, da Interferenzen durch den zugesetzten Mediator auf ein Minimum reduziert werden.

Zentrales Thema des dritten Projekts war die Charakterisierung zweier Gruppen von bordotierten Diamantelektroden mit und ohne Vorbehandlung durch ein spezielles Polierprotokoll. Außerdem beinhalteten beide Sätze BDD-Proben mit unterschiedlichen Bordotierungsgraden im Bereich von 500 bis 8000 ppm. Zuerst wurden vier typische SECM-Mediator für den möglichen Einsatz zur Darstellung von Reaktivitätsunterschieden der BDD-Proben getestet. Die höchste Qualität wurde dabei mit Ferrocenmethanol erreicht. Die Vergleichsstudie zeigte, dass die unbehandelten Proben nicht nur leitende Bereiche auf ihrer Oberfläche hatten, sondern auch nichtleitende. Im Gegensatz dazu wurden an den behandelten Proben keine nichtleitenden Bereiche vorgefunden. Weiterhin zeigten die unbehandelten Proben eine ausgeprägte Heterogenität der elektrochemischen Aktivität, selbst beim höchsten Bordotierungsgrad. Die elektrochemische Aktivität der behandelten Proben war weitestgehend homogen. Darüber hinaus waren die Unterschiede zwischen beiden Gruppen bei niedriger Bordotierung stärker ausgeprägt. Weitere Experimente wurden durchgeführt, um die Kinetik der Proben lokal zu untersuchen. Dafür wurden Proben mit 4000 ppm Bordotierungsgrad eingesetzt. Eine höhere durchschnittliche Reaktionskonstante und eine geringere lokale Variation wurden für die behandelte Probe festgestellt.

In einem Nebenprojekt wurden gestempelte Platinelektroden mittels SECM charakterisiert. Durch das simple Auftragen einer nichtleitenden Lackschicht mit definierter Form konnten verschiedene Mikrostrukturen auf einer Makroelektrode erzeugt werden. In SECM-Experimenten wurden drei Strukturen, eine punktförmige, eine bandförmige und eine kreisförmige untersucht. Dabei wurden die erhaltenen Größen und die erhaltene Qualität der

Mikrostrukturen bestimmt und außerdem die Stabilität und isolierenden Eigenschaften der umgebenden Lackschicht.

Zusammengefasst wurde die SECM-Thematik durch instrumentelle und methodische Entwicklung mit besonderem Fokus auf LIB-Untersuchungen verbessert. Eine unkomplizierte und leicht anzuwendende SICM-Methode wurde vorgestellt und gekoppelt mit SECM eingesetzt. Der kombinierte Aufbau wurde verwendet in LIB-Elektrolytlösungen. Weiterhin wurde ein neuartiges Konzept zum reduzierten Mediatoreinsatz während *in situ* oder *in operando* Studien an LIBs entwickelt. Messungen an einem Modellsubstrat und an einer LIB-Graphitelektrode demonstrierten die Leistungsfähigkeit des MD-Aufbaus. Außerdem wurden SECM-Studien an verschiedenen Elektrodenmaterialien in wässrigen Lösungen im Rahmen weiterer Projekte durchgeführt. Zwei verschiedenen Gruppen bordotierter Diamantelektroden wurden untersucht. Dabei wurde der Einfluss einer Vorbehandlung durch ein spezielles Polierprotokoll und unterschiedliche Bordotierungen ermittelt. Darüber hinaus wurden Mikrostrukturen, welche auf Platinmakroelektroden gestempelt wurden, hinsichtlich ihrer Qualität beurteilt.

7 Eidesstattliche Erklärung

Ich habe die vorliegende Arbeit selbstständig verfasst, keine anderen als die angegebenen Quellen und Hilfsmittel benutzt und bisher keiner anderen Prüfungsbehörde vorgelegt. Von den in §27 Abs. 5 vorgesehenen Rechtsfolgen habe ich Kenntnis genommen.

Regensburg, den 05.08.2024

Eidenschink Johannes